BIOMATERIAL STRATEGIES FOR IMPROVED BONE HEALING WITH BONE MORPHOGENETIC PROTEIN-2 DELIVERY

A Dissertation

Presented to

The Academic Faculty

by

Lauren B. Priddy

In Partial Fulfillment

of the Requirements for the Degree

Doctor of Philosophy in the

Program of Bioengineering

Georgia Institute of Technology

August 2015

BIOMATERIAL STRATEGIES FOR IMPROVED BONE HEALING WITH BONE MORPHOGENETIC PROTEIN-2 DELIVERY

Approved by:

Dr. Robert E. Guldberg, Ph.D., Advisor
School of Mechanical Engineering
Georgia Institute of Technology

Dr. Johnna S. Temenoff, Ph.D.
Department of Biomedical Engineering
Georgia Institute of Technology

Dr. Edward A. Botchwey, Ph.D.
Department of Biomedical Engineering
Georgia Institute of Technology

Dr. Lisa N. Tran, D.D.S., M.D.
Department of Surgery
Emory University School of Medicine

Dr. Andrés J. García, Ph.D.
School of Mechanical Engineering
Georgia Institute of Technology

Date Approved: July 8, 2015

To my loving family.

ACKNOWLEDGEMENTS

The road to the PhD is not a straight or predictable road, and I have many people to thank for helping me along the way. First, thanks to my thesis advisor Dr. Robert Guldberg, who helped me become an independent researcher by pushing me to think critically about my work and demonstrating the traits of a successful researcher and mentor. I hope to be as successful as he is one day with my own lab. I am also grateful for the collective insight of my thesis committee members Dr. Johnna Temenoff, Dr. Andrés García, and Dr. Edward Botchwey who helped steer my research by their constructive criticism and guidance. A special thanks to Dr. Lisa Tran, whose enthusiasm and encouragement were greatly appreciated. Thank you for reminding me of the relevance of my work and how it fits into clinical orthopedics, as well as for your hours spent helping with surgeries on your days off.

A big thanks goes out to all members of the Guldberg lab, both past and present, for their contributions to my work. The days of surgeries would not have been possible without the collaborative group effort, and I truly enjoyed the camaraderie. I am grateful for both the intellectual contributions and friendship of Hazel Stevens, who keeps the Guldberg lab ticking and was my sounding board on many occasions when I needed advice. I am honored to have had the opportunity to work alongside Dr. Laxmi Krishnan, who is an endless source of knowledge and was always eager to help. Thanks to Dr. Nick Willett, Dr. Joel Boerckel, and Dr. Brent Uhrig for helping me get started with in vivo work. I am also very thankful to Nick for his advice and encouragement during my job search. Thanks to Angela Lin for assistance with micro-CT and mechanical testing. Dr. Tamim Diab, Dr. Chris Dosier, and Dr. Jessica Green also provided valuable input in my projects early on. I am truly grateful for the companionship of Dr. Tanu Thote (my mentor during recruitment) and

Dr. Ashley Allen (my post-recruitment mentor)—both were great advocates for the family that is the Guldberg lab—as well as my former back row buddy Dr. Alice Li. Tanu, Alice, and Ashley, I am forever grateful for your guidance and for being able to share the PhD experience with you. Each of you made it a truly fun time that I will always remember fondly. Tanu, thank you for blazing the trail and for taking lunch breaks outside with me. Alice, thank you for helping me explore new and interesting foods that I otherwise never would have tried, and for commiserating about crazy kitties with me. You always knew the right research questions to ask, and I appreciate your help with planning experiments early on and navigating the nuances of the PhD process later. Ashley, thank you for encouraging me in my running—it has truly changed my life! I will miss our run-chats and your constant positive outlook on life. Ending the PhD process with you has been a very memorable experience. Dr. Tara McFadden, thank you for going to football games with me and for sharing your (especially strong) Irish tea. Jason Wang, thank you for being my quals study partner and for sharing your genuine love of teaching. Marian Hettiaratchi, Giuliana Salazar-Noratto, and Marissa Ruehle, it's been fun with you on the back row. And also to David Reece, Olivia Burnsed, Brennan Torstrick, Albert Cheng, Andrew Miller, and Brett Klosterhoff, the Guldberg lab is in great hands with you all. Thank you for your friendship and intellectual input in my work. You all made work more enjoyable, and I am grateful for each and every one of you. The students I mentored—Camden Esancy, Kalah Haley, Nikhil Gupte, Sukhita Karthikeyakannan, and Amanda Schaefer—also deserve a big thanks for their contributions to my projects. Finally, thanks to the rest of my colleagues in wing 2D who were there when I needed a break from research.

Many members of the IBB community deserve thanks for their assistance throughout my time at Tech. Vivian Johnson was my constant advocate and was always

willing to help. Chris Ruffin was a pleasure to work with during my time leading BGSAC, and he will be forever missed. Laura Paige has kept me informed of all the deadlines for graduating and has shared enough BioE shirts with me for every day of the week. The IBB staff including Megan McDevitt, Floyd Wood, Alyceson Andrews, James Godard, Steve Woodard, Colly Mitchell, Allen Echols, and Karen Ethier have generously provided their time and help. Thanks also to Aqua Asberry for assistance with histology procedures.

I would like to thank my teaching mentor Dr. Brani Vidakovic, who not only provided me with valuable experience in the classroom, but also devoted additional time for me to participate in the Center for the Enhancement of Teaching and Learning's (CETL) Tech to Teaching Program, which allowed me to further explore how learning works and provided me with a solid foundation of techniques I can use in the classroom to promote learning. Thanks to the folks in CETL and communications who mentored me, including Dr. Damon Williams, Dr. Dave Lawrence, Lori Critz, Dr. Caroline Noyes, and Dr. Wendy Newstetter. I am grateful for my experiences in Women in Engineering (WIE) and the Society of Women Engineers (SWE) with Dr. Christine Valle, who has been a mentor to me and advocate for women in STEM, and has given me many opportunities to share my enthusiasm for promoting women in STEM. Thank you to Dr. Laura O'Farrell, Kim Benjamin, Andrea Gibson, Ogeda Blue, and all the PRL staff for taking care of our animals, making my time in the PRL more enjoyable, and reminding me of the importance of our work with animals. I would also like to acknowledge my research collaborators Dr. Ovijit Chaudhuri, Dr. Dalia Arafat, and Dr. Tom Koob for their contributions to this work. The NIH Graduate Training for Rationally Designed, Integrative Biomaterials Fellowship provided me with funding for two years, valuable research and classroom experience in the field of biomaterials, and opportunities to build relationships with a great group of people,

especially through the Graduate Leadership Program. I am also grateful for my experiences in the BioEngineering Graduate Association (BGA, but will forever be BGSAC to me) and the broader Bioengineering and Bioscience Unified Graduate Students (BBUGS) group. Finally, a big thanks is due to friends I haven't mentioned yet, including Dr. Ashley Brown, Jen Lei, Dr. Laura Hansen, Dr. Patricia Pacheco, Dr. Alex Caulk, Charla Howard, Dr. Katie Mowry, Dr. Joe Chen, Amanda McGowin, Brooke Williams, Blair White, and many others: thank you for your friendship and support over the years.

I am truly grateful for the constant love and support from my family. Mom and Dad, you have always been my biggest fans, encouraging me to believe in myself and follow my dreams. Thank you for all you have done and continue to do to help them come true. I would like to thank all of my family for helping me become the person I am today. Each one of you holds a special place in my heart. Your love and support means the world to me.

Last, but certainly not least, I am thankful for the love and support of my husband Matthew. Thank you for driving me to and from work every day, even though the traffic drove us both crazy sometimes. Thank you for making me laugh, even when I'm so mad that I don't want to. The little moments that happen every day mean so much. Thank you for your understanding and encouragement during the trying times. I am so proud of you, and I am honored to share this journey with you. You are my inspiration.

TABLE OF CONTENTS

LIST OF TABLES

LIST OF FIGURES

LIST OF SYMBOLS AND ABBREVIATIONS

αMEM	alpha-Minimum Essential Medium
AA2P	Ascorbic acid 2-phosphate
ACS	Absorbable collagen sponge
ALP	Alkaline phosphatase
ANOVA	Analysis of variance
bFGF	Basic fibroblast growth factor
BMD	Bone mineral density
BMP-2	Bone morphogenetic protein-2
BMU	Basic multicellular unit
BSA	Bovine serum albumin
BV	Bone volume
cDNA	Complementary deoxyribonucleic acid
Ct	Cycle threshold
dHACM	Dehydrated human amnion/chorion membrane
ECM	Extracellular matrix
ELISA	Enzyme-linked immunosorbent assay
FBS	Fetal bovine serum
FDA	Food and Drug Administration
FDR	False discovery rate
FOP	Fibrodysplasia ossificans progressiva
GAGs	Glycosaminoglycans
GCSF	Granulocyte colony stimulating factor

H&E	Hematoxylin & eosin
HBSS	Hank's Buffered Salt Solution
HSV	Hue, Saturation, Value
IACUC	Institutional Animal Care and Use Committee
IHC	Immunohistochemistry
IL	Interleukin
IL-1Ra	Interleukin-1 receptor antagonist
IM	Intramuscularly
Micro-CT	Micro-computed tomography
MC3T3-E1	Mouse clonal pre-osteoblasts
MMP	Matrix metalloproteinase
MSC	Mesenchymal stem cell
NSAIDs	Nonsteroidal anti-inflammatory drugs
OCN	Osteocalcin
OCT	Optimum cutting temperature
OPG	Osteoprotegerin
OPN	Osteopontin
OSX	Osterix
PBS	Phosphate buffered saline
PCA	Principal component analysis
PCL	Poly(ε-caprolactone)
PDGF	Platelet-derived growth factor
pMOI	Polar moment of inertia

p-NPP	p-Nitrophenyl Phosphate
PSL	Penicillin-streptomycin-L-glutamine
qPCR	Quantitative real-time polymerase chain reaction
RANKL	Receptor activator of nuclear factor kappa-B ligand
RGD	Arginine-glycine-aspartic acid
rhBMP-2	Recombinant human bone morphogenetic protein-2
RNA	Ribonucleic acid
RSA	Rat serum albumin
RUNX2	Runt-related transcription factor 2
SDF-1	Stromal cell-derived factor-1
SDS	Sodium dodecyl sulfate
SEM	Standard error of the mean
SIS	Small intestinal submucosa
TGF-β	Transforming growth factor-beta
TNF-α	Tumor necrosis factor-alpha
VEGF	Vascular endothelial growth factor
VOI	Volume of interest

SUMMARY

Musculoskeletal injuries account for two-thirds of all injuries that occur in the United States annually, and among these injuries, large bone defects are particularly challenging to repair. Although bone morphogenetic protein-2 (BMP-2) delivered on an absorbable collagen sponge (ACS) has shown clinical success in long bone healing, complications associated with the empirical use of supraphysiological doses of BMP-2, including heterotopic mineralization and inflammation, necessitate the development of a biomaterial carrier that localizes growth factors to the site of injury. In the development of bone tissue engineering strategies, another critical design parameter is the timing of delivery vehicle degradation, since bone regeneration may be impeded by the presence of residual biomaterials at the injury site. Furthermore, bioactive, naturally derived extracellular matrix (ECM) products with pro-healing and immunomodulatory properties are attractive therapeutics with rapid translatability that may function to attenuate heterotopic mineralization often observed with high dose BMP-2 treatment.

The goal of this work was to investigate hybrid biomaterial systems with controlled strategies for BMP-2 delivery to promote structural and functional restoration of segmental bone defects. Using a critically sized rat segmental bone defect model, we (i) evaluated the effects of alginate hydrogel oxidation on BMP-2 release and bone regeneration, (ii) elucidated the spatiotemporal effects of high dose BMP-2 on bone healing and gene expression, and (iii) investigated the ability of amniotic membrane to attenuate heterotopic mineralization in critically sized bone defects. Modification of the delivery vehicle to modulate growth factor availability may help minimize adverse side effects associated with high dose BMP-2 delivery, while harnessing the healing efficacy of BMP-2 for bone tissue engineering applications.

This thesis evaluated novel translatable strategies for promoting biomaterial degradation and growth factor localization, as well as attenuating heterotopic mineralization in a challenging segmental bone defect model. Of significance, our rat model recapitulated adverse effects associated with orthotopic high dose BMP-2 delivery, particularly heterotopic mineralization and systemic inflammatory effects. The spatiotemporal differences in gene expression as a function of BMP-2 dose may, in part, explain the heterotopic mineralization and tissue swelling seen clinically with high doses of BMP-2. By providing insight into the complex process of bone healing in the context of growth factor delivery, we may more effectively harness endogenous repair mechanisms for successful bone regeneration.

I. SPECIFIC AIMS

Treatment of large bone defects resulting from traumatic injury or tumor resection presents a significant clinical challenge. The gold standard of care, the autograft, still involves complications such as pain at the donor site, lack of revascularization at the injury site, and non-union, necessitating repeated surgeries or in rare cases, amputation. Since bone tissue can regenerate after injury, the development of tissue engineering strategies that support the endogenous bone repair process is crucial for successful healing.

As alternatives to autograft treatment, the osteoinductive growth factors BMP-2 and BMP-7 have been used successfully for regeneration of bone in the clinic. However, the use of BMPs at supraphysiological doses often leads to complications including heterotopic mineralization and inflammation. Adverse effects such as these are compounded by the delivery of BMP within a collagen sponge, which has limited ability to retain growth factor. Furthermore, since residual biomaterial at the injury site can hinder the formation of new tissue, modifying the biomaterial to accelerate degradation may augment bone healing.

Growth factor delivery vehicles capable of mitigating BMP-2-induced adverse effects represent a significant clinical need. To develop such therapies, one must first understand the mechanisms of bone healing and inflammation in the context of critically sized bone defects. To this end, we utilized a well-established rat segmental bone defect model to evaluate the therapeutics of interest. Previously with this model, irradiated alginate hydrogels enclosed with a poly(ε-caprolactone) (PCL) nanofiber mesh allowed for a more sustained release of BMP-2 and enhanced bone regeneration compared to delivery with collagen sponge. Using this model as a platform, our goal was to recapitulate the negative effects of a more clinically relevant (higher) dose of BMP-2. Subsequently, the effects of BMP-2 dose on gene expression in the bone defect and surrounding soft tissue were examined during early

bone healing. Additionally, biomaterial parameters (e.g., degradation, growth factor release/bioactivity) were modulated to evaluate their effects on bone regeneration. This model was then used to assess the efficacy of ECM-derived material to spatially restrict bone formation with high dose BMP-2 delivery. The *overall objective* of this work was to investigate hybrid biomaterial systems with controlled strategies for BMP-2 delivery to promote structural and functional restoration of segmental bone defects. The *central hypothesis* was that a biomaterial delivery vehicle that allows for localized growth factor availability and minimal heterotopic bone formation will facilitate structural and functional restoration of segmental bone defects. We tested this hypothesis via the following specific aims:

Aim 1: Evaluate the effects of alginate hydrogel oxidation on BMP-2 release and bone regeneration

The interplay between carrier degradation, growth factor release, and tissue ingrowth remains poorly understood. With these design parameters in mind, this aim evaluated the regenerative capacity of an oxidized-irradiated alginate hydrogel as a delivery vehicle for BMP-2 in a large bone defect model. We *hypothesized* that oxidized-irradiated alginate would accelerate the release of BMP-2, degrade faster *in vivo*, and facilitate the formation of higher quality, more mature bone. Release kinetics and bioactivity of BMP-2 released from and retained within alginate hydrogels *in vitro* were quantified via ELISA and alkaline phosphatase (ALP) induction assays, respectively. Critically sized (8-mm) rat femoral segmental defects were treated with low dose recombinant human BMP-2 (rhBMP-2) in irradiated alginate or oxidized-irradiated alginate, surrounded by a PCL nanofiber mesh. Bone regeneration was assessed via radiography, micro-CT, and mechanical testing. Histology was conducted to identify residual alginate and newly formed bone within the defect region.

Aim 2: Elucidate the spatiotemporal effects of high dose BMP-2 on bone healing and gene expression

Clinically, the use of high doses of BMP-2 is associated with many adverse effects including heterotopic bone formation and tissue swelling. However, the consequences of supraphysiological doses of BMP-2 on bone healing and inflammation have not been well characterized. Therefore, in this aim we examined bone regeneration and inflammation associated with high dose BMP-2 delivery in a critically sized bone defect model. Release kinetics of high dose BMP-2 from collagen sponge, collagen sponge+mesh, and irradiated alginate+mesh *in vitro* were compared. Critically sized segmental bone defects were treated with high dose rhBMP-2 in collagen sponge or irradiated alginate, both surrounded by a mesh. Bone regeneration was assessed via radiography, micro-CT, and mechanical testing. Routine histology and immunohistochemistry (IHC) was conducted to observe spatial distribution of mineralization and identify inflammatory mediators within the defect space. We first *hypothesized* that the alginate delivery system would lead to reduced heterotopic mineralization compared to the collagen sponge system. Subsequently, we further characterized mechanisms of bone formation and inflammation in the context of critically sized bone defects as a function of BMP-2 dose. Using quantitative real-time polymerase chain reaction (qPCR), the effects of BMP-2 dose on osteogenic and inflammatory gene expression profiles in the bone defect and surrounding soft tissue were assessed. Our *hypothesis* here was that high dose BMP-2 would elicit greater osteogenic and inflammatory gene expression in both the bone defect and muscle tissue compared to low dose BMP-2.

Aim 3: Investigate the ability of amniotic membrane to attenuate heterotopic mineralization in critically sized bone defects

The amniotic membrane is a natural ECM material containing structural collagens and proteoglycans, as well as potent anti-inflammatory cytokines and growth factors, making it an ideal candidate for tissue healing applications. Based on our results from Aim 2 demonstrating the presence of heterotopic mineralization adjacent to bone defects treated with high dose BMP-2, we believed amniotic membrane (dehydrated human amnion/chorion membrane, dHACM) surrounding the bone defect space would serve as an effective barrier to mitigate heterotopic mineralization. Release kinetics of BMP-2 from amnion and PCL nanofiber mesh were evaluated *in vitro* by ELISA. Subsequently, two clinically available delivery systems—collagen sponge alone and collagen sponge surrounded by amnion—were used to deliver high dose BMP-2 in our rat critically sized segmental bone defect model. Outcome measures included radiography, micro-CT, mechanical testing, and histology. We *hypothesized* that amniotic membrane surrounding collagen sponge would result in less heterotopic mineralization compared to collagen sponge alone.

Significance and Scientific Impact

This thesis provides significant insights into strategies for promoting biomaterial degradation and growth factor bioactivity and localization, as well as reducing heterotopic mineralization in a challenging segmental bone defect model. Importantly, our rat model recapitulated adverse effects observed clinically with orthotopic high dose BMP-2 delivery, specifically heterotopic mineralization, prolonged local inflammation, and systemic inflammatory effects. Although the hybrid alginate-PCL delivery system did not reduce heterotopic ossification with high dose BMP-2, it enhanced bone formation within the defect space compared to the collagen-PCL vehicle, likely due to the prolonged, enhanced bioactivity of the BMP-2 remaining in the alginate constructs.

By identifying specific alterations in gene expression as a function of time and BMP-2 dose, this thesis contributes to our understanding of the complex process of bone healing during the early stages of large bone defect regeneration. Of significance, an earlier resolution of inflammation in the bone defect microenvironment following treatment with low dose BMP-2 was observed. The spatiotemporal differences in gene expression as a function of BMP-2 dose may, in part, explain the heterotopic mineralization and tissue swelling seen clinically with high doses of BMP-2.

Extracellular matrix-derived amniotic membrane surrounding collagen sponge scaffolds resulted in less heterotopic mineralization compared to collagen sponge alone. This finding may be attributed to the amnion functioning as a biological sink for BMP-2 (retained more BMP-2 than standard PCL mesh membrane) and/or the immunomodulatory factors present in the amnion. The reduction in heterotopic ossification is especially important because these materials are available for use clinically, which may drastically accelerate the translation of the amnion for bone regeneration applications.

The findings here support the overall hypothesis that a biomaterial delivery vehicle that allows for localized growth factor availability and minimal heterotopic bone formation would facilitate structural and functional restoration of segmental bone defects. By considering these fundamental biomaterial parameters, we may more effectively harness endogenous repair mechanisms for successful bone regeneration.

II. BACKGROUND[1] [2]

2.1 Bone Physiology

Bone Structure and Function

As an organ, bone plays crucial roles in homeostasis both physiologically and structurally. The primary metabolic actions of bone include regulation of calcium, phosphate, and growth factor availability; coordination of hormone levels with other organs; production and maintenance of hematopoietic stem cells in the marrow space; and reservoir of mesenchymal stem cells (MSCs) that contribute in the formation of bone [1, 2]. Structurally, bone also performs many essential functions: (i) providing the frame that both supports the body's weight and protects vital organs, and (ii) serving as the insertion point for muscles (via tendons) and the attachment to other bones (via ligaments) to allow for movement.

Bone can be classified as cortical (compact) bone or trabecular (cancellous) bone. Cortical bone serves mainly structural and protective roles as the dense outer shell of bones and is coated by the periosteum. The bones of the limbs and limb girdles (appendicular skeleton) are composed primarily of cortical bone. Human cortical bone is organized into units called osteons that each contain a central Haversian canal, which allows for nutrient and waste exchange in the highly dense tissue. Conversely, the axial skeleton bones (bones of

[1] Portions of this chapter were adapted from Priddy L B, Chaudhuri O, Stevens H Y, Krishnan L, Uhrig B A, Willett N J, Guldberg R E. Oxidized alginate hydrogels for bone morphogenetic protein-2 delivery in long bone defects. *Acta Biomaterialia*, 10(10), 4390-4399, 2014. License No. 3603720780456

[2] Portions of this chapter were adapted from Allen A B, Priddy L B, Li M T, Guldberg R E. Functional augmentation of naturally-derived materials for tissue regeneration. *Ann Biomed Eng*, 43(3), 555-567, 2015. License No. 3630480316395

the skull, spine, ribs, and sternum) and the metaphyses of long bones are made mainly of trabecular bone surrounded by a thin cortical shell. Trabecular bone plays primarily a metabolic role and is present in long spicules called trabeculae that are oriented along lines of principal stresses (Wolff's law [3]), thus providing further mechanical strength to bone.

Bone is a dynamic tissue that adapts to environmental stimuli, particularly mechanical loads, by resorbing or forming bone. Bone tissue is composed mainly of osteoblasts, osteocytes, and osteoclasts [2]. Osteoblasts are cells of the mesenchymal lineage, derived specifically from osteoprogenitor cells. The major sources of these cells are the bone marrow, periosteum, and the surrounding soft tissue [4]. Osteoprogenitor cells play two primary roles in bone homeostasis: (i) secretion of cytokines to recruit additional MSCs and pre-osteoblasts, and (ii) differentiation and production of mineralized matrix, leading to the formation of bony tissue [5]. During early osteogenic differentiation, cells secrete factors such as alkaline phosphatase (ALP) and collagen type I, and as they become mature osteoblasts they produce proteins including osteopontin (OPN) and osteocalcin (OCN). The secreted proteins and ground substance make up the organic portion of bone matrix, referred to as osteoid, which is subsequently mineralized when calcium and phosphate precipitates form hydroxyapatite crystals.

Collagen type I comprises 90% of the organic portion of bone extracellular matrix (ECM) [6] and confers bone its tensile strength [7]. Besides comprising collagen type I, bone matrix also serves as a reservoir for other proteins and growth factors that participate in bone maintenance. One such growth factor (discussed in detail in Section B.3) is bone morphogenetic protein-2 (BMP-2), which is chemotactic to many cell types and was first discovered as an inducer of osteogenesis in the 1960s [5]. Hydroxyapatite is the main inorganic component of bone matrix. The high compressive strength of bone is due to the

presence of hydroxyapatite crystals within collagen fibrils as well as the alignment of the collagen fibers within the matrix.

Once osteoblasts are surrounded by bone matrix, they are referred to as osteocytes. Osteocytes make up 90-95% of all bone cells and are located within lacunae and communicate via gap junctions [8]. Although once thought to be quiescent cells, osteocytes are now recognized as the bone cells chiefly responsible for sensing mechanical stimuli and responding via bone formation and/or resorption [9].

Osteoclasts are large, multinucleated cells of hematopoietic origin that reside on bone surfaces. Active osteoclasts migrate to resorption pits called Howship's lacunae where they resorb bone. Within Haversian canals, osteoclasts comprise the leading edge (cutting cone) of bone resorption, followed by osteoblasts secreting osteoid. The coupling mechanism by which osteoclasts and osteoblasts communicate during bone remodeling is described in detail below.

On the microscale, bone can be classified by the degree of organization of the collagen fibers [10]. Woven bone is characterized by disorganized collagen fibers that are laid down quickly. After a fracture, woven bone is the first type of bone to form. In contrast, lamellar bone is composed of parallel collagen fibers within concentric sheets called lamellae, with the fibers alternating their orientation from one lamella to the next. Due to its highly organized structure, lamellar bone has greater mechanical integrity than woven bone. Regardless of the mechanism by which bone develops (endochondral or intramembranous ossification, discussed below), woven bone forms first and is subsequently remodeled into lamellar bone.

Bone Development and Remodeling

The two classes of bone development, or ossification, are known as endochondral ossification and intramembranous ossification. Endochondral ossification is the primary mechanism by which long bones develop [11]. During endochondral ossification, bone is formed from a cartilage template composed of proliferating and hypertrophic chondrocytes that then becomes calcified. The chondrocytes undergo apoptosis and are cleared by invading osteoclasts, and new bone matrix is secreted by osteoblasts. At the point of skeletal maturity (18-25 years), the cartilage in the growth plates of bones has been replaced entirely by bone tissue. Intramembranous ossification is the process by which flat bones (e.g., skull bones, scapulae) develop. In this process, bone is formed directly from mesenchymal tissue instead of from cartilage [10]. High concentrations of osteoprogenitor cells differentiate into osteoblasts, which secrete bone matrix. Typically, bone healing after injury involves both endochondral and intramembranous ossification [12].

Once bone tissue is present, it is constantly resorbed and formed in a process known as remodeling. Every year, approximately 10% of the adult skeleton (by mass) undergoes remodeling [13]. As a result of daily loading of bone, microcracks in osteocytes cause the secretion of soluble paracrine factors that recruit osteoclasts to resorb the damaged bone. Osteoblasts and osteoclasts together form structures known as basic multicellular units (BMUs) that orchestrate both bone development (modeling) and remodeling. In short, receptor activator of nuclear factor kappa-B ligand (RANKL) on the surface of an osteoblast binds to RANK on an osteoclast, activating the osteoclast. Once active, the osteoclast forms a tight seal with the bone surface and begins resorbing bone, releasing factors from the matrix (e.g., BMPs, transforming growth factor-beta (TGF-β)) that recruit osteoprogenitor cells to the resorption site. These cells then differentiate into osteoblasts, which form new

bone. In a negative feedback loop, once the matrix is mineralized, osteoblasts regulate the bone remodeling process by secreting osteoprotegerin (OPG), a decoy receptor that binds RANKL, preventing its interaction with RANK and thus inhibiting osteoclast activation. By continuously remodeling itself, bone tissue maintains a state of equilibrium, except during growth and disease. Osteoporosis is the state whereby more bone is resorbed than is formed; conversely, osteopetrosis involves bone formation that outpaces resorption [14].

2.2 Bone Regeneration

Clinical Motivation

Musculoskeletal injuries account for two-thirds of all injuries each year in the United States [15, 16]. Of the 6.3 million bone fractures that occur annually in the United States, over 500,000 require bone grafts, accounting for approximately $2.5 billion in medical expenses [17]. Substantial loss of bone tissue caused by traumatic injury or tumor resection presents a significant clinical challenge for reconstruction. Among these injuries, critically sized bone defects are particularly difficult to repair and often require subsequent surgeries or result in a non-union or amputation. An estimated 185,000 persons per year undergo amputation of a limb [18]. Currently, the gold standard of care for critically sized bone defects is autograft harvested from the iliac crest, but the limited graft tissue available and associated donor site pain and morbidity [19] warrant the study of more effective therapeutics.

Bone tissue has an innate capacity to regenerate after injury. Thus, tissue engineering and regenerative medicine approaches, based on the delivery of osteoinductive cells, growth factors, and matrix materials, have emerged as a promising alternative to autograft treatment. One clinically viable tissue engineering strategy is to deliver an osteogenic growth factor

within a biomaterial scaffold to the site of injury and thereby stimulate the endogenous bone repair process [20]. A critical factor in the effectiveness of the carrier is the ability to provide the necessary temporal and spatial presentation of the growth factor for sufficient recruitment and differentiation of endogenous stem cells [20]. In particular, the surrounding soft tissue serves as a crucial source of stem cells, especially for large bone defects that result in significant loss of periosteum and marrow tissue [21].

As members of the transforming growth factor-beta (TGF-β) super family of growth factors, bone morphogenetic proteins (BMPs) promote migration of many cells including osteoprogenitors [22], and osteogenic differentiation of mesenchymal stem cells [23, 24]. Both BMP-2 and BMP-7 are approved by the Food and Drug Administration (FDA) for clinical use [25, 26], and BMP-2 has been widely studied as an osteoinductive protein for bone regeneration. Although BMP-2 delivered on an absorbable collagen sponge has shown success in long bone healing and spinal fusion [27, 28], concerns regarding the use of supraphysiological doses and associated complications including heterotopic mineralization and inflammation [29] necessitate the development of biomaterial carriers that promote greater regenerative efficacy with lower doses of growth factor [30].

Biomaterials in Bone Tissue Engineering

Alginate Hydrogels

A critical factor in the effectiveness of the biomaterial carrier is its ability to provide the necessary temporal and spatial presentation of the growth factor for sufficient recruitment and differentiation of endogenous stem cells [20]. Hydrogels as a class of biomaterials possess many advantages for growth factor delivery, including biocompatibility, ease of growth factor incorporation, and tunable degradation rates. In particular, alginate

hydrogels have been used as delivery vehicles for a multitude of proteins, including BMP-2 [31-34]. As alginate is a plant polysaccharide, it does not degrade enzymatically in animal species because they lack alginases [34]. Instead, alginate degrades slowly and in an uncontrolled manner due to the dissociation of ionic crosslinks [35]. Release of growth factors from unmodified alginate relies mainly on diffusion. However, modifying the structure of the alginate polymer can alter the rate of degradation of alginate, thus allowing more control over protein release [36].

Modification techniques utilized to increase alginate degradation rate and its associated growth factor release include gamma-irradiation and partial oxidation. Gamma-irradiation lowers the molecular weight of alginate and allows for improved cellular infiltration and tissue healing compared to non-irradiated alginate [34, 37]. Irradiated alginate hydrogels have been used to deliver proteins such as BMP-2 and facilitated functional regeneration in a critically sized rat femoral defect model [38-41]. Further, irradiated alginate hydrogels surrounded by a PCL nanofiber mesh provided a more sustained release of BMP-2 and augmented bone regeneration compared to the clinically-used collagen sponge in a rat model [39, 40]. However, a portion of the alginate material was shown to persist at 30 weeks and may have hindered integration of the newly formed bone tissue [42]. Partial oxidation, whereby a small percentage of the uronate residues are oxidized, allows the polymer chains to be more susceptible to hydrolysis and increases the degradation rate *in vitro* [43-45]. Unlike the degradation of unmodified alginate, oxidized alginate breakdown occurs primarily via hydrolysis, specifically at the oxidized sugar residues [43]. Oxidation of the alginate creates a more open-chain structure while maintaining the ionic cross-linking capacity [44] and biocompatibility of the alginate [43].

Scaffold degradation is a crucial regulator of not only growth factor retention but also extracellular matrix deposition [46]. As the scaffold degrades, space for new bone is created. As such, the rate of scaffold degradation would ideally be similar to the rate of new tissue formation to allow for successful coalescence of the newly formed bone. In previous subcutaneous implant studies, irradiation of the alginate led to a greater amount [34, 37] and superior quality [37] of bone tissue compared to non-irradiated alginate. Furthermore, oxidized alginate hydrogels facilitated an increase in cellular infiltration and matrix formation subcutaneously [44], and mitigated tissue loss in a mouse hind limb ischemia model [45].

Collagen Sponge Scaffolds

As collagen is a primary constituent of the ECM, collagen-based biomaterials are one of the most common classes of natural biomaterials used in tissue engineering applications. In the clinic, absorbable collagen sponge (ACS) scaffolds of bovine origin are approved for use in spinal fusions, open tibial fractures, and non-unions as carriers of rhBMP-2 and rhBMP-7 [25, 26]. One of the benefits of collagen scaffolds is their ability to be enzymatically degraded, and the time line of degradation can be extended by, for example, physical or chemical crosslinking of the scaffold [47, 48]. However, a major limitation of growth factor delivery via collagen sponge is the rapid release of growth factor. It has been reported between 40-90% of the loaded growth factor is released in an initial burst pattern [25, 29, 39, 49]. Despite this drawback, collagen scaffolds continue to be used often for the regeneration of bone in the clinic.

Extracellular Matrix-Derived Materials

Native ECM materials such as amniotic membrane and small intestinal submucosa (SIS) represent a class of naturally derived biomaterials already employed in the clinic for

tissue healing applications. With their intrinsic structural properties (proteins, glycosaminoglycans (GAGs), adhesive ligands, etc.) and ability to bind growth factors, these natural scaffolds provide an environment beneficial for resident and recruited cells [50, 51].

Amniotic membrane was used as early as 1910 for skin grafting [52] and has been used successfully for the regeneration of many tissues, including cornea [53, 54], tendon [20], and cartilage [55]. The amniotic membrane is a bioactive ECM composed of an epithelial layer, a basement membrane, a thick fibrous layer (fibroblasts within loosely crosslinked collagen, glycoproteins, and proteoglycans), and avascular connective tissue [56, 57]. Amniotic membrane contains large amounts of collagens type I and III and hyaluronan [58-60], as well as many growth factors, inflammatory mediators [51, 61], and angiogenic cytokines [62]. Some of the many factors present in the tissue include platelet-derived growth factors (PDGFs), transforming growth factor-beta 1 (TGF-β1), basic fibroblast growth factor (bFGF), and granulocyte colony-stimulating factor (GCSF), as well as interleukin-4 (IL-4), IL-6, IL-8, and IL-10 [51].

Although amniotic membrane materials are being increasingly used clinically, few studies have investigated the mechanisms behind the positive effects that result from their use. Cells harvested from amniotic membrane have been shown to express immunosuppressive factors such as IL-1 receptor antagonist (IL-1Ra) and IL-10 [63]. Additionally, Lindenmair et al. demonstrated the osteogenic potential of amniotic membrane tissue *in vitro* [64]. Besides the limited knowledge on mechanisms of action of the amnion, processing of the graft materials varies and is often not standardized. One patented procedure (PURION®) for amnion/chorion involves gentle cleansing, lamination of the amnion and chorion, dehydration, and devitalization (leaving cellular debris) [65]. Recently, amniotic membrane sheets processed by this method greatly improved the healing of

diabetic foot ulcers compared to the clinical standard treatment [66], and micronized, injectable amniotic membrane was shown to slow the progression of osteoarthritis in a rat model [67].

SIS is one of the most commonly used ECM materials, comprising a dense collagen network (mainly types I, III, and VI) [68], glycoproteins, GAGs, and a cocktail of bioactive growth factors [69] that contribute to the scaffold's angiogenic [70], chemotactic [71], and immunosuppressive [72, 73] roles. Typically, SIS processing involves physical removal of the outer layers (leaving the submucosa and adjoining layers) followed by decellularization [74]. SIS was first used clinically in the 1960s as autograft or allograft tissue to replace dysfunctional vasculature [75]. Today, SIS grafts are primarily decellularized, porcine-derived materials, many of which are approved for clinical use and have had successful outcomes in the treatment of a variety of damaged tissues and diseases. For example, although limited mostly to case studies, CorMatrix© has been shown to function in the repair of cardiac tissues [76, 77]. In some cases, however, augmentation of diseased tissue with SIS had no benefit, or resulted in deleterious effects. Similarly to amniotic membrane, SIS formulations have been tailored for different uses, including micronized SIS for cell delivery in a murine wound healing model, [78] and SIS gel for cardiac repair after myocardial infarction in the mouse [79]. For an in-depth review of SIS, see Andree et al. [50]. Despite progress towards the characterization of SIS materials, the large degree of biological variability of native matrices such as these warrants improvements of standardized processing methods.

Evaluating the biocompatibility, as well as biological and mechanical function of ECM materials post-processing is crucial for improving the biointegration and remodeling of these scaffolds. In particular, few studies have examined the host response to ECM-derived biological materials. Allogenic and xenogenic ECM materials, even after decellularization, are

capable of eliciting an immune response due to the presence of ECM proteins, which have been shown to stimulate the migration of neutrophils and macrophages [80-82]. Differences in the inflammatory profiles resulting from the use of noncrosslinked Restore™ SIS (pro-healing M2 macrophages) and crosslinked CuffPatch™ SIS (pro-inflammatory M1 macrophages) have been observed in a rat abdominal wall defect model [83].

Synthetic Materials

In some cases, the addition of synthetic materials to natural scaffolds can allow for more control over structural properties, while taking advantage of the innate benefits provided by the endogenous scaffold [84]. As the provisional ECM during the natural healing cascade, fibrin is a well-characterized, natural and pro-angiogenic biomaterial explored in a variety of tissue engineering applications. Commercial fibrin products traditionally require high fibrinogen and thrombin concentrations (at least an order of magnitude higher than physiologic levels) for mechanical stability. However, this leads to faster polymerization and a denser fibrin network, which limits cell infiltration [85]. The native biology of fibrin polymerization, specifically fibrin knobs which have inherent binding affinity to fibrin holes, can be harnessed and modified to provide control over the resulting structural, mechanical, and degradation properties. In particular, augmentation of fibrin knobs with synthetic, poly(ethylene glycol) (PEG)-based functionalities led to altered polymerization by engagement of hole 'b' with PEGylated knob 'B' units. The resultant fibrin hydrogels exhibited greater mechanical strength and slower enzymatic degradation, yet surprisingly, enhanced porosity (and correspondingly, diffusivity) [86].

Synthetic hydrogel materials have also served as effective carriers of BMP-2 for bone tissue regeneration. In particular, PEG-based hydrogels modified with matrix metalloproteinase (MMP) cleavable linkages were used to delivery BMP-2 and demonstrated

improved cranial defect healing compared to BMP-2 delivery via collagen sponge [87, 88]. Similar results were observed in a mouse radial defect model, where enhanced bone regeneration occurred with MMP-degradable PEG-maleimide hydrogels loaded with BMP-2 compared to collagen sponge carriers [89]. For certain applications, synthetic scaffolds may be advantageous over natural materials because of the precise control and reproducibility of material properties.

Growth Factor Delivery

Tibial fractures have a 10-30% rate of non-union, with even higher rates (50%) in open tibial fractures [90, 91]. To treat these challenging injuries, tissue engineering strategies such as the delivery of osteogenic growth factor(s) within a biomaterial scaffold to the site of injury are being explored, with the goal of harnessing the bone healing capacity of the endogenous stem cells [20]. Numerous growth factors with osteoinductive properties, including BMPs, TGF-β1, PDGF, and vascular endothelial growth factor (VEGF), have been examined for the treatment of bone defects [25, 92]. The addition of BMP has been shown to significantly improve the success rates in tibial non-unions compared to autograft tissue alone [91]. Even when a combination of bone grafts, ACS, or bulking agents was applied, BMP-2 augmented the healing outcomes. Furthermore, incorporating higher doses of BMP-2 led to improved bone regeneration in canine tibial and ulnar segmental defect models [93, 94]. However, the lack of spatial and temporal control over growth factor delivery can lead to adverse systemic effects and/or incomplete healing due to insufficient concentration of growth factor at the injury site [95]. Also, growth factor use is costly, particularly with the supraphysiological doses often used.

Bone Morphogenetic Protein-2 (BMP-2)

As members of the TGF-β superfamily of growth factors, BMPs are highly conserved, potent osteogenic proteins. More than twenty BMPs have been identified to date, with diverse functions in many developmental processes including embryogenesis, skeletal development, and hematopoiesis [96]. BMPs were initially isolated from decellularized, demineralized bone matrix [5, 97] and were found to initiate the formation of cartilage and bone *in vitro* and ectopically [98-100]. In particular, BMP-2 has been widely studied as an osteoinductive protein for bone regeneration, as it and BMP-7 are currently approved by the FDA for clinical use [25, 26].

BMP-2 is a dimeric protein that plays a role in both bone development and post-natal fracture healing [101]. One function that BMP-2 serves is promoting chemotactic migration of many cells including osteoprogenitors [22]. Additionally, BMP-2 stimulates osteogenic differentiation of mesenchymal stem cells by binding to cell surface receptors, which initiates the activation of downstream signaling pathways via phosphorylation of Smad 1/5/8, leading to the upregulation of transcription factors including runt related transcription factor 2 (RUNX2) and osterix (OSX), as well as other osteogenic genes previously mentioned, ultimately resulting in matrix secretion and mineralization [23, 102]. Of note, nanograms of endogenous BMPs are sufficient to induce osteogenesis, while it has been found that exogenous recombinant human BMPs are required at higher doses for efficacy [103-105].

It is well understood that the biological effects of a growth factor are a function of the dose of growth factor delivered. Although BMP-2 delivered on an absorbable collagen sponge (ACS) has shown success in long bone healing and spinal fusion [106, 107], the use of supraphysiological doses of BMP-2 has caused concern due to complications including

heterotopic mineralization and hematoma [29]. The consequences of supraphysiological doses of BMPs on bone healing and inflammation have not only been observed clinically but also examined in preclinical animal models. The inflammatory response following BMP-2 and BMP-7 delivered subcutaneously or intramuscularly (IM) in collagen sponge revealed, with increasing BMP dose (1-20 μg), larger volumes of soft tissue edema and granuloma-like masses at both implantation sites and greater areas of inflammatory zones surrounding the IM implants [108]. However, regardless of BMP dose, soft tissue edema volumes peaked at 3 hours in the subcutaneous implants and 2 days for the IM implants. Regarding orthotopic delivery of BMP-2, a dog model of critically sized radial defects treated with up to 2.4 mg of BMP-2 resulted in regenerated bone with cyst-like voids and impaired mechanical properties compared to bone formed with the lowest dose of BMP-2 (150 μg) [25]. Zara et al. determined a minimum threshold dose of BMP-2—11.25 μg in a critically sized rat bone defect model—at and above which poor bone quality and heterotopic mineralization were observed [109]. Likewise in a similar rat bone defect model, 10 μg BMP-2 resulted in improved bone healing compared to higher and lower doses [110]. The osteogenic effects of other growth factors (e.g., TGF-β, fibroblast growth factor-2) have also followed a biphasic dose response, whereby osteoinductive activity and bone healing peaked at mid-range concentrations [111-113]. Despite progress, our current understanding of the effects of BMP-2 dose has primarily been based on gross, tissue level analyses. Notably, the majority of the literature describing the biomolecular factors that participate in the bone healing process have been determined using fracture models, not critically sized bone defects [114].

Inflammation in Bone Healing

After injury, the natural healing cascade involves a coordinated series of events: inflammation, proliferation/repair, and remodeling. Occurring immediately after injury, inflammation is characterized by increased blood vessel permeability, hematoma, and edema, along with the secretion of a multitude of cells and growth factors. This initial response is crucial for proper repair, as removal of the hematoma (especially days post-injury) led to impaired fracture healing in a rat model [115]. The highly regulated cascade of cytokines that constitute the acute inflammatory response subsequently participate in instructing the bone healing process [116-118]. Bone injury results in the expression of a wide array of pro-inflammatory cytokines, which, along with many growth factors, particularly those from the transforming growth factor-beta (TGF-β) super family, result in inflammatory cell migration, angiogenesis, and mesenchymal stem cell (MSC) migration and differentiation [119-121]. For example, signaling molecules such as interleukin-6 (IL-6), tumor necrosis factor alpha (TNF-α), and stromal cell-derived factor-1 (SDF-1) promote MSC migration *in vivo* [92, 122-124]. Osteoprogenitor cells secrete BMPs [25, 119], which together with inflammatory cytokines further enhance MSC migration, proliferation, and differentiation [125-127]. Although levels of pro-inflammatory modulators are minimal during the subsequent proliferative/repair phase, their expression increases again during bone remodeling, when osteoblasts secrete IL-1, IL-6, IL-11, and other factors that promote osteoclastogenesis [127]. At this point, osteoblasts and chondrocytes become the main source of pro-inflammatory factors [120].

Typically, inflammatory cytokine expression levels return to baseline approximately one week post-injury [119-121]. In particular, MSCs have been found to play an immunomodulatory role during fracture healing [128]. However, the normal inflammatory response can be perturbed by factors such as trauma or disease [129, 130], and a significant

contributor to delayed bone healing or eventual non-union is an unresolved inflammatory response. For example, heightened and prolonged inflammation was associated with impaired bone healing in a sheep osteotomy model [131]. Although the pro-inflammatory cytokines IL-6 and TNF-α were found to be necessary for bone healing in murine models [132, 133], prolonged exposure to these molecules was associated with impaired bone volume and function [134-136]. Osteoinductive factors such as BMP-2 also play key roles in many signaling pathways related to inflammation. BMP-2 induces chemotaxis of inflammatory cells, namely lymphocytes, monocytes, and macrophages [137]. Additionally, BMP-2 supports osteoclast survival and differentiation through the enhancement of RANKL [138, 139]. Recently, Lee et al. determined that BMP-2 and BMP-7 induced an increase in IL-6 production in human promonocytic leukemia THP-1 cells over cells incubated with lipopolysaccharide alone, suggesting BMPs may have a more direct role in promoting inflammation [108].

Heterotopic Ossification

Heterotopic ossification is the process whereby bone formation occurs in nonosseous tissue, often causing pain and impaired mobility. Histologically and biochemically, heterotopic bone "lesions" are indistinguishable from orthotopic bone [140, 141]. The most debilitating form of heterotopic ossification in humans is the rare genetic disorder fibrodysplasia ossificans progressiva (FOP), which is caused by a mutation in a receptor for BMP type-I [142]. More commonly, heterotopic bone forms as a result of trauma such as acetabular or elbow fracture, total hip arthroplasty, burn, or injury to the brain or spinal cord [143]. In particular, heterotopic ossification caused by combat-related injuries has become a more prominent occurrence from military operations in the Middle

East [144]. Treatment options are limited to the removal of heterotopic bone by surgery, but repeated surgeries to debride the tissue have been associated with recurrence of heterotopic ossification. Prophylactic alternatives include radiation therapy and administration of nonsteroidal anti-inflammatory drugs (NSAIDs). Though these can be effective in reducing or preventing heterotopic ossification [145], most combatants who have undergone complex traumatic injuries have multiple contraindications to these treatment options [144].

Regardless of etiology, heterotopic ossification involves a complex coordination of cellular and molecular mechanisms. During heterotopic ossification, connective tissues are presumably replaced by bone tissue through a complex process involving inflammation, muscle cell death, fibrous tissue proliferation, angiogenesis, and ossification (often endochondral) [146]. Expectedly, local tissue environmental factors (e.g., source of BMP stimulus, ability to recruit osteoprogenitor cells and induce their differentiation into bone tissue) play a major role in the extent to which heterotopic ossification occurs [141]. For example, osteogenic genes were upregulated in wounds with heterotopic mineralization compared to wounds without [147]. Despite progress in understanding the role of BMP signaling pathways in heterotopic mineralization, the cells that contribute to the pathology remain under investigation. Due to the proximity of muscle progenitors/myoblasts to bone and their ability to differentiate down the osteogenic lineage when exposed to BMP-2 [148], these cells may contribute directly to heterotopic bone formation. Muscle-derived progenitor cells from wounds that subsequently developed heterotopic bone were present in greater numbers and exhibited increased osteogenic differentiation compared to cells from wounds that did not form heterotopic bone [149]. However, Lounev and colleagues, using two mouse models involving intramuscular BMP-2 injection or muscle injury via cardiotoxin injection, found that muscle satellite cells comprised a very minimal portion of the

heterotopic bone, while endothelial precursor cells contributed significantly to all three stages of heterotopic ossification (fibroproliferative, chondrogenic, and osteogenic) [150]. Furthermore, their findings suggested both dysregulation of BMP signaling and an inflammatory environment are necessary for heterotopic ossification to occur. Inflammatory cells of hematopoietic origin have been shown to contribute to heterotopic ossification [151, 152]. Moreover, elevated levels of inflammatory cytokines both locally and systemically were associated with the development of heterotopic mineralization following combat injury [153], suggesting that local and circulating factors play a role in heterotopic bone deposition.

III. OXIDIZED ALGINATE FOR BMP-2 DELIVERY[3]

3.1 Abstract

Autograft treatment of large bone defects and fracture non-unions is complicated by limited tissue availability and donor site morbidity. Polymeric biomaterials such as alginate hydrogels provide an attractive tissue engineering alternative due to their biocompatibility, injectability, and tunable degradation rates. Irradiated RGD-alginate hydrogels have been used to deliver proteins such as bone morphogenetic protein-2 (BMP-2), to promote bone regeneration and restoration of function in a critically sized rat femoral defect model. However, slow degradation of irradiated alginate hydrogels may impede integration and remodeling of the regenerated bone to its native architecture. Oxidation of alginate has been used to enhance the degradation of alginate matrices. The *objective* of this study was to evaluate the effects of alginate oxidation on BMP-2 release and bone regeneration. We *hypothesized* that oxidized-irradiated alginate hydrogels would elicit an accelerated release of BMP-2, but degrade faster *in vivo*, facilitating the formation of higher quality, more mature bone compared to irradiated alginate. Indeed, oxidation of irradiated alginate did accelerate *in vitro* BMP-2 release. Notably, the BMP-2 retained within both constructs was bioactive at 26 days, as observed by induction of alkaline phosphatase activity and positive Alizarin Red S staining of MC3T3-E1 cells. From the *in vivo* study, robust bone regeneration was observed in both groups through 12 weeks by radiography, micro-computed tomography analyses,

---

[1] Portions of this chapter were adapted from Priddy L B, Chaudhuri O, Stevens H Y, Krishnan L, Uhrig B A, Willett N J, Guldberg R E. Oxidized alginate hydrogels for bone morphogenetic protein-2 delivery in long bone defects. *Acta Biomaterialia*, 10(10), 4390-4399, 2014. License No. 3603720780456

and biomechanical testing. Bone mineral density was significantly greater for the oxidized-irradiated alginate group at 8 weeks. Histological analyses of bone defects revealed enhanced degradation of oxidized-irradiated alginate and suggested the presence of more mature bone after 12 weeks of healing.

3.2 Introduction

Alginate hydrogels have been used as delivery vehicles for a multitude of proteins, including BMP-2 [33, 34, 154, 155]. Alginate is a polysaccharide derived from algae that exhibits minimal binding interactions with cells and can be ionically crosslinked into hydrogels using divalent cations such as calcium [156]. Alginate does not degrade enzymatically [34], but alginate hydrogels can degrade slowly due to dissociation of the ionic crosslinks [157]. Scaffold degradation is a crucial regulator of not only growth factor release but also extracellular matrix deposition [46]. Ideally, as the scaffold degrades, space for new bone is created. As such, the rate of scaffold degradation should be similar to the rate of new tissue formation to allow for successful coalescence of the newly formed bone. In the case of alginate, various modification techniques, including gamma-irradiation and partial oxidation, have been utilized to enhance degradation of the scaffold [37, 43-45, 158].

Gamma-irradiation lowers the molecular weight of the alginate polymer chains, allowing the polymers to more readily dissociate from the alginate matrix [37]. Previously, irradiated alginate led to improved cellular infiltration and tissue healing compared to unmodified alginate [34, 37]. Irradiated alginate hydrogels have been used to deliver proteins such as BMP-2 and facilitated functional regeneration in our critically sized rat femoral segmental defect model [38-41]. In previous subcutaneous implant studies, irradiation of the alginate led to enhanced tissue infiltration, bone architecture, and bone area fraction [34, 37],

as well as greater mineral density and extent of alginate degradation [37] compared to unmodified alginate.

Partial oxidation—whereby a small percentage of the uronate residues are oxidized—allows the polymer chains to be more susceptible to hydrolysis and increases the degradation rate *in vitro* [43-45, 158]. Unlike the degradation of unmodified alginate, oxidized alginate breakdown occurs primarily via hydrolysis, specifically at the oxidized sugar residues [43]. Oxidation of the alginate creates a more open-chain structure while maintaining the ionic cross-linking capacity [44] and biocompatibility of the alginate [43]. In previous work, oxidized alginate hydrogels served as a carrier for chondrocytes [44] and growth factors (BMP-2 and TGF-β3) [158], and in both studies facilitated an increase in cellular infiltration and matrix formation subcutaneously compared to unmodified alginate. Additionally, oxidized alginate hydrogels loaded with vascular endothelial growth factor (VEGF) mitigated tissue loss in a mouse hind limb ischemia model [45]. Oxidized-irradiated alginate hydrogels were used recently for adipose stem cell delivery, promoting the formation of new adipose tissue subcutaneously [159]. In the present study, we utilized this same alginate modified by both irradiation and oxidation—i.e., a lower molecular weight and hydrolytically degradable alginate—as a growth factor delivery system for bone tissue engineering in an orthotopic model.

In our rat segmental defect model, irradiated alginate hydrogel surrounded by a PCL nanofiber mesh provided a more sustained release of BMP-2 and augmented bone regeneration compared to the clinically-used collagen sponge [39, 40]. However, a portion of the alginate material was shown to persist at 30 weeks and may have hindered functional remodeling of the newly formed bone tissue [42]. The interplay between carrier degradation, growth factor availability, and tissue ingrowth remains poorly understood. With these design

parameters in mind, this work evaluated the regenerative capacity of an oxidized-irradiated alginate hydrogel as a delivery vehicle for BMP-2 in a well-established rat long bone defect model. The *objectives* of the study were: (i) to compare BMP-2 release and bioactivity from irradiated alginate and oxidized-irradiated alginate, and (ii) to evaluate bone regeneration, alginate degradation, and quality of regenerated bone *in vivo* using these two alginate formulations. We *hypothesized* that the oxidized-irradiated alginate hydrogels would elicit an accelerated release of BMP-2, but degrade faster *in vivo*, facilitating the formation of higher quality, more mature bone.

3.3 Materials and Methods

Alginate hydrogel preparation

Sodium alginate rich in guluronic acid blocks (MVG alginate, FMC BioPolymer) was used for all experiments. A low molecular weight alginate formulation was made by treating MVG alginate with gamma-irradiation, reducing its molecular weight from ~250 kDa to ~50 kDa [45]. For preparation of the oxidized-irradiated alginate, irradiated alginate was exposed to sodium periodate, resulting in ~1% oxidation of the uronate residues and creating a hydrolytically labile polymer [44]. The alginates were functionalized with RGD peptide sequences (2 sequences per polymer chain) [37] to promote cell adhesion. Alginates were reconstituted in alpha-Minimum Essential Medium (αMEM, Gibco) and mixed with recombinant human BMP-2 (rhBMP-2, R&D Systems) in 0.1% rat serum albumin (RSA, Sigma). Hydrogels (2% (w/v) alginate) were prepared by mixing the alginate+rhBMP-2 solution with calcium sulfate slurry (0.21 g/mL) at a ratio of 25:1 [40]. All hydrogels were incubated at room temperature for 30 minutes before further manipulation. Hydrogels used for *in vivo* delivery were stored at 4°C overnight.

Nanofiber mesh production

Nanofiber meshes were fabricated as previously described [40]. Briefly, poly(ε-caprolactone) (PCL) was dissolved in a 90:10 volume ratio of hexafluoro-2-propanol:dimethylformamide (Sigma-Aldrich) to a 12% (w/v) concentration. The solution (5 mL) was electrospun onto a static collector plate for 5-6 hours. Using a VLS3.50 laser cutter (Universal Laser Systems) and CorelDRAW software, PCL sheets were cut into 12x19-mm rectangles, each with 24 1-mm diameter perforations, and rolled to form tubes 4.5 mm in diameter and 12 mm in length. Meshes were sterilized by ethanol evaporation overnight, rinsed three times in phosphate buffered saline (PBS, Cellgro), and stored in PBS. The meshes used *in vivo* were transferred to αMEM approximately 12 hours before surgery.

rhBMP-2 release kinetics

To investigate the release kinetics of BMP-2, 2% (w/v) alginate hydrogels (n=8) containing 500 ng rhBMP-2 per 150 μL were injected into PCL nanofiber meshes and incubated at 37°C in 1 mL PBS, as previously described [40]. PBS was collected and replaced at 3 and 15 hours, and at 1, 2, 3, 5, 8, 14, and 26 days. The BMP-2 remaining in the constructs at 26 days was then eluted by rinsing vigorously with PBS. The BMP-2 not removed by PBS rinsing was eluted by incubation with 1 mL 0.1% sodium dodecyl sulfate (SDS) on a rocker plate for 1 hour. SDS was removed from solution by an SDS-Out™ Precipitation Kit (Thermo Scientific). The BMP-2 in solution was quantified using an enzyme-linked immunosorbent assay (ELISA, R&D Systems) according to the manufacturer's protocol.

Using least-squares nonlinear regression analysis (SigmaPlot 11.0), the data of BMP-2 retained in the constructs was fit to a three-term exponential decay function of the form

$$y(t) = a * \exp^{-\lambda t} + c$$

where y is the percentage of BMP-2 retained in the constructs at time t, λ is the decay constant, or rate of decay, a+c is the initial value of y (100% at t=0), and the function is asymptotic to y=c ($t \rightarrow \infty$).

Alkaline phosphatase induction assay

The bioactivity of released and retained BMP-2 was determined using an alkaline phosphatase (ALP) induction assay [160] (n=6–7). Mouse clonal pre-osteoblasts (MC3T3-E1s, American Type Culture Collection) were seeded in 96-well plates at a density of 62,500 cells/cm^2 and incubated at 37°C, 5% CO_2 in αMEM with 20% fetal bovine serum (FBS, Atlanta Biologicals) and 1% penicillin-streptomycin-L-glutamine (PSL, Invitrogen) for 6 hours. Media was then replaced with a 1:1 volume ratio (200 μL total) of: (i) αMEM with 2% FBS and 0.2% ascorbic acid 2-phosphate (AA2P); and (ii) PBS containing released BMP-2 collected at 3 and 15 hours, and 1, 2, 3, and 5 days—or PBS/SDS containing BMP-2 remaining in the constructs at 26 days (all samples in triplicate). As a positive control, 20 ng BMP-2 in PBS was used. Wells without BMP-2 served as a negative control. After 3 days of culture, MC3T3s were washed 3 times with Hank's Buffered Salt Solution (HBSS, Thermo Scientific), fixed in 2% paraformaldehyde in 0.1 M sodium phosphate buffer for 10 minutes, and washed 3 times with sodium phosphate buffer (pH 7.4) for 3 minutes. MC3T3s were incubated with 100 μL/well of 7.6 mM p-Nitrophenyl Phosphate (p-NPP) in 50 mM Tris/HCl (pH 10.3) for 10 minutes at 37°C. The reaction was terminated by the addition of 100 μL/well of 0.2 M NaOH, and the absorbance was read at 405 nm using a microplate spectrophotometer (PowerWave X5, Gen5 Software; Biotek Instruments, Inc.). Absorbance values were converted to ALP activity (nmol/hr) using the linear relationship between p-NP

standards (0-800 nmol/mL) and absorbance. Subsequently, mineralization in the MC3T3 cultures was observed by staining with Alizarin Red S.

Surgical procedure

Bilateral critically sized femoral segmental defects were created in 13-week-old female SASCO Sprague-Dawley rats (Charles River Laboratories) as previously described [38, 41]. Briefly, a radiolucent polysulfone fixation plate was affixed to the femur for limb stabilization, and an 8-mm defect was created in the mid-diaphysis of the femur. The defect was enclosed with a PCL nanofiber mesh and treated with 2 μg rhBMP-2 in 150 μL of irradiated alginate hydrogel or oxidized-irradiated alginate hydrogel (n=8). It was determined previously that 2 μg of rhBMP-2 promoted consistent bridging of the defects [39]. Subcutaneous injection of slow-release buprenorphine (Wildlife Pharmaceuticals) was provided for analgesia before surgery. Animals were euthanized by CO_2 inhalation at 12 weeks post-surgery. All procedures were approved by the Georgia Institute of Technology Institutional Animal Care and Use Committee (IACUC).

Radiography and micro-computed tomography

Bone regeneration was assessed qualitatively via radiography (Faxitron MX-20 Digital, Faxitron X-ray Corp.) at 2, 4, 8, and 12 weeks post-operatively. New bone formation was quantified by micro-computed tomography (micro-CT; Viva-CT 40, Scanco Medical) at 4, 8, and 12 weeks after surgery. The bone defect regions were scanned at medium resolution with a 38.9 μm voxel size, a voltage of 55 kVp, and a current of 145 μA. The volume of interest (VOI) for evaluation comprised the central 168 slices, or about 6.4 mm of the 8-mm defect region. A global threshold of 408 mg hydroxyapatite/cm^3, corresponding to approximately 50% of the density of the native cortical bone, was applied to segment bone tissue. Noise was suppressed using a Gaussian filter (sigma = 1.2, support = 1).

Biomechanical testing

Torsional tests to failure were performed on femora (n=5) after harvest at 12 weeks post-surgery as previously described [41]. Briefly, the fixation plate was removed, the surrounding soft tissue was excised, and the native bone ends were potted in Wood's metal (Alfa Aesar). Femora were displaced at 3° per second to failure (ELF 3200; Bose ElectroForce Systems Group). Maximum torque, toughness (energy to failure), and torsional stiffness (linear region of the torque-rotation curve) were calculated for each sample.

Histological analyses

Histology was conducted on femora at 12 weeks (n=3) to identify newly formed bone and residual alginate within the defect region. Upon harvesting, femora were fixed with 10% neutral buffered formalin for 48 hours and decalcified under gentle agitation in a formic acid solution (Cal-ExII, Fisher Scientific), which was changed three times per week for two weeks. After paraffin processing, 5-μm mid-sagittal sections were cut and stained with hematoxylin and eosin (H&E), Safranin O (for alginate) and Fast green (for tissue infiltration) [39], Masson's trichrome (for bone) [109, 161], or Picrosirius red (for lamellar bone) [161]. Safranin O stained sections viewed by bright field microscopy were used for area quantification of alginate. The carboxyl groups in the alginate polymer contribute to its negative charge, which allows for staining with Safranin O [162, 163]. Although Safranin O also stains cartilage, chondrocytes are easily distinguishable from densely stained, acellular alginate. Picrosirius red stained sections were used for highlighting organized, lamellar bone under polarized light. The highly organized collagen of the native bone ends appeared green/yellow, so these colors were used to select mature, lamellar bone within the defect region [161]. For three consecutive sections per sample, five low magnification (10x) images from comparable areas within the bone defect region were used for automated image

analysis, for a total of 15 images per sample. The location of each image was determined using the nanofiber mesh (which bordered the defect on both sides) as a marker. Image locations were as follows: top left corner of defect, bottom right corner of defect, and three central images distributed equally along the vertical length of the defect.

A custom MATLAB script (MATLAB 7.11.0 (R2010b)) was employed for automated and unbiased measurements on 10x magnification images (15 per sample, n=3) of de-identified sections. For images from Safranin O stained sections, areas of alginate (red), tissue (blue), and background (white) were identified by converting the images to HSV (Hue, Saturation, Value) color space [164]. The indices of the color areas were used to create a binary representation from which the areas of the image occupied by the red stained alginate, blue stained bone and fibrous tissue, and white backgrounds were estimated. For analysis of each image, red alginate areas were calculated as percentages of total area and binned from 0-100%. Alginate pieces constituting less than 1% of the total stained area were considered noise and excluded from analysis. This representation provided a comparison of the relative sizes of the residual alginate aggregates and served as a measure of alginate breakdown/fragmentation.

Similarly, for Picrosirius red stained images, the white colored tissue loci were demarcated by converting the image to YUV (luma and chrominance) and HSV color spaces. Subsequently, the original image, converted to HSV space, was used to identify loci of green/yellow color. Binary representations were built to calculate the relative areas of the respective colors. Additionally, a 50-pixel connectivity size filter (1.6 pixels/μm) was used to identify the larger contiguous areas in the green/yellow area binary representation. Mature, lamellar bone (green/yellow) area was calculated as a percentage of total stained area for

each image. For a more detailed description of histomorphometric analysis methods, see Appendix A.1.

Statistical analyses

All data were analyzed in GraphPad Prism 5 (GraphPad Software, Inc.) and reported as mean ± standard error of the mean (SEM). Two-way repeated measures analysis of variance (ANOVA) was performed on cumulative BMP-2 release. Decay constant and BMP-2 recovered from the constructs at 26 days were analyzed via t-tests. ALP activity of cells treated with released BMP-2 was evaluated using two-way ANOVA, while ALP activity of cells treated with construct-bound BMP-2 was performed by one-way ANOVA. Micro-CT parameters were evaluated using two-way repeated measures ANOVAs. For each ANOVA, a Bonferroni post-hoc test for pairwise comparisons was performed. Paired t-tests were performed on biomechanical data to evaluate differences between the two alginate formulations, while comparison to intact femora required additional (unpaired) t-tests. Histomorphometry of alginate area and lamellar bone area were analyzed by t-tests. A *p*-value less than 0.05 was considered statistically significant.

3.4 Results

rhBMP-2 release kinetics

The release of BMP-2 from irradiated and oxidized-irradiated alginate hydrogels loaded with 500 ng BMP-2 was assessed over 26 days. An initial burst release of BMP-2 from both alginate types was observed (Figure 1A). Cumulative release was significantly greater for oxidized-irradiated alginate at days 2 and 3 ($p<0.05$). However, by day 5 these differences were no longer significant. Of the BMP-2 that was released (~20% of loaded), more than 95% was released by day 3 and day 8 for the oxidized-irradiated and irradiated alginates, respectively. The BMP-2 release data was also expressed as percent retained in the

constructs through 26 days, and was fit to a three-term exponential decay function (Figure 1B) to determine the decay constant, or rate of decay λ. The decay constant was significantly greater for the oxidized-irradiated alginate hydrogels ($p<0.05$) (Figure 1C).

Approximately 35% of the loaded BMP-2 remained in the constructs at 26 days as measured by vigorous washing with PBS and SDS (Figure 1D). A larger portion of the construct-bound BMP-2 was eluted during rinsing with PBS (~30% of loaded), as compared to the BMP-2 obtained from the SDS wash (~5% of loaded). In a separate experiment after 3 weeks incubation with 500 ng BMP-2, significantly more BMP-2 was recovered from hybrid constructs (alginate+mesh) compared to either component alone (Figure 2), suggesting both components of the delivery system were necessary for prolonged binding of BMP-2.

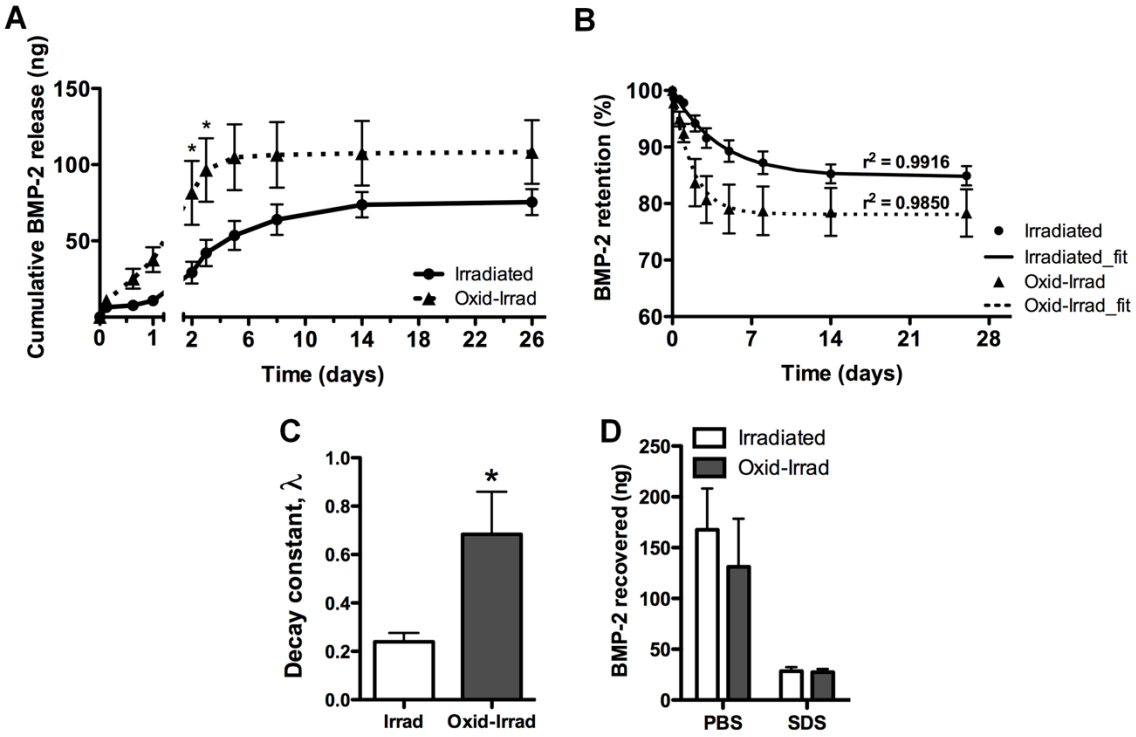

Figure 1. Released and retained BMP-2. (A) Release kinetics of BMP-2 from alginate gels. Significantly more BMP-2 had been released from oxidized-irradiated alginate at days 2 and 3 (*$p<0.05$). (B) Percentages of BMP-2 retained in the constructs over time were fit to exponential decay functions (denoted by _fit). (C) Decay constant λ was significantly greater for the oxidized-irradiated alginate (*$p<0.05$). (D) Approximately 35% of the BMP-2 was recovered from the constructs at 26 days.

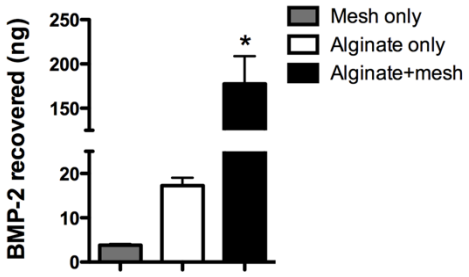

Figure 2. BMP-2 retained in PCL mesh and alginate. After 3 weeks in culture with 500 ng of BMP-2 initially, minimal BMP-2 remained in nanofiber mesh constructs (BMP-2 added to media) and alginate constructs (BMP-2 incorporated into hydrogel) compared to alginate+mesh constructs (*$p<0.01$).

Alkaline phosphatase induction assay

Levels of ALP activity, an early marker of osteoblastic differentiation, were examined to evaluate the functional ability of the released BMP-2 to induce mineralization in MC3T3-E1 cells after 3 days of culture. ALP activity was significantly enhanced for cells treated with BMP-2 released through 1 day for the irradiated group and through 15 hours for the oxidized-irradiated group compared to the negative control (no BMP-2) ($p<0.05$) (Figure 3A). BMP-2 released at 1 day from irradiated alginate elicited significantly higher ALP activity compared to the oxidized-irradiated group at that time point ($p<0.05$). ALP activities after day 1 were negligible. Although minimal BMP-2 was released after 8 days, BMP-2 remaining in both constructs at 26 days (obtained from PBS rinse) was bioactive, as indicated by ALP activity significantly greater than the negative control (Figure 3B). Minimal ALP activity was measured by the subsequent SDS wash (data not shown). Alizarin Red S staining of calcium deposits in these same MC3T3 cultures treated with PBS/BMP-2 retained in the constructs at 26 days served as further evidence of BMP-2 bioactivity (Figure 3C, D).

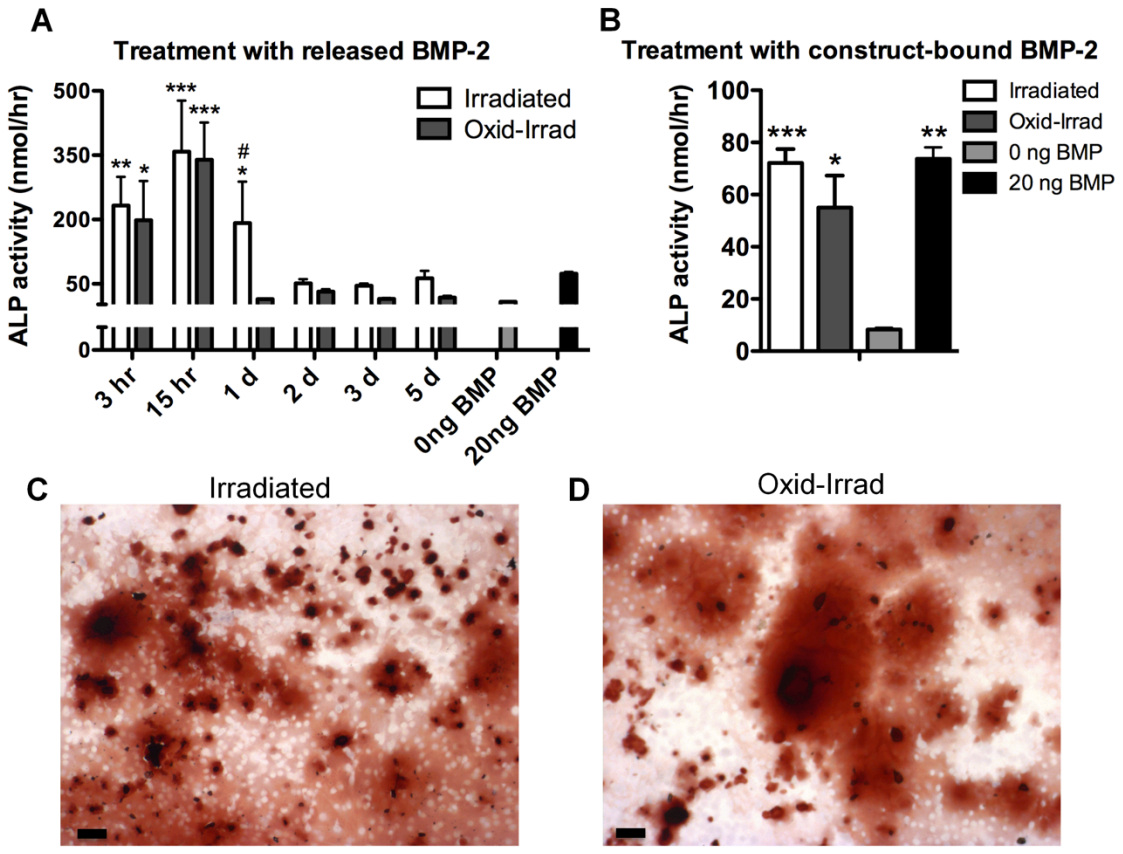

Figure 3. Bioactivity of released and retained BMP-2. (A) ALP activity was highest for MC3T3-E1 cells incubated with PBS/BMP-2 collected at 15 hr. Bioactivity of BMP-2 released from irradiated hydrogels through 1 day, and from oxidized-irradiated hydrogels through 15 hr, was significantly greater than the negative control (***$p<0.001$, **$p<0.01$, *$p<0.05$). BMP-2 released from irradiated alginate at 1 day showed significantly higher ALP activity than BMP-2 from oxidized-irradiated alginate at the same time point (#$p<0.05$). (B) BMP-2 remaining in the constructs at 26 days was bioactive, as all groups were significantly greater than the negative control. (C-D) Alizarin Red S staining of calcium deposits in MC3T3 cultures treated with BMP-2 retained in the constructs at 26 days. Scale bar = 100 μm.

Radiography and micro-computed tomography

The *in vivo* comparison of bone regeneration with 2 μg BMP-2 in the two alginate formulations indicated similar, robust bone formation from radiographs and micro-CT. Radiographs at 2, 4, 8, and 12 weeks post-surgery revealed comparable bone formation for the irradiated alginate and oxidized-irradiated alginate groups (Figure 4). For both groups, 7

of 8 defects showed bridging of the defect site by 4 weeks, and all 8 defects were bridged by 8 weeks, as is typical with this model and dose of BMP-2.

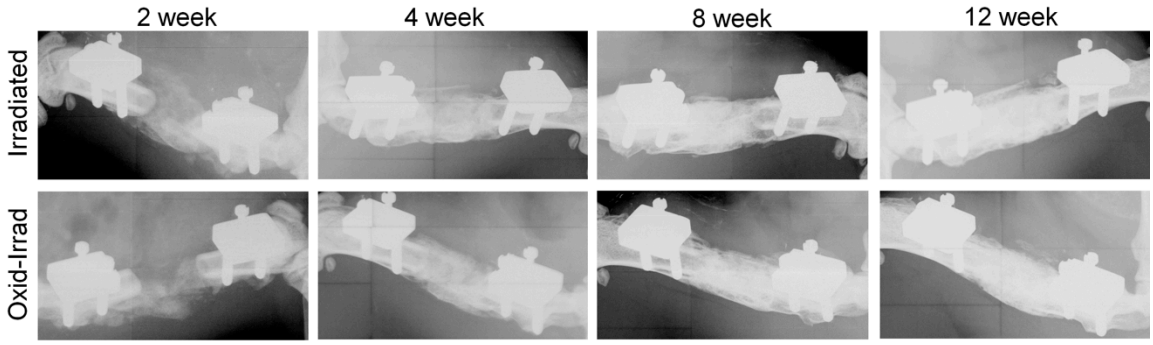

Figure 4. Longitudinal radiographs of bone regeneration. Representative radiographs of defects treated with BMP-2 in irradiated alginate (top) or oxidized-irradiated alginate (bottom) at 2, 4, 8, and 12 weeks post-operatively. All defects showed complete bridging by 8 weeks.

Micro-CT data at 4, 8, and 12 weeks post-surgery were consistent with the results from radiography. Bone volume increased over the course of the study for both groups but was not significantly different between the two groups at any time point (Figure 5A). Bone mineral density (BMD) at 8 weeks was significantly greater in the oxidized-irradiated alginate group ($p<0.05$, Figure 5B). The spatial distribution of BMD in a mid-sagittal slice within the defect region further demonstrated this difference at 8 weeks (Figure 5C). By 12 weeks, however, these differences were no longer significant.

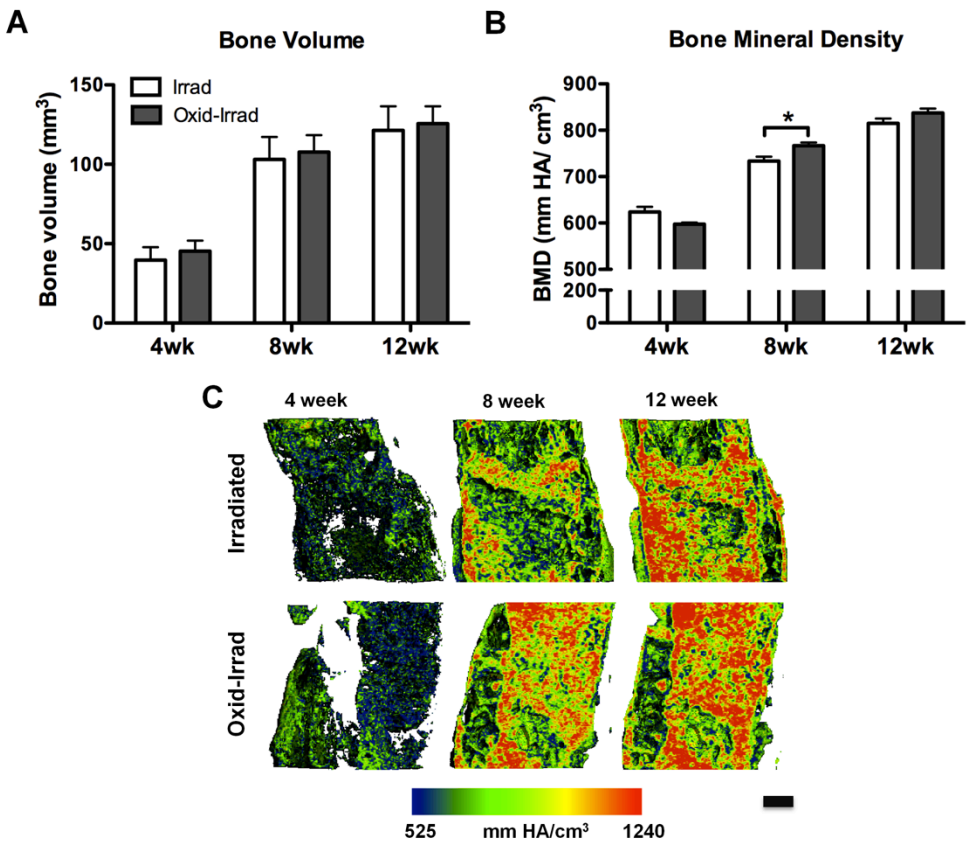

Figure 5. Bone volume and mineral density over time. (A) Bone volume increased over time, but no differences were observed between groups. (B) Bone mineral density (BMD) also increased over time for both groups and was significantly greater in the oxidized-irradiated alginate group at 8 weeks (*$p<0.05$). (C) Density mapping of mid-sagittal cross-sections of newly formed bone in the central defect region further illustrated this higher density at 8 weeks in the oxidized-irradiated alginate group. Scale bar = 1 mm.

Biomechanical testing

Torsional testing to failure provided a measure of functional recovery of the newly regenerated bone at 12 weeks post-surgery. Data were also compared to historical data of age-matched, intact femora [40]. Maximum torque at failure was significantly attenuated in the irradiated alginate group compared to intact controls ($p<0.05$), while max torque for the oxidized-irradiated group was statistically equivalent to the irradiated group and control bone (Figure 6A). Toughness, or area under the torque-rotation curve to failure, was not different

between groups (Figure 6B). Torsional stiffness was similar between groups and significantly greater than intact controls for both groups ($p<0.01$, Figure 6C).

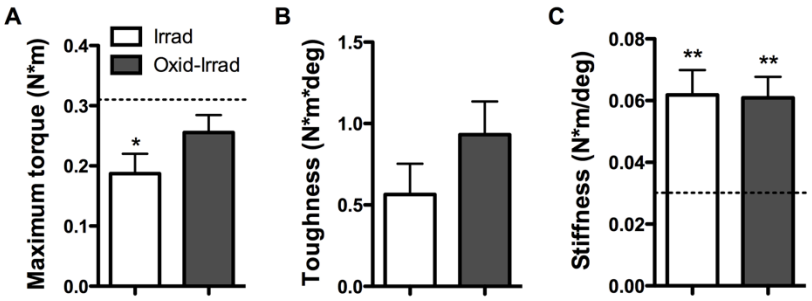

Figure 6. Biomechanical properties of regenerated bone tissue. Functional assessment of the regenerated bone at 12 weeks. Dashed lines indicate mean values for historical naïve intact control bone [40]. (A) Maximum torque to failure was not significantly different between test groups. However, max torque for the irradiated alginate group was significantly lower than intact controls (*$p<0.05$). (B) Toughness, or energy to failure, was not different between groups. (C) Torsional stiffness for both groups was significantly greater than intact controls (**$p<0.01$).

Histological analyses

Hematoxylin and eosin (H&E) staining of new bone (pink) and residual alginate (purple) showed distinct areas of bone and alginate in the irradiated group (Figure 7A), and co-localization of bone and alginate in the oxidized-irradiated group (Figure 7B). Masson's trichrome staining revealed bone tissue (red) within the defect region (Figure 7C-D). The presence of globular fatty cells and marrow-like structures observed with both stains was indicative of physiological bone regeneration.

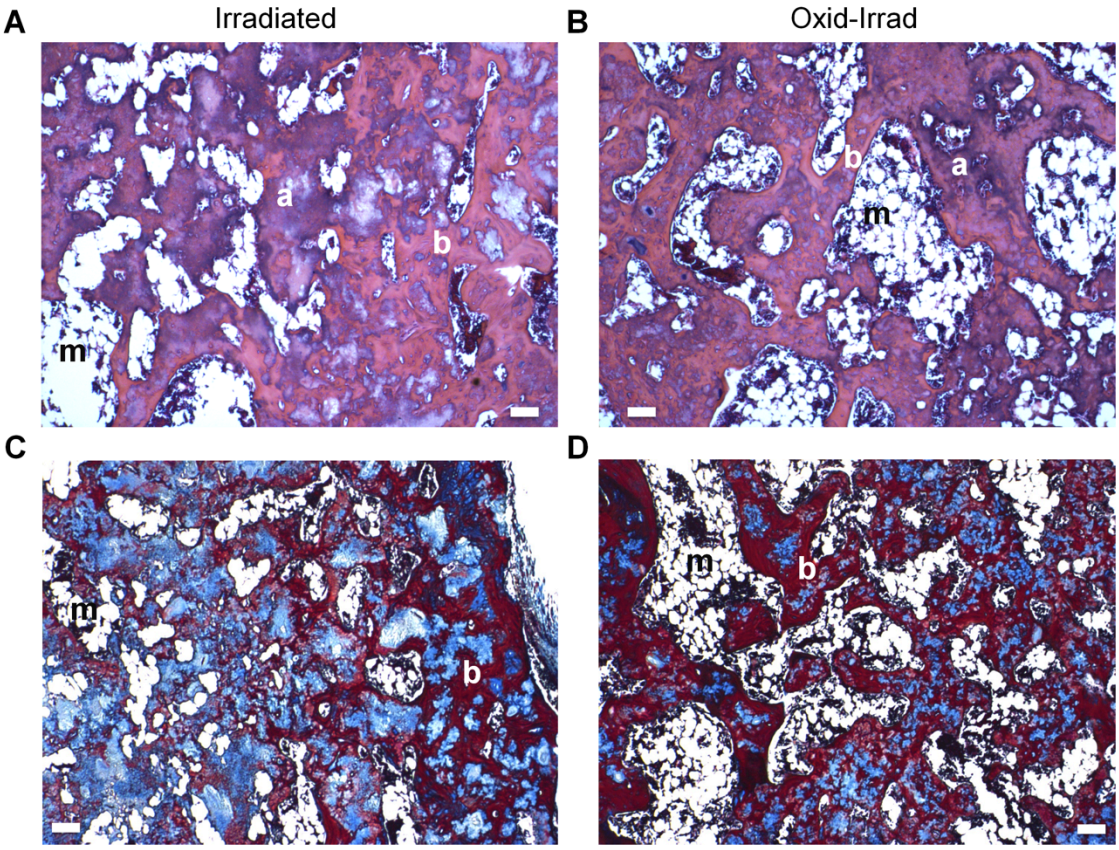

Figure 7. 12 week histology of mid-sagittal sections of bone defect tissue. (A, B) H&E staining revealed areas of new bone (pink, b) and residual alginate (purple, a), which appeared more interspersed/co-localized in the oxidized-irradiated group. (C, D) From Masson's trichrome staining, bone tissue stained red (b). (A-D) Globular, marrow-like structures (m) suggested physiological bone healing. Scale bar = 100 μm.

Safranin O staining of the defect regions distinguished infiltrating bone tissue (blue) and residual alginate (red acellular areas) (Figure 8A). Notably, no chondrocytes were present in the bone defect region. Although a considerable amount of both alginate types remained in the defect area, the oxidized-irradiated alginate was more diffuse and fragmented than the residual irradiated alginate. Histomorphometry was used to quantify residual alginate as a percentage of total image area. The number of alginate pieces comprising 1-10% area was greater for the oxidized-irradiated group. However, the average count of larger alginate pieces (>10% area) was significantly higher for the irradiated alginate group ($p<0.05$, Figure

8B). Collectively, irradiated alginate occupied ~40% of total image area, while oxidized-irradiated alginate occupied ~30% (Figure 8C).

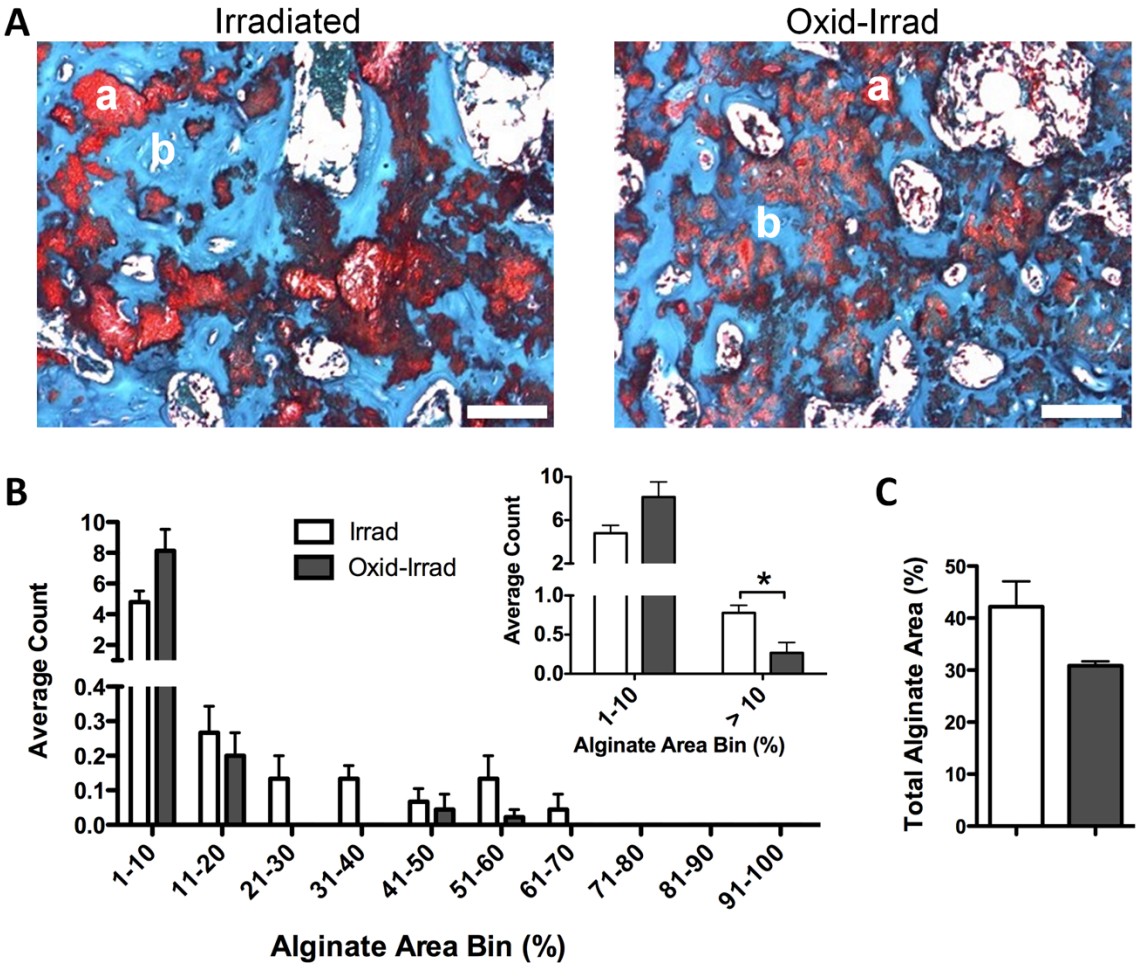

Figure 8. Histomorphometry of alginate in 12 week bone defect samples. (A) Alginate stained red (a) and newly formed bone stained blue (b) with Safranin O. Residual oxidized-irradiated alginate was more diffuse and fragmented than irradiated alginate. (B) Frequency distribution of percent area of alginate pieces. Significantly more large (>10%) irradiated alginate pieces remained (*$p<0.05$). (C) Overall, irradiated alginate occupied ~40% of total area, while oxidized-irradiated comprised ~30%, although these differences were not statistically significant ($p=0.0831$). Scale bar = 100 μm.

Picrosirius red staining highlighted birefringent collagen under polarized light (Figure 9A). While most of the collagen in the irradiated group was poorly organized woven bone, the oxidized-irradiated group appeared to contain more organized, lamellar bone (bright green/yellow). In both groups, woven bone (red) had formed in the available space created

by degraded alginate and had integrated with the residual alginate. From histomorphometric analysis, lamellar bone area as a percentage of total stained area was statistically equivalent between groups (Figure 9B).

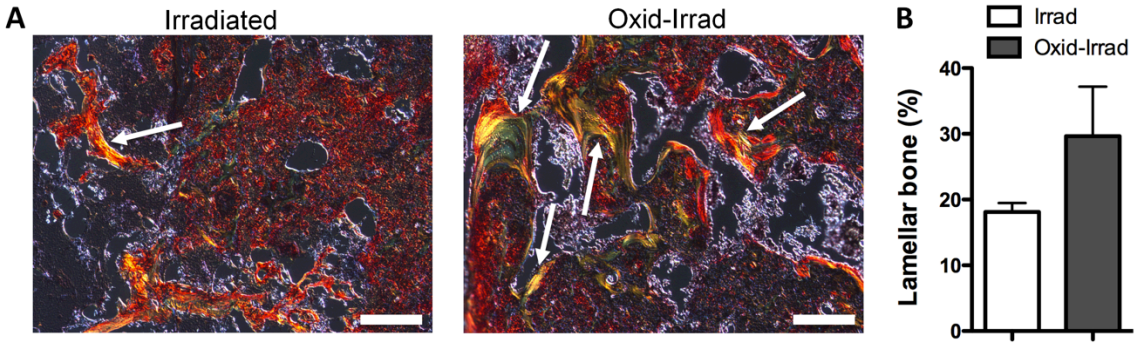

Figure 9. Histomorphometry of lamellar bone in 12 week bone defect samples. (A) Picrosiruis red staining viewed under polarized light highlighted organized, lamellar bone (bright green/yellow, arrows), which appeared more abundant in the oxidized-irradiated alginate group. (B) Quantification of lamellar bone as a percentage of stained area. Scale bar = 100 μm.

3.5 Discussion

Irradiated alginate has previously been used to deliver BMP-2 in our critically sized rat bone defect model, facilitating enhanced bone regeneration over the clinically used collagen sponge [39, 165]. However, a portion of the alginate material remained in the defect beyond the typical 12-week time course of healing. Since bone tissue formation and remodeling may be impeded by the presence of residual biomaterial at the injury site, understanding the timelines of protein release and biomaterial degradation is crucial for complete restoration of the form and function of bone tissue. In introducing oxidation as an additional structural modification of the alginate, the goal was to maintain the appropriate functionality (e.g., biocompatibility and injectability) of the irradiated alginate, while accelerating alginate degradation to augment bone tissue formation and maturation. In this work, an oxidized-irradiated alginate hydrogel served as an effective carrier for BMP-2 in a

critically sized segmental bone defect model, transiently improving mineral density of the bone tissue and enhancing alginate degradation at 12 weeks compared to a BMP-2-loaded irradiated alginate hydrogel.

In contrast to the relatively uncontrolled release of growth factors from unmodified, non-degradable alginate, which relies primarily on diffusion, growth factor release from irradiated and oxidized alginate hydrogels is accelerated by degradation of the alginate matrix [44]. Previous work has employed irradiation and oxidation as methods to modify alginate to allow for more tunable protein release kinetics, and the effects of varying the degree of alginate modification have been thoroughly examined [37, 43, 45]. In this work, the release of BMP-2 from oxidized-irradiated alginate was accelerated compared to that from irradiated alginate, as measured by a larger decay constant (rate of release) for the oxidized-irradiated group. Others have observed a similar difference in release profiles of VEGF from oxidized-irradiated alginate compared to irradiated alginate [45]. However, the accelerated release (greater amount at early time points) of BMP-2 from oxidized-irradiated alginate did not translate to an increase in ALP activity for pre-osteoblasts *in vitro*. Furthermore, beyond day 1, ALP activity for BMP-2 released from both alginate types was negligible, suggesting that released BMP-2 did not maintain its bioactivity *in vitro*. ALP activity normalized to protein content revealed similar relationships between the groups (data not shown). The discrepancy between the ELISA and ALP results might be attributed to partial denaturation or misfolding of the protein once released, such that a portion of the BMP-2 was detected by ELISA but was not bioactive. Nonetheless, a burst release followed by minimal release of BMP-2 was observed from both alginates. Previously, *in vivo* BMP-2 release was tracked in our segmental defect model, and only ~10% of the protein remained at 21 days [39]. While Jeon et al. measured an increase in bone volume from a slow, sustained release of BMP-2

[166], others reported improved bone healing when an initial burst release was followed by a smaller sustained release [39, 167, 168].

Although minimal amounts of BMP-2 were released from both alginate types after one week (as seen previously with irradiated alginate [40]), approximately one-third of the loaded BMP-2 remained bound to the alginate/PCL nanofiber mesh constructs and was bioactive through 26 days. The bioactivity of the bound BMP-2 may have been prolonged due to retention of the protein within the constructs. Maintenance, and even possible enhancement, of bioactivity of VEGF, another heparin-binding growth factor, has been observed in the presence of alginate [45, 169]. Furthermore, BMP-2 bioactivity has been sustained on the order of weeks using various delivery vehicles, including PCL [170]. However, to our knowledge, this is the first demonstration of prolonged bioactivity of BMP-2 retained within alginate hydrogels, specifically an alginate/PCL mesh carrier. Likely, both the alginate hydrogel and the nanofiber mesh contributed to the binding of BMP-2, as BMP-2 retention was enhanced in the hybrid delivery system compared to both the mesh only and alginate only constructs. However, the precise roles of each are yet to be delineated. The initial PBS wash removed most of the bound BMP-2, which we believe was loosely bound, while the remaining ~5% of loaded BMP-2 was eluted via SDS, which may have been bound more strongly to the mesh. An intermediate wash with sodium citrate (to dissolve the alginate) was performed, resulting in negligible amounts of BMP-2 measured. Alternatively, immediate hydrogel dissolution with sodium citrate at day 0 resulted in recovery of only ~200 ng of BMP-2 (data not shown), so a significant portion of BMP-2 seemed to be lost in the preparation of the hydrogels. In both cases, approximately half of the loaded BMP-2 was accounted for. It is possible that both the initial burst release and the localized retention of BMP-2 in the constructs facilitated bone regeneration, the former by recruiting the initial

wave of osteoprogenitor cells to the defect site, and the latter by influencing the differentiation of osteoprogenitor cells once present within the defect space [168, 171]. Collectively, these findings suggest the bioavailability of BMP-2 for an extended time frame (~weeks) may be required for complete restoration of critically sized bone defects.

The degradation of hydrogels used in bone tissue engineering should ideally act in concert with the formation of new bone, so that by the completion of the regeneration process, only native bone fills the defect space. The increased degradation rate of oxidized alginate hydrogels compared to unmodified alginate hydrogels and irradiated alginate hydrogels has been characterized *in vitro* [43-45]. Qualitatively, the residual oxidized-irradiated alginate in the 12-week bone defect samples alginate appeared further degraded (less densely stained) than the irradiated alginate. Although no differences were observed in total alginate area, significantly fewer large fragments of oxidized-irradiated alginate were present. This difference in size distribution of residual alginate suggested that oxidation of irradiated alginate increased the degree of hydrolytic degradation. The more diffuse and fragmented oxidized-irradiated alginate may have allowed for an increase in cellular infiltration into the defect space, thereby promoting more rapid formation of organized, lamellar bone. Indeed, histomorphometry of lamellar bone area from Picrosirius red staining suggested a trend towards increased formation of lamellar bone in the oxidized-irradiated group. However, the multitude of factors contributing to the degradation of alginate *in vivo* makes understanding the role of each extremely difficult. In particular, a limitation of this work was the analysis of alginate degradation at a single time point (12 weeks); thus, the time course of alginate degradation in an orthotopic model remains unknown.

The breakdown of the oxidized-irradiated alginate may have been accelerated as the material degraded due to greater cellular invasion into the defect space. The well-understood

role of the osteoprogenitor cells is two-fold: (i) secretion of cytokines to recruit additional mesenchymal stem cells and pre-osteoblasts, and (ii) differentiation and production of mineralized matrix, leading to the formation of bony tissue [5]. The cells' ability to deposit matrix relies on the concomitant degradation of the scaffold, creating space for and promoting consolidation of the newly formed bone tissue [37]. In this study, bone mineral density was significantly greater at 8 weeks in the oxidized-irradiated group. However, enhanced fragmentation of oxidized-irradiated alginate did not translate into augmented bone repair, as biomechanical function at 12 weeks was similar between groups. The limited degree of bone remodeling in the rat species and/or the small sample size may have hindered our ability to detect differences in this study, possibly leading to a type II error. Despite the lack of differences in bone healing, we observed robust bone regeneration with both alginate formulations, suggesting early release and local retention of BMP-2 may be an advantageous approach for growth factor delivery.

In conclusion, we observed prolonged bioactivity of BMP-2 at 26 days *in vitro* in both the irradiated and oxidized-irradiated alginate hydrogel/nanofiber mesh delivery systems. The oxidized-irradiated alginate hydrogel carrier for BMP-2 led to augmented mineral density, albeit temporarily, in a critically sized bone defect model. Furthermore, the residual oxidized-irradiated alginate was more diffuse and fragmented relative to the irradiated alginate at 12 weeks *in vivo*, although the hydrogels were not fully degraded at this time point. Thus, scaffold degradation remains a critical design parameter for evaluating the efficacy of growth factor delivery vehicles in tissue engineering.

IV. EFFECTS OF BIOMATERIAL IN HIGH DOSE BMP-2 DELIVERY

4.1 Abstract

Bone morphogenetic protein-2 (BMP-2) delivered on absorbable collagen sponge has shown clinical success in bone healing. However, complications associated with supraphysiological BMP-2 doses including heterotopic mineralization (bone formation in nonosseous tissue) and inflammation often cause pain and impaired mobility. These issues have prompted investigation into improved retention of growth factors for guided bone regeneration. The *objective* of this work was to evaluate the spatiotemporal effects of high dose BMP-2 as a function of delivery vehicle on bone healing. We *hypothesized* that an alginate delivery system would elicit a more localized mineralization pattern compared to the collagen sponge. Release kinetics of BMP-2 *in vitro* were accelerated with collagen sponge compared to alginate constructs. Critically sized rat femoral segmental defects were enclosed with a nanofiber mesh and treated with 30 μg rhBMP-2 in alginate hydrogel or collagen sponge. Bone regeneration was assessed longitudinally via radiography and micro-CT. Polar moment of inertia, maximum torque, and stiffness provided measures of the functional recovery of regenerated bone. Histology was conducted to further characterize the spatial distribution of bone. Total bone volume was significantly higher in the alginate group at 12 weeks. Further, bone volume within the central defect region was significantly greater in the alginate group at 8 and 12 weeks. However, heterotopic bone volume was similar between groups. Histological analyses corroborated these findings and revealed mineralization outside the bone defect space for both delivery vehicles. Overall, this work recapitulated the heterotopic mineralization often observed with high dose BMP-2 delivery, and demonstrated

that the volume and distribution of BMP-mediated bone formation depend on delivery matrix.

4.2 Introduction

It is estimated that limb fractures account for more than 25% of the musculoskeletal injuries that occur annually (12.36 million). Of these injuries, approximately 5-10% suffer from delayed union or non-union, requiring multiple interventions that are very costly [110]. Although autograft remains the gold standard in clinical care, failure rates with bone grafts range from 13-35% [172]. Bone morphogenetic protein-2 (BMP-2) has emerged as an effective alternative or adjuvant to autograft tissue, demineralized matrices, or similar scaffolds in the treatment of bone defects based on extensive animal and clinical studies supporting its efficacy [25-28]. Roughly a quarter of the approximate 500,000 bone grafting procedures treat cases of trauma [172]. With rising numbers of high-impact and multi-tissue injuries in both military and civilian populations, and their potential complications like non-union, BMP-2 therapy may offer an alternative whereby modest increases in surgical costs with the use of BMP-2 may lead to overwhelming socioeconomic benefits by avoiding the true economic burden of amputations, estimated at $400,000 throughout the patient's lifetime [173].

The discovery of BMP-2 in decellularized, demineralized bone matrix led to the evolution of BMP-2 as a therapeutic target in bone regeneration [5]. Subsequently, animal models have used a wide range of doses in different scaffolds to regenerate bone defects [171]. BMP-2 injected intravenously has a physiological half-life of only 7-30 minutes and localizes to high flow areas including the liver and kidneys [174, 175]. Further, it is expected that a significant amount of locally delivered BMP-2 may be removed into the circulation and excreted [176]. Biomaterial scaffolds have therefore attempted to retain BMP-2 at the

site of delivery to prolong local bioavailability of BMP-2. For example, the absorbable collagen sponge (ACS) scaffold commonly used in the clinic releases BMP-2 over a period of days. Specifically, the ACS scaffold has been shown to retain 40-50% of the BMP-2 within 3 to 4 days, and 10% 1 to 2 weeks after delivery [39, 49, 171, 177] both at a subcutaneous implant site [177] and in a critically sized femoral segmental defect [39]. This release profile is an improvement in comparison to that of BMP-2 delivery without a carrier, where the fraction of BMP-2 retained at the site of delivery sharply dropped to 10% within 3 to 4 days. It is thought that a biphasic release profile is beneficial in the chemotactic recruitment of progenitor cells to the site of delivery and subsequent differentiation of these cells to osteoblasts [171]. Observations by Brown et al. showing improved bone formation using a carrier with a biphasic BMP-2 release profile compared to only sustained release supports this hypothesis [178].

Regardless of whether it is an ideal carrier, ACS has shown great efficacy as a BMP-2 delivery vehicle for bone regeneration, and the variability in dose selection clinically could stem from the perceived higher needs in more challenging injury scenarios. The disparity in the physiological quantities of BMP-2 (picograms-nanograms) in the healing osteogenic environment and the supraphysiological quantities of recombinant human BMP-2 (rhBMP-2) delivered locally (milligrams) as a therapeutic are well recognized [103-105]. The discrepancy has been attributed to both the lower activity of the rhBMP-2 compared to endogenous BMP-2, as well as its temporal bioavailability, which in turn is a function of delivery scaffold [39, 110, 179]. The rationale for the use of high doses of BMP-2, however, remains unclear. Yet spinal fusion surgeries have reported BMP-2 doses ranging from 20-200 mg per patient delivered on ACS [180, 181]. Higher doses of BMP-2 were considered necessary for mineralized bridging in the absence of bone grafting or bulking agents,

suggesting the spatiotemporal distribution of BMP-2 may function in its efficacy [180]. Early evidence using polylactic acid (PLA) carriers showed no appreciable differences in healing or adverse effects in a canine spinal fusion model with BMP-2 doses ranging 40-fold in concentrations (58-2300 μg) [182], suggesting a threshold dose effect. However, subsequent studies have clearly demonstrated an incremental effect on bone regeneration with increasing BMP-2 dose in a canine model using an ACS scaffold [183]. Similarly, an incremental response to increasing dose of BMP-2 has been observed in a mouse calvarial defect model [184] and a rabbit radial defect model using a PLA scaffold (17-70 μg BMP-2) [185]. Thus, the wide range of release profiles, combined with anatomical and other pathophysiological differences in animal species and models, may explain the extent to which different biomaterial carriers promote osteoinduction at varying doses of BMP-2 [186].

The lack of a precise dose response relationship and limited data on the efficacy of high doses of rhBMP-2 notwithstanding, supraphysiological doses are relatively common in clinical use and have been linked to inflammatory reactions such as increased secretion of inflammatory cytokines [187], as well as heterotopic mineralization and diminished bone quality [109]. Few studies have examined the effects of high dose BMP-2 in the regeneration of large segmental bone defects, and the variable results regarding the extent of heterotopic ossification may be a function of the carrier used for BMP-2 delivery. The use of ceramic bulking agents when combined with BMP-2 on ACS did not produce heterotopic bone formation [93]. In contrast, BMP-2 on ACS in canine radial osteotomies (2.5 cm) led to the formation of cyst-like voids and heterotopic bone with higher doses of BMP-2 in a dose dependent manner (150-2400 μg) [183]. Furthermore, the lowest dose of 150 μg resulted in improved mechanical properties and gross structure on radiographs similar to normal bone. Using an apatite-coated PLGA delivery system to treat critically sized femoral segmental

defects in rats, Zara et al. have reported a dose of 2.25 μg of BMP-2 to be necessary for mineralized bridging of the defect, but found no dose dependent increase in bone volumes over a range of 2.25 μg to 45 μg [109]. More recently, in a study of early stage healing (4 weeks) in critically sized femoral segmental defects in rats, a reduction in bone volume was reported with 20 μg of BMP-2 in ACS compared to 10 μg [110]. However, the quantification of heterotopic bone formation, its evolution over time, and its influence on ultimate biomechanical function remain unknown. Furthermore, the role of the scaffold in both heterotopic bone formation and the functional outcome of the healed segmental defect are yet unclear.

Alginate hydrogel based delivery of BMP-2, with a burst release and a subsequent slower release profile, has shown remarkable successes in pre-clinical animal models of both ectopic bone formation and segmental bone defect regeneration [34, 37-41, 165, 188, 189]. Using a critically sized femoral segmental defect in the rat, we have previously demonstrated improved functional bone regeneration compared to autograft [190] and ACS [39, 165], specifically at lower doses and with better spatiotemporal control than commonly seen with ACS [39, 40, 165]. Though differences in degradation rate and hence BMP-2 release profile between alginate formulations did not show significant difference in mineralized bridging or mechanical properties, a larger distribution of more mature (lamellar) bone structures were found with the faster degrading alginate [189]. Nevertheless, the improvement in bone regeneration with alginate-based delivery in comparison to collagen sponge may be attributed to its more optimum BMP-2 release profile, likely resulting in a more sustained chemotactic gradient. The performance of this system with supraphysiological doses of rhBMP-2 has not yet been evaluated. Thus, the aim of this study was to provide a direct comparison of the effects of delivery system—clinically used ACS and the alginate hydrogel

based system—on heterotopic bone formation resulting from a supraphysiological dose of rhBMP-2. This work provides a quantitative description of heterotopic mineralization in segmental defects, elucidates the effects of heterotopic bone on mechanical properties, and ultimately serves as a platform for further mechanistic investigations.

4.3 Materials and Methods

Delivery vehicle preparation

Irradiated sodium alginate was functionalized with the cell adhesion peptide RGD (FMC BioPolymer) and reconstituted in alpha-minimum essential medium (αMEM, Gibco). Recombinant human BMP-2 (rhBMP-2, Pfizer, Inc.) in 0.1% rat serum albumin (RSA, Sigma) in 4 mM HCl was added to the alginate solution, followed by a calcium sulfate slurry for crosslinking, which resulted in a 2% (w/v) hydrogel [40]. Alginate hydrogels contained 30 μg BMP-2 per 150 μL hydrogel. Hydrogels were stored at 4°C overnight before use.

Collagen sponge cylinders (4 mm in diameter, 10 mm in length) were prepared from a manufacturer-sterilized collagen sponge sheet (Kensey-Nash Corp.) using a biopsy punch. rhBMP-2 was suspended in 0.1% RSA in HCl at a concentration of 30 μg/150 μL. The solution was added drop wise to the scaffold, which was incubated 15 minutes for sufficient absorption prior to use.

Nanoporous poly(e-caprolactone) (PCL) nanofiber meshes with 1 mm diameter perforations were produced as described previously [40, 189]. The nanofiber mesh was used to contain alginate hydrogel and collagen sponge. Alginate hydrogel was injected via syringe through the pores in the mesh. Collagen sponge was placed inside the mesh prior to the addition of the BMP-2 solution. Similarly prepared delivery vehicles were used for *in vitro* and *in vivo* experiments.

rhBMP-2 release kinetics

The *in vitro* release profile of BMP-2 from three constructs was assessed: alginate hydrogel surrounded by a mesh, collagen sponge surrounded by a mesh, and collagen sponge alone. BMP-2 release was evaluated through 26 days as previously described [189]. Constructs (n=6-7) containing 30 μg rhBMP-2 were incubated in 1 mL PBS, which was collected and replaced at 3 and 6 hours, and at 1, 2, 3, 5, 8, 14, and 26 days. Following the day 26 collection, a vigorous PBS wash was performed to capture residual BMP-2 remaining in the scaffolds. The BMP-2 released in the media at each time point was quantified using an enzyme-linked immunosorbent assay (ELISA, R&D Systems). The release data for each sample was converted to decay data (theoretical percentage retained in the constructs), which was analyzed by least-squares nonlinear regression analysis (SigmaPlot 11.0) as previously described [189].

Alkaline phosphatase induction assay

An alkaline phosphatase (ALP) induction assay [160] was performed to measure the bioactivity of BMP-2 released through 5 days and BMP-2 remaining in the constructs at 26 days (n=6-7) as previously described [189]. Briefly, mouse clonal pre-osteoblasts (MC3T3-E1s, American Type Culture Collection) were cultured at high density (62,500 cells/cm^2) for 72 hours in equal volumes of αMEM and PBS containing released/retained BMP-2, supplemented with 0.1% ascorbic acid 2-phosphate (AA2P) and 1% fetal bovine serum (FBS, Atlanta Biologicals). MC3T3s were incubated with 7.6 mM p-nitrophenyl phosphate (p-NPP) in 50 mM Tris/HCl (pH 10.3) for 10 min at 37°C. After termination of the reaction with 0.2 M NaOH, the absorbance was read at 405 nm on a microplate spectrophotometer (PowerWave X5, Gen5 Software; Biotek Instruments, Inc.).

Surgical procedure

Unilateral critically sized (8-mm) segmental bone defects were created in the left femora of 13-week-old female SASCO Sprague-Dawley rats (Charles River Laboratories) as detailed previously [41]. After excision of bone, the defects were stabilized with a radiolucent polysulfone plate. Defects were treated with 30 μg rhBMP-2 in collagen sponge or irradiated RGD-alginate, surrounded by a PCL nanofiber mesh (n=9-11). For analgesia, slow-release buprenorphine (Wildlife Pharmaceuticals) was given subcutaneously prior to surgery. Animals were euthanized by CO_2 inhalation. All procedures were approved by the Georgia Institute of Technology Institutional Animal Care and Use Committee (IACUC).

Radiography and micro-computed tomography

Longitudinal bone regeneration was assessed via radiography and micro-computed tomography (micro-CT) through 12 weeks. Radiographs (Faxitron MX-20 Digital, Faxitron X-ray Corp.) were taken 2, 4, 8, and 12 weeks post-operatively for qualitative observation.

De novo mineral within and surrounding the defect space was quantified using micro-CT (Viva-CT 40, Scanco Medical) at 4, 8, and 12 weeks. Parameters for scans were medium resolution, 38.9 μm voxel size, 55 kVp voltage, 145 μA current, and a global threshold of 386 mg hydroxyapatite/cm^3 (50% of the density of cortical bone) to segment newly formed bone tissue. A Gaussian filter (sigma = 1.2, support = 1) was used for noise suppression. Along the long axis of the femur, the central 136 slices (~5.3 mm) were evaluated. To clearly differentiate the new bone formation within the bone defect enclosed by the nanofiber mesh from the adjacent heterotopic bone outside the defect, two volumes of interest (VOIs) were evaluated. First, a 6-mm diameter VOI was used to characterize mineralization within and immediately bordering the outside of the mesh. This VOI corresponds to the typical VOI that is used for evaluating mineral formation following delivery of low dose BMP-2 in this

defect model [189]. Secondly, a large diameter VOI was used to encompass all bone formation within the thigh. The bone volume from the 6-mm VOI was subtracted from the bone volume from the corresponding large diameter VOI, and this bone was defined as heterotopic bone.

Femora were harvested at 12 weeks post-operatively for *ex vivo* micro-CT scans. All scan parameters were the same as above, except the voxel size was 21.5 μm. Here, the large diameter VOI, encompassing both the defect and heterotopic bone, comprised 495 slices (~10.6 mm) of the femur length and included part of the native bone ends that were subsequently subjected to torque during mechanical testing. The "Bone Midshaft" evaluation script (Scanco Medical) was used to calculate polar moment of inertia (pMOI) for each slice from CT scans [188]. All pMOI values within the sample were then averaged to provide a global measure of the distribution of bone with respect to the longitudinal axis of each sample.

Biomechanical testing

Torsional testing of regenerated femora *ex vivo* was performed as previously described [41]. Briefly, after removal of the fixation plate and clearing of soft tissue, the bone ends were affixed in Wood's metal (Alfa Aesar). Displacement-controlled loading at 3°/s was performed on femora (n=7-9) to failure (ELF 3200; Bose ElectroForce Systems Group). From torque-rotation curves, maximum torque and torsional stiffness were calculated.

Histology

One sample from each group was harvested at 2 weeks, fixed, and embedded in optimum cutting temperature (OCT) compound to further characterize the distribution of newly formed bone, especially the heterotopic mineralization at the early phase of bone regeneration in the presence of a high dose of BMP-2. Mid-sagittal 7 μm non-decalcified

sections were obtained from the defect center by a tape transfer technique [191] (Section Labs, Hiroshima, Japan) on an NX-70 cryostat (Thermo Scientific). Mineral distribution was identified by von Kossa staining (5% silver nitrate under UV light for 40 minutes followed by a sodium thiosulfate wash), and slides were counterstained with eosin. Sequential sections were also stained with routine hematoxylin and eosin (H&E) for morphology comparisons.

Representative sections were also stained for the presence of macrophages using CD68, a pan-macrophage marker. Sections were washed in PBS to remove OCT, permeabilized with 0.5% Triton X-100, blocked, and stained overnight at 4°C with the primary antibody (Mouse anti-rat CD68 (AbD Serotec®), 1:100). Sections were then incubated with the appropriate fluorescent secondary antibody (Alexa Fluor® 488 Donkey anti-mouse (Life Technologies), 1:50) for 1 h at room temperature, washed in PBS, and stained with DAPI (4',6-diamidino-2-phenylindole, Life Technologies, 1:1000) for 2 min to identify nuclei.

One representative sample from each group was also harvested at 4 and 12 weeks, fixed using 10% neutral buffered formalin, and decalcified in a mild formic acid solution (Immunocal, Decal Chemical Corp.), which was changed three times a week for two weeks. Samples were paraffin embedded and sectioned using a tape transfer technique (Section Labs, Hiroshima, Japan). Sagittal sections obtained from the mid-defect region were deparaffinized and stained with H&E to characterize tissue morphology, safranin-O and fast green to identify alginate and cartilage, and Mallory's modified aniline blue stain for identification of mature and immature osteoid, as described extensively for this experimental model [9, 22-25].

Statistical Analyses

Data were analyzed using GraphPad Prism 5 (GraphPad Software, Inc.) with a significance level of $p<0.05$ and reported as mean ± standard error of the mean (SEM). Release kinetics and longitudinal micro-CT parameters were assessed by two-way repeated measures analysis of variance (ANOVA). BMP-2 recovered from the constructs and decay constants were analyzed by one-way ANOVA. ALP activity of cells cultured with released and retained BMP-2 was evaluated using two-way ANOVA. Post-hoc pairwise comparisons for each ANOVA were performed using the Bonferroni method. Biomechanical properties, including pMOI from micro-CT analyses, were evaluated using Student's t-tests.

4.4 Results

rhBMP-2 release kinetics

The cumulative release of BMP-2 did not differ statistically among the construct groups, though the initial burst release from the collagen sponge groups were higher and occurred earlier than that from the alginate. The initial burst release from the collagen sponges, irrespective of the presence of the enveloping mesh, occurred within a day, while that from the alginate occurred between 2 and 5 days (Figure 10A). Though not significantly different, the presence of the mesh around collagen sponge appeared to retard BMP-2 release after the initial burst. The *apparent* retained quantity of BMP-2 in the alginate constructs had a slower rate of decay than collagen, as determined by non-linear regression analysis ($r^2=0.95$, Figure 10B). From these curves, the decay constant was significantly lower in the alginate group compared to both collagen groups (Figure 10C; $p<0.05$, Kruskal-Wallis test). The amount of BMP-2 recovered from the constructs at 26 days was not significantly different among groups, but a higher average amount of BMP-2 was recovered from alginate constructs (Figure 10D).

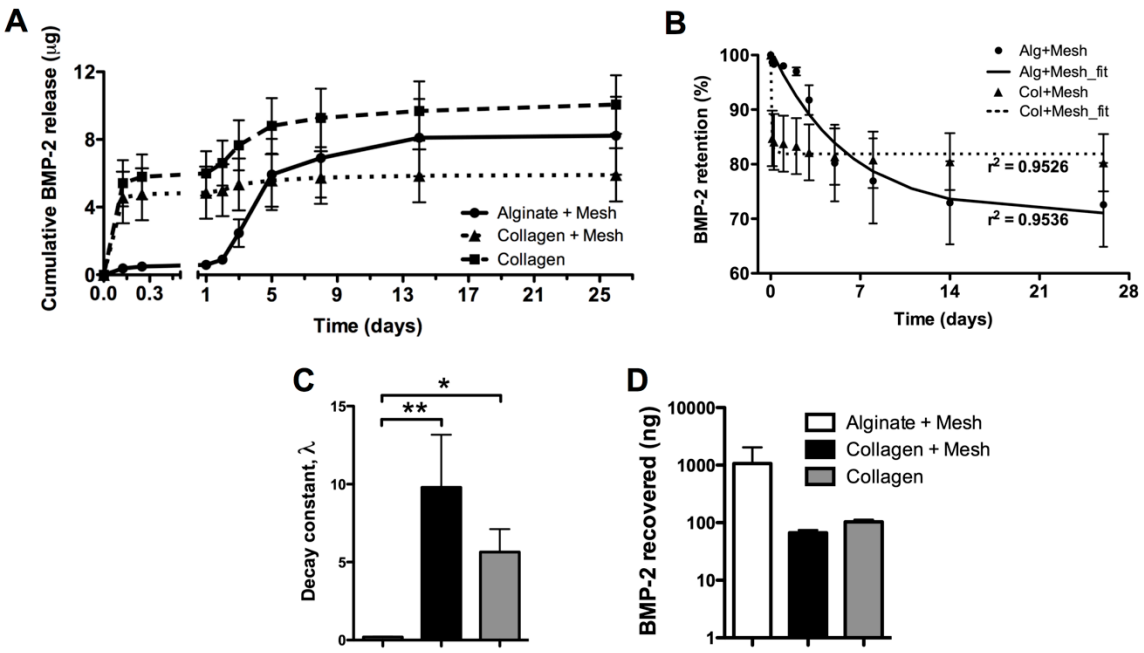

Figure 10. Release kinetics of BMP-2 from constructs *in vitro*. (A) Cumulative BMP-2 release through 26 days indicated delayed release through day 5 from alginate+mesh constructs. (B) *Apparent* percent BMP-2 retained in the constructs over time was plotted alongside the average exponential curve fits (denoted by _fit). (C) Decay constant λ was significantly higher for the collagen+mesh constructs (**$p<0.01$) and collagen constructs (*$p<0.05$) compared to alginate+mesh constructs. (D) Minimal BMP-2 was measured in the constructs at 26 days.

Alkaline phosphatase induction assay

Functional assessment of the bioactivity of BMP-2 released and bound in the constructs was measured by an ALP assay with MC3T3-E1 cells. ALP activity was normalized to the amount of BMP-2 in the samples measured by ELISA (Figure 11). All samples induced measurable ALP activity, but no differences were observed among the groups from released BMP-2 at any time point. However, the BMP-2 remaining in the alginate+mesh constructs at 26 days elicited significantly higher ALP activity compared to BMP-2 retained in the collagen+mesh and collagen constructs ($p<0.01$).

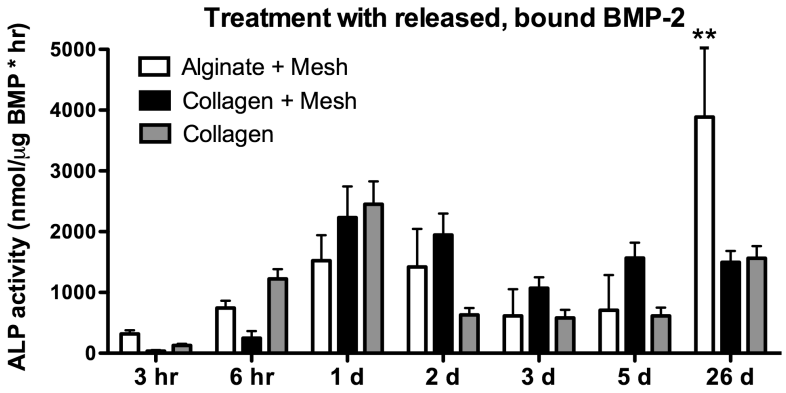

Figure 11. ALP activity normalized to BMP-2. ALP activity was induced in MC3T3 cells incubated with samples containing BMP-2 from all time points analyzed (released at 3 hr through 5 d, and bound at 26 d). No differences in ALP activity from BMP-2 released at any time point were observed among groups. However, BMP-2 retained in the alginate delivery system promoted significantly higher ALP activity compared to that retained in both collagen delivery systems (**$p<0.01$).

Radiography and micro-computed tomography

Longitudinal radiographs of defects treated with high dose BMP-2 in alginate and collagen sponge revealed an early heterotopic mineralization response at 2 weeks, which appeared more prevalent in the collagen sponge group. Qualitatively, the heterotopic bone was less prominent in both groups by 8 to 12 weeks, particularly for the alginate group (Figure 12). More than 90% of the defects in both groups showed mineralized bridging of the defect site by 8 weeks (9/9 of the collagen treated defects and 10/11 of the alginate treated defects).

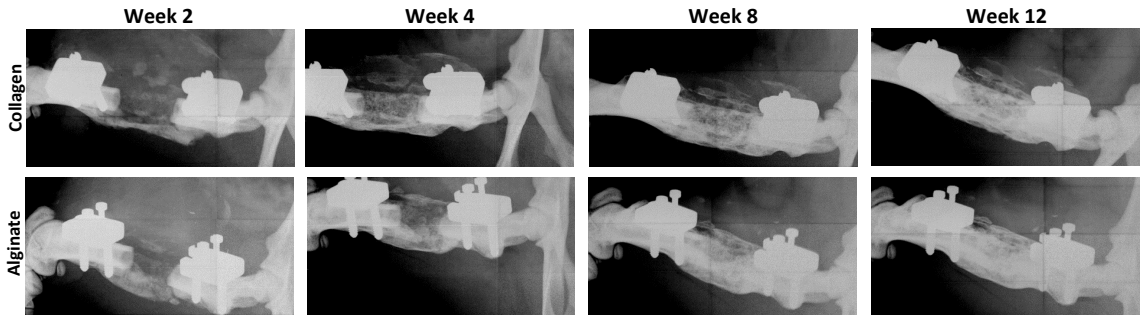

Figure 12. Longitudinal radiographs of regenerating bone defects. Defects were treated with high dose BMP-2 in collagen sponge scaffold (top) or alginate hydrogel (bottom). Heterotopic ossification, although present by 2 weeks in both groups, was less pronounced over time, especially in the alginate group.

Quantitative comparison of mineral volume showed an increase in total bone volume over the course of the study for both groups, and total bone volume was significantly greater at 12 weeks in the alginate treated defects ($p<0.05$, Figure 13A). Further, bone volume within the defect space was significantly higher for the alginate group at 8 and 12 weeks ($p<0.01$, Figure 13B). However, no differences in heterotopic mineralization were observed (Figure 13C). Nonetheless, as a proportion of total bone volume, heterotopic bone volume was significantly attenuated in the alginate group at 8 and 12 weeks ($p<0.05$, Figure 13D). At all time points, over 50% of the total bone volume in the collagen treated defects was heterotopic bone, while approximately 30% of the total bone in the alginate group was outside the defect.

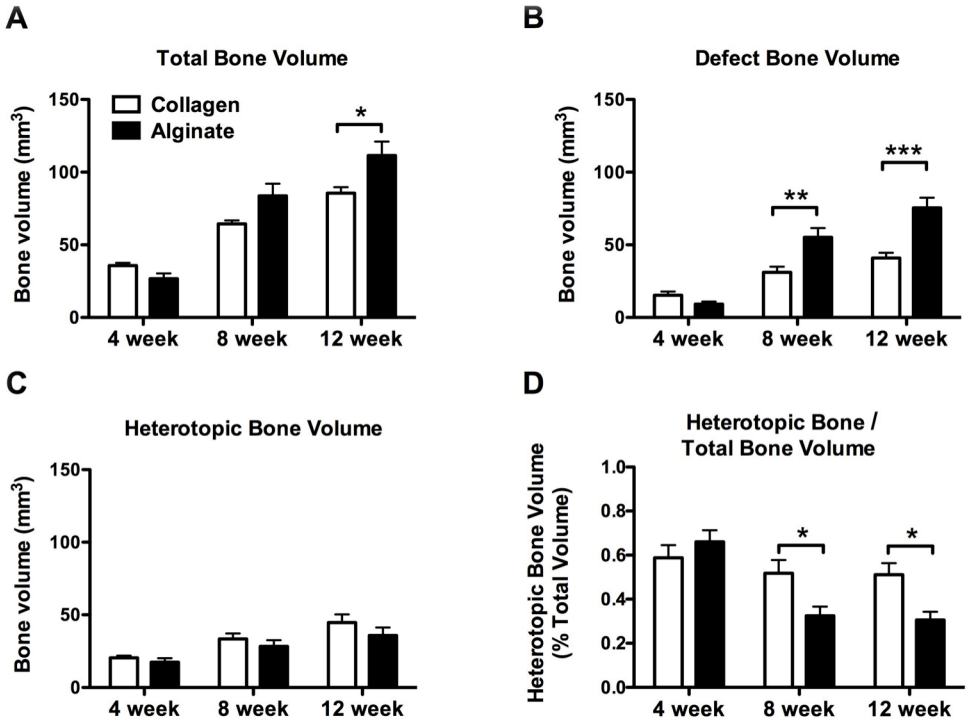

Figure 13. Regenerated bone volumes through 12 weeks. (A) Total bone volume (BV) increased over time and was significantly higher in the alginate group at 12 weeks (*$p<0.05$). (B) Bone volume within the defect region (defect BV) was significantly greater in the alginate group at 8 and 12 weeks (**$p<0.01$, ***$p<0.001$). (C) No differences in the amount of heterotopic bone were observed. (D) Nonetheless, as a proportion of total bone volume, heterotopic bone was significantly lower for the alginate group at 8 and 12 weeks (*$p<0.05$).

The units of mineral (termed trabeculae) both within and surrounding treated defects were further characterized. While there were no significant differences between the two groups in the number of trabecular structures (Figure 14A), the thickness of these structures was significantly higher in the alginate group at both 8 and 12 weeks of healing ($p<0.01$, Figure 14B). Correspondingly, the trabecular connectivity was reduced significantly in the alginate group at 12 weeks ($p<0.05$, Figure 14C), indicating a lower number of connections between the thicker trabeculae. The polar moment of inertia (pMOI) for the collagen group had a higher average value, but was not significantly different from the alginate group (Figure 14D).

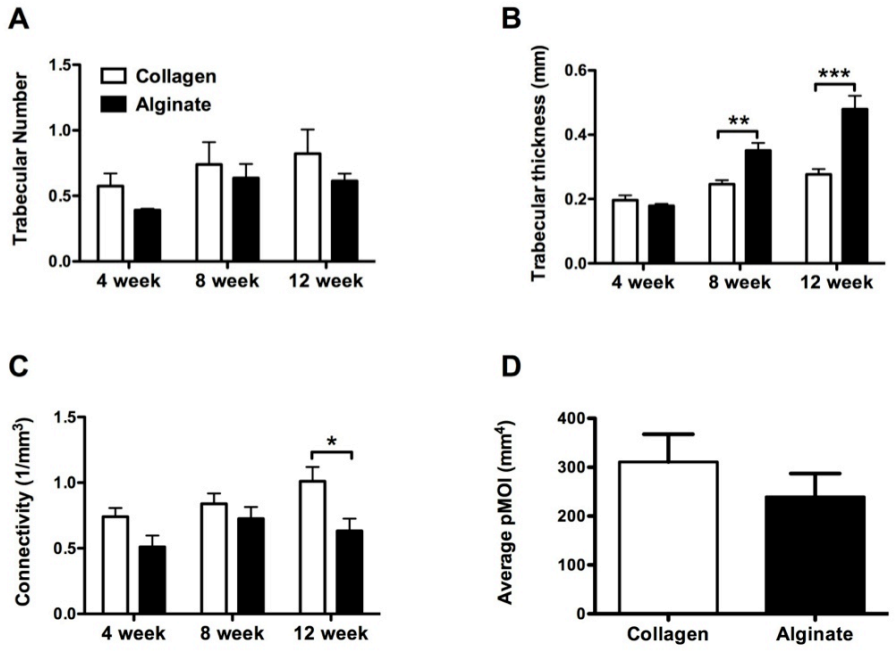

Figure 14. Properties of total bone regenerated through 12 weeks. (A) The number of bone (trabecular) structures present was not signficantly different between groups. (B) Trabecular thickness was significantly increased at 8 and 12 weeks in the alginate group (**$p<0.01$, ***$p<0.001$). (C) Correspondingly, connectivity density, a representation of the number of connections per unit volume, was augmented in the collagen treated defects at 12 weeks (*$p<0.05$). (D) Average polar moment of inertia (pMOI) evaluated from micro-CT reconstructions of 12 week samples was not significantly different between groups.

Biomechanical testing

No statistically significant differences in the maximum torque at failure or the torsional stiffness between the two groups were noted (Figure 15A, B). Further, the maximum torque for both groups did not differ from that of intact bone [40]. The average torsional stiffness, a material property, was significantly higher than historical values reported for intact bone [40], but was not significantly different between the two scaffold groups.

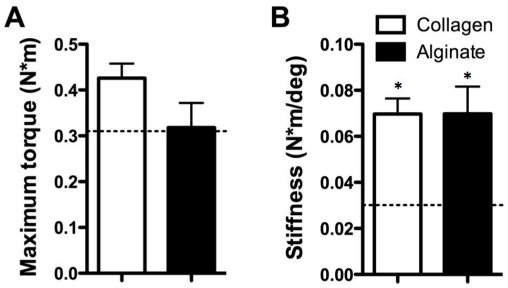

Figure 15. Biomechanical properties of regenerated bone defect tissue. Dashed lines indicate mean values for historical intact control bone [40]. From torsional testing of bone defect tissue at 12 weeks, no differences in maximum torque to failure (A) or torsional stiffness (B) were observed. However, torsional stiffness values were significantly greater than those of intact bone (*$p<0.05$).

Histology

Staining of cryosections at 2 weeks revealed heterotopic bone formation in the surrounding soft tissue. The spatial extent and appearance of heterotopic mineral was similar in both groups (Figure 16). Areas of mineralization and cartilage formation in the region around the mesh were evident from H&E staining (Figure 16A, D). Furthermore, von Kossa staining confirmed the presence of mineralized nodules (Figure 16B, E). In the defect region, many macrophages were observed with collagen sponge (Figure 16C), compared to fewer macrophages, and cells in general, in the alginate group (Figure 16F).

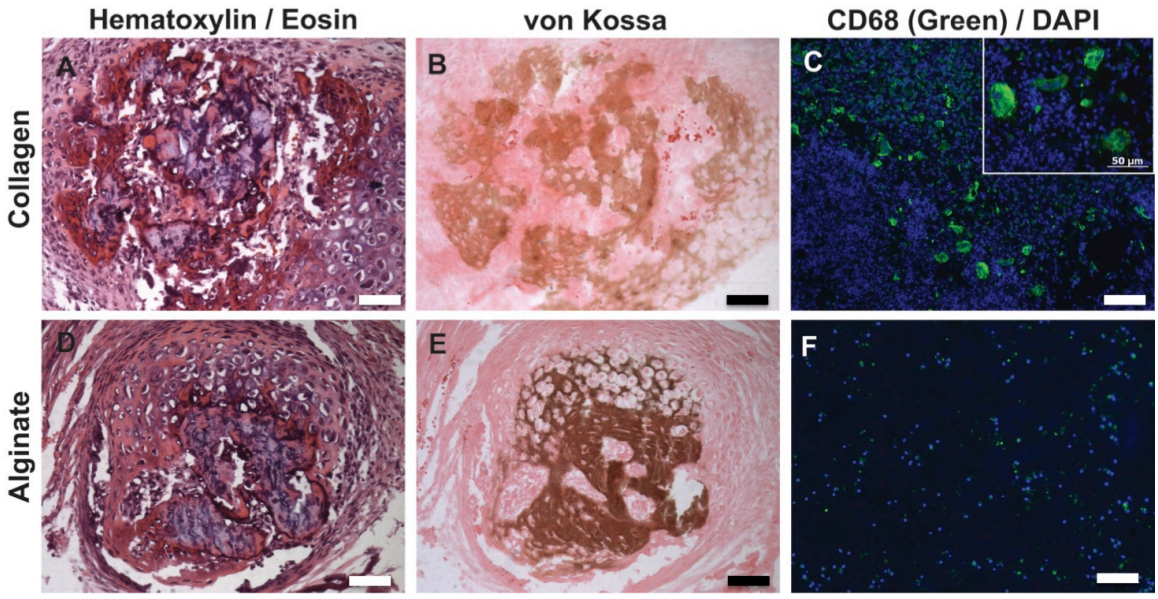

Figure 16. Heterotopic bone and macrophages at 2 weeks. (A, D) H&E staining indicated the presence of cartilage nodules outside the defect region in both groups. (B, E) von Kossa staining demonstrated that these nodules were mineralized (20x magnification, scale bar=50 µm). (C, F) CD68 staining identified more macrophages (and cells in general) in the collagen group (10x magnification, scale bar=100 µm, except inset in C).

Representative paraffin sections captured the evolution of mineralization over time from 4 weeks to 12 weeks of healing. In the defect center, the collagen treated group contained trabecular, strut-like osteoid elements interspersed with abundant space that was filled with marrow and adipose like structures, giving the appearance of spongy bone (Figure 17A) with few cartilage structures (Figure 17B) at 4 weeks. Most bone in the defect area appeared to be mature bone based on the dark red staining with Mallory's modified aniline blue stain (Figure 17C) [190]. In contrast, the alginate group showed areas of bone interrupted by large pieces of alginate (Figure 17D, E) and negligible marrow and adipose like structures. The bone also appeared more immature (orange-red, Figure 17F) compared to bone in the collagen treated group.

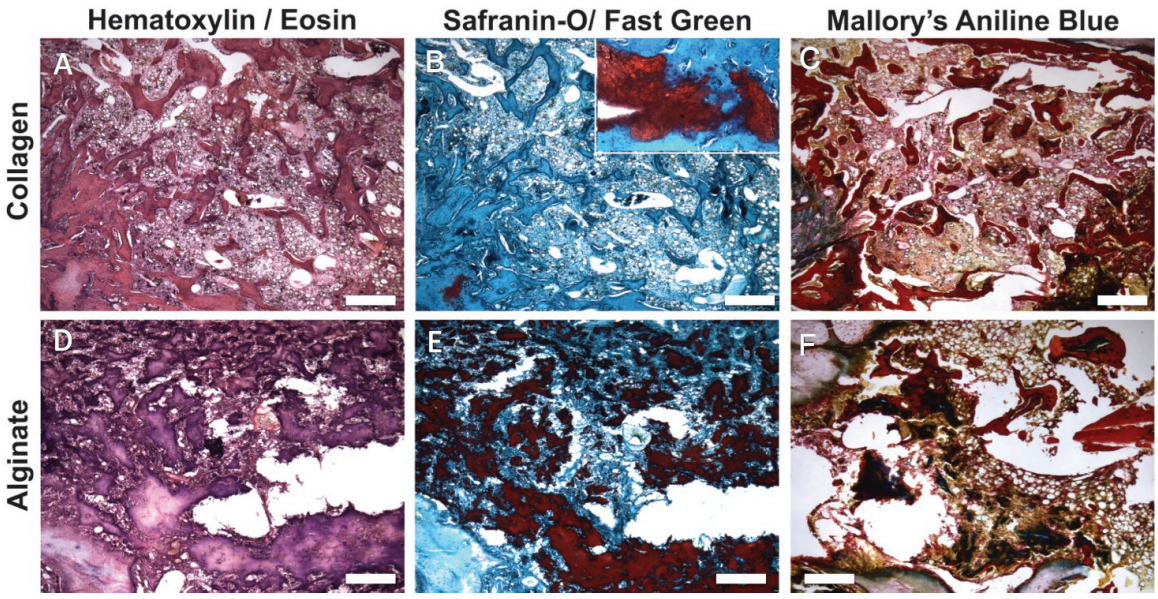

Figure 17. Bone defect tissue at 4 weeks. (A-C) Defect tissue in the collagen group contained trabecular structures surrounded by marrow and adipose tissue. (B) Small pockets of cartilage (inset) were present in the collagen sponge group. (C) Further, the bone tissue present appeared to be mature osteoid. (D-F) In the alginate group, although similar amounts of bone tissue were observed, a large portion of the alginate remained (E). (F) The bone tissue appeared to be more immature bone (4x magnification, except B inset is 10x. Scale bar=100 μm).

By 12 weeks, the appearance of spongy bone with thin, mature trabeculae was unmistakable in the collagen treated group with no cartilage detected at this stage (Figure 18A-C). A large portion of the section appeared to be loose adipose tissue with marrow structures. In sharp contrast, the alginate group showed more bone areas with some marrow-like infiltration between them (Figure 18D-F), as well as smaller persisting pieces of alginate (Figure 18E) adjacent to mature bone (Figure 18F).

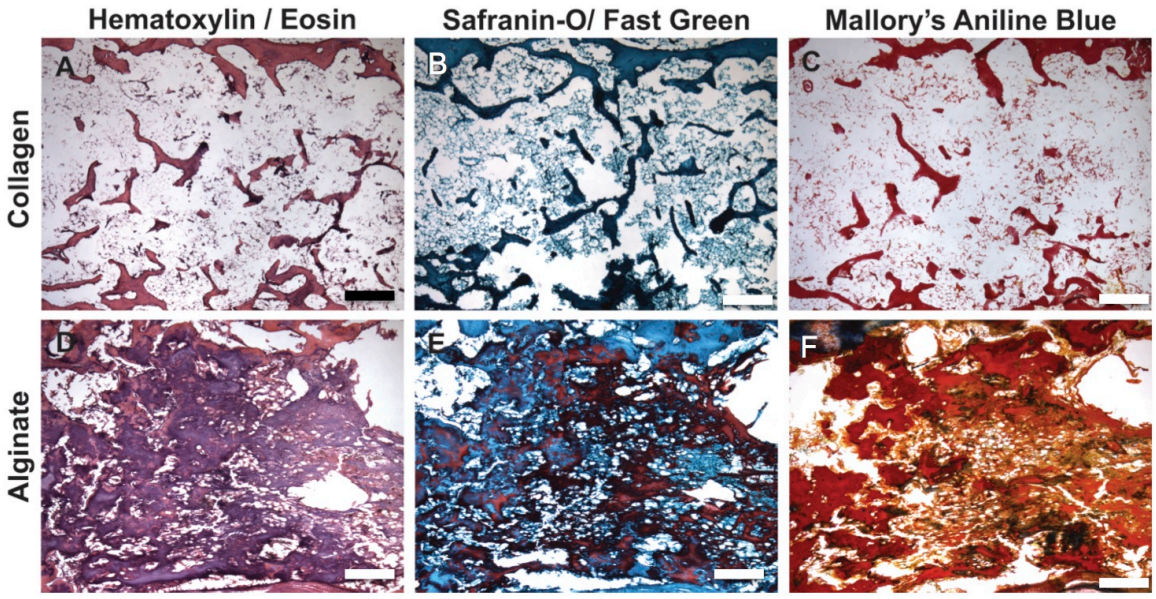

Figure 18. Bone defect tissue at 12 weeks. (A-C) Defects treated with collagen sponge had primarily mature bone spicules present. (D-F) In contrast, alginate treated defects resulted in the formation of denser tissue comprising both residual alginate (E) and mature bone (F) (4x magnification, scale bar=100 μm).

In both groups, the heterotopic bone had a similar appearance and was closely associated with the surrounding soft tissue (Figure 19). Furthermore, the morphology of the heterotopic bone did not appear to change significantly between 4 and 12 weeks. Surprisingly, most heterotopic bone seen in the representative sections appeared to be more mature bone, regardless of the scaffold used or time of observation.

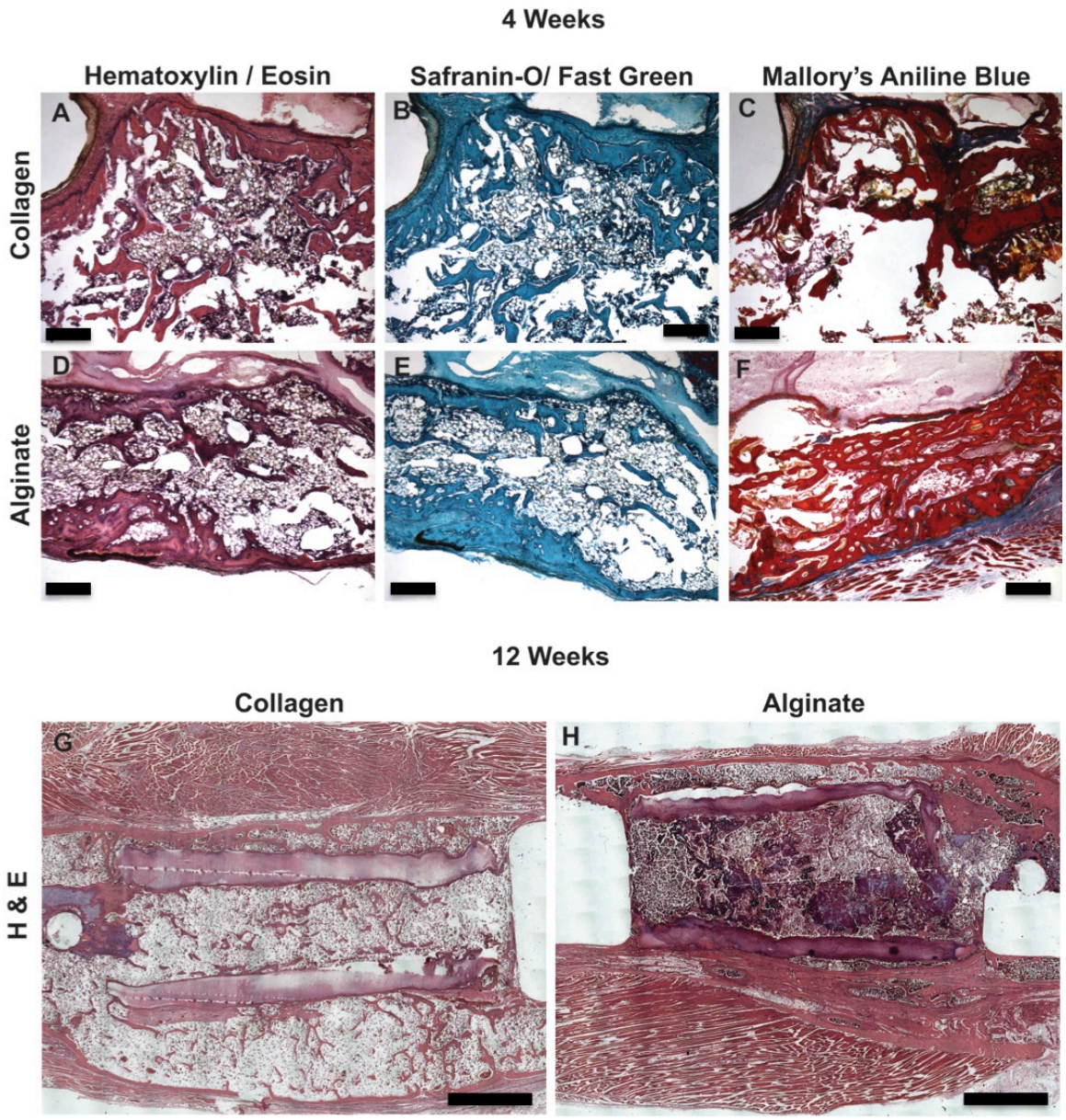

Figure 19. Heterotopic bone at 4 and 12 weeks. (A-F) Heterotopic bone was present adjacent to the surrounding soft tissue and appeared to be mature bone (C, F) (4x magnification, scale bar=100 μm). (G-H) Global heterotopic mineralization occurred to a similar extent in both groups (4x magnification, scale bar=2 mm).

4.5 Discussion

Delivery of BMP-2 in absorbable collagen sponge (ACS), though the clinical standard, is associated with high incidence of side effects, attributable to both the

supraphysiological doses of BMP-2 used, as well as the poor retention of BMP-2 by the collagen matrix. Complications with the use of BMP-2 occur in 10-50% of cases and include uncontrolled overgrowth of bone, osteolysis, and inflammation [192]. Nonetheless, a wide therapeutic dose of BMP-2 and a variety of carriers evaluated in the clinic and in pre-clinical animal models have yielded excellent bone regeneration. Despite the astounding success of this clinical therapeutic and many successful animal studies on dose and carriers, the lack of appropriate dose-effect or bioavailability-effect relationships have hampered the selection of effective dose. Here, we have directly compared the effect of delivery scaffolds, including the clinically used collagen sponge, for the delivery of high dose BMP-2. Contributions of this work include: (i) characterization of an orthotopic model that recapitulates adverse effects associated with high dose BMP-2 delivery and investigation of the factors contributing to these consequences, and (ii) evaluation of the hybrid alginate-PCL mesh delivery system for enhanced localized bone formation with high dose BMP-2 treatment.

Improving spatiotemporal delivery and/or presentation of growth factors is a topic of intense research, with strategies ranging from simple delaying of diffusion, to complex three-dimensional localization within bioprinted matrices [193]. Modifications of the BMP-2 protein can also improve the residence time of the BMP-2 in ACS [194], but may be challenging for clinical translation. The rapid diffusion of BMP-2 away from the delivery site may quickly reduce the local growth factor concentrations, which may remain at physiologically insufficient levels for chemotactic recruitment or differentiation of regenerative cells in adequate numbers, necessitating supraphysiological doses [195]. Thus, improved delivery systems capable of maximizing growth factor potency while mitigating harmful side effects represent a significant clinical need. However, no clear relationship has been identified between side effects of BMP-2 and BMP-2 release kinetics from the

scaffolds, altered bone structure, or bone mechanical properties [109, 110, 182, 183]. In addition to being a function of delivery system, release profiles might differ vastly by animal species and anatomical location of delivery [172]. Despite evidence to the successful use of lower doses of BMP-2 with biomaterial scaffolds, it is believed that the rodent and small animal models heal more efficiently and at lower relative BMP-2 doses than large animals. This study used a BMP-2 dose of 120 μg/kg (30 μg per average 250 g rat), which falls in the typical range of supraphysiological doses used in clinical settings: 50-800 μg/kg (based on an 80 kg individual) [181, 196].

Improved healing with the alginate based delivery system in comparison to both collagen sponge and autograft, with lower doses of BMP-2, as well as improved retention of BMP-2 at the defect site *in vivo* are well established [39, 40, 165, 189, 190]. However, contrary to our hypothesis, the alginate delivery system did not reduce the amount of heterotopic mineralization compared to the collagen sponge in high dose BMP-2 delivery. The burst release of a large proportion (>25%) of the delivered BMP-2 within the first 5 days from both delivery systems may have resulted in the large heterotopic bone formation seen in both groups. The initial delay in burst release from the alginate group was insufficient in significantly reducing the heterotopic bone formation in the surrounding soft tissue. However, the higher average retention of the BMP-2 at 26 days and its significantly higher bioactivity in the alginate group likely facilitated the increases in bone deposition in the defect center and total bone volume at 12 weeks, as BMP-2 remaining in alginate constructs at 26 days has been shown to induce high levels of ALP activity [189]. Though not directly quantified, the presumed earlier collapse of the local chemotactic gradient for collagen sponge, as can be inferred by the high decay constant and the lower amount of BMP-2 recovered *in vitro* at day 26, could further explain the differences in bone formation patterns

between the two delivery systems. The rapid efflux of BMP-2 from collagen without the mesh, particularly between days 1 and 5, suggested a retarding or binding effect of the BMP-2 with the nanofiber mesh as observed previously [189]. Despite the lack of a significant biological effect of the mesh in our *in vitro* studies, the mesh was invaluable in establishing the limits for the defect margin *in vivo* and thus enabled consistent quantification of heterotopic bone formation in this longitudinal study.

Micro-CT data showed that the alginate delivery system facilitated significantly more bone deposition in the central defect region. This is likely due in part to delayed degradation and increased retention of BMP-2 in the alginate compared to the faster degrading collagen sponge [197]. Approximately 75% of the total bone in the alginate group was centrally located at 8 and 12 weeks, compared to less than 50% for the collagen group. These stark differences in amount and distribution of *de novo* bone suggest the alginate hybrid delivery system may be superior to the collagen sponge for high dose BMP-2 treatment of large bone defects. The structure-function relationship of this newly formed bone was further characterized to identify differences in mineralization and the impact on mechanical properties. Thicker trabeculae with lower connectivity observed in the alginate group from micro-CT quantifications agreed with its histological appearance, where the central defect region showed augmented mineralization. For collagen, this appearance recapitulated the more trabecular structure with larger marrow infiltration [109]. This histological appearance of a predominantly trabecular structure was in contrast with our previous characterization of bone formation with a lower dose of BMP-2 [165]. In that study, collagen sponge used without the peripheral mesh showed a lower density of connections at the early stage (4 weeks) but was ultimately equivalent to the alginate+mesh group by 12 weeks. Taken with the increasing total bone volume over time within each scaffold, it is likely that continued

mineralization of the alginate, especially in the defect region, may have resulted in a reduction in the appearance of trabecular-like structures. Surprisingly, the total bone volume in this study was comparable to that seen with lower doses of BMP-2 in alginate hydrogel [189, 190].

The lack of significant differences between the two scaffolds in their functional biomechanical properties, as evaluated by failure in torsion, was as expected based on the extent of heterotopic bone formation, both in its volume and spatial extent (pMOI) for both scaffold groups. Though better central bone formation was seen with alginate group, the comparable functional mechanics obtained even from the more heterotopically distributed bone in the collagen scaffolds provided insights into the continued use of these scaffolds in clinical care, especially since the torsional stiffness values were more than twice that of intact bone. Not surprisingly, these values were also higher than those reported for a six-fold lower dose of BMP-2 or autograft treatment [190].

Histological analyses corroborate the differences in bone volume, as the defect space appeared to contain more bone in the alginate group at 12 weeks, and heterotopic bone was observed with both delivery systems. Though not quantified in this study, participation of muscle derived cells in the healing of open fractures [198] and the osteogenic differentiation of muscle derived stromal cells located adjacent to a fracture site are established [123]. Further, the muscle resident stem cell population (satellite cells) is activated after muscle injury and with chemotactic migration, incorporates into the healing callus in the case of bone injury [123, 198, 199]. The formation of the fracture callus in rat, rabbit, and sheep tibial fractures has been observed in the space between the fracture site and the intact muscle surrounding the injury [200]. Importantly, a short exposure of muscle stem cells to appropriate cytokines can be sufficient for osteoinduction [123, 148, 199]. As such, bone

healing in our segmental defect model was impaired when combined with a large volumetric muscle injury adjacent to the bone injury site [201]. Considered with our findings reported here, rapid osteoinduction of the neighboring muscle derived progenitor cells by the supraphysiological doses of BMP-2, and/or the large bone defect and necessary injury to the muscle, may have induced the heterotopic mineralization response, regardless of the scaffold used. We provide partial evidence of this phenomenon in the skeletal tissue surrounding the bone injury. The localization of mineral staining around the muscle fibers was suggestive of a rapid osteoinduction of muscle-derived progenitors, known to preferentially localize within myofibers [202].

Contrary views exist on the source of the progenitor cells that form heterotopic mineral under the influence of BMP-2 in muscle tissue, but the pathogenesis is thought to progress from inflammation through the process of endochondral ossification [146]. Previous reports have been conflicting on the effect of BMP-2 on cellular infiltrate, suggested a reduced macrophage presence over time with BMP-2 [185], and conversely, an increase in inflammatory cells due to the presence of BMP-2 [109]. The heightened early cellular infiltration seen in the collagen sponge treated defects may be a result of the accelerated release of BMP-2 or the presence of the (bovine) collagen sponge itself. This study demonstrated highly mineralized cartilage nodules in the soft tissue surrounding the defects at 2 weeks, as also reported previously in relation to increasing doses of BMP-2 in a subcutaneous implant model [99]. Nonetheless, muscle mineralization was not extensively noted in either group and could have been more thoroughly characterized by examining even earlier time points.

In summary, BMP-2 retained in the alginate construct at 26 days *in vitro* demonstrated significantly higher bioactivity. In the segmental bone defect model, the

alginate delivery system facilitated significantly more bone deposition in the defect center. Despite enhanced centralized bone formation with the alginate system, the volume of heterotopic bone was not different between groups, possibly due to the early burst release of BMP-2 from both delivery systems. Likewise, mechanical properties from *ex vivo* torsional testing were comparable between groups. Histologically, mineral deposition was observed in the soft tissue beginning at 2 weeks in both groups. Nonetheless, the alginate delivery system had lower cellular infiltration early, and condensed mineral in the defect space later. Overall, this work recapitulated the heterotopic ossification often associated with high dose BMP-2 delivery, and demonstrated that the total amount and pattern of BMP-mediated bone formation depend on delivery matrix.

V. SPATIOTEMPORAL GENE EXPRESSION PATTERNS AS A FUNCTION OF BMP-2 DOSE

5.1 Abstract

Successfully healing critically sized bone defects is challenging and necessitates treatment with autograft bone tissue and/or osteogenic growth factors such as bone morphogenetic proteins (BMPs). Despite the potent osteoinductive properties of BMP-2, the use of BMP-2 at supraphysiological doses is associated with many adverse effects including heterotopic bone formation and tissue swelling. Using a proportionately high dose of BMP-2 in a well-established rat segmental bone defect model, we have also observed heterotopic mineralization in the soft tissue adjacent to bone defects. Based on these findings, the objective of this work was to examine the effects of BMP-2 dose on osteogenic and inflammatory gene expression profiles in the bone defect and surrounding soft tissue. Our hypothesis was that high dose BMP-2 would elicit greater osteogenic and inflammatory gene expression in both the bone defect and muscle tissue compared to low dose BMP-2. Critically sized rat femoral segmental defects were treated with 2.5 μg (low dose) or 30 μg (high dose) BMP-2 in RGD-alginate hydrogel injected into a poly(ε-caprolactone) (PCL) nanofiber mesh. Bone and muscle samples from operated limbs and contralateral, unoperated limbs were harvested at 3, 7, 14, and 21 days for analysis by quantitative real-time polymerase chain reaction (qPCR). Bone defects treated with high dose BMP-2 exhibited increasing expression of osteogenic genes through 21 days. However, these levels began to plateau for the low dose group by day 14. Inflammatory gene expression peaked at day 3 for the low dose group, while two pro-inflammatory genes (CCR7, IFNG) remained elevated through 21 days in high dose BMP-2 treated defects, suggesting earlier resolution of

inflammation with low dose BMP-2. In the direct comparison between BMP-2 doses, low dose BMP-2 elicited heightened inflammatory gene expression at day 3 in bone defect tissue. In contrast, high dose BMP-2 resulted in increased osteogenic gene expression in bone defects at day 3, and heightened expression of inflammatory and osteogenic genes in intact muscle, indicating local and systemic effects, respectively. In conclusion, these spatiotemporal differences in gene expression may, in part, explain the heterotopic mineralization and tissue swelling seen clinically with high doses of BMP-2.

5.2 Introduction

Large bone defects resulting from trauma or tumor resection require augmentation of the tissue with allograft, autograft, or other bone substitute to heal these challenging injuries. The gold standard of care, the autograft, still involves complications such as pain at the donor site, lack of revascularization at the injury site, and non-union, necessitating repeated surgeries or in rare cases, amputation. Since bone tissue has an innate capacity to regenerate after injury, the development of tissue engineering strategies that support the endogenous bone repair process is crucial for healing of these most traumatic injuries.

Growth factor delivery has shown promise for augmenting the treatment of large bone defects, albeit with limitations at present. As alternatives to autograft treatment, the osteoinductive growth factors BMP-2 and BMP-7 have been used successfully for regeneration of bone in the clinic [26, 203]. However, controversy surrounds the clinical use of BMP-2, particularly for spinal fusion procedures, which is often associated with inflammatory reactions such as pain, swelling, and hematoma [29, 204]. Adverse effects such as these are compounded by the delivery of BMP-2 within a collagen sponge, which has limited ability to retain growth factor [25, 29, 39]. Nonetheless, minimal complications were observed when dose and containment were carefully considered [30].

After injury, the natural healing cascade involves a coordinated series of events: inflammation, proliferation/repair, and remodeling. Occurring immediately after injury, inflammation is characterized by increased blood vessel permeability, hematoma, and edema, along with the homing of a multitude of cells and secretion of growth factors. The highly regulated cascade of cytokines that constitute the acute inflammatory response also participate in instructing the bone healing process [116-118]. Bone injury results in the expression of a wide array of pro-inflammatory cytokines, which, along with many growth factors, particularly those from the transforming growth factor-beta (TGF-β) superfamily, result in inflammatory cell migration, angiogenesis, and mesenchymal stem cell (MSC) migration and differentiation [119-121]. For example, signaling molecules such as interleukin-6 (IL-6), tumor necrosis factor-alpha (TNF-α), and stromal cell-derived factor-1 (SDF-1) promote MSC migration *in vivo* [92, 122-124]. Osteoprogenitor cells secrete BMPs [25, 119], which together with inflammatory cytokines further enhance MSC migration, proliferation, and differentiation [125-127]. MSCs themselves have been found to play an immunomodulatory role during fracture healing [128]. Although levels of pro-inflammatory modulators are minimal during the subsequent proliferative/repair phase, their expression increases again during bone remodeling, when osteoblasts secrete IL-1, IL-6, IL-11, and other factors that promote osteoclastogenesis [127]. At this point, osteoblasts and chondrocytes become the main source of pro-inflammatory factors [120].

Typically, inflammatory cytokine and gene expression levels return to baseline approximately one week post-injury [119-121]. Resolution of inflammation is crucial; however, the inflammatory response can be perturbed by factors such as trauma or disease [129, 130], and persistent inflammation has been associated with impaired bone healing [131]. Although the inflammatory cytokines IL-6 and TNF-α were found to be necessary for

bone healing in murine models [132, 133], prolonged exposure to these molecules was associated with diminished bone volume and function [134-136]. Osteoinductive factors such as BMP-2 also play key roles in many signaling pathways related to inflammation. BMP-2 induces chemotaxis of inflammatory cells, namely lymphocytes, monocytes, and macrophages [137]. Additionally, BMP-2 supports osteoclast survival and differentiation through the enhancement of receptor activator of nuclear factor kappa-B ligand (RANKL) [138, 139]. Recently, Lee et al. determined that BMP-2 and BMP-7 induced an increase in IL-6 production in human promonocytic leukemia THP-1 cells over cells incubated with lipopolysaccharide alone, suggesting BMPs may have a more direct role in stimulating inflammation [108].

Heterotopic ossification involves a complex coordination of cellular and molecular mechanisms. During heterotopic ossification, it is thought that connective tissues are replaced by bone tissue through a process involving inflammation, muscle cell death, fibrous tissue proliferation, angiogenesis, and ossification (often endochondral) [146]. Expectedly, local tissue environmental factors (e.g., source of BMP stimulus, ability to recruit osteoprogenitor cells and induce their differentiation into bone tissue) play a major role in the extent to which heterotopic ossification occurs [141]. For example, osteogenic genes were upregulated in wounds with heterotopic mineralization compared to wounds without [147]. Despite progress in understanding the role of BMP signaling pathways in heterotopic mineralization, the cells that contribute to the pathology remain under investigation.

It is well understood that the biological effects of a growth factor are a function of the dose of growth factor delivered. Further, the consequences of supraphysiological doses of BMPs on bone healing and inflammation have not only been observed clinically but also examined in preclinical animal models. The inflammatory response following BMP-2 and

BMP-7 delivered subcutaneously or intramuscularly (IM) in collagen sponge revealed, with increasing BMP dose (1-20 μg), larger volumes of soft tissue edema and granuloma-like masses at both implantation sites and greater areas of inflammatory zones surrounding the IM implants [108]. However, regardless of BMP dose, soft tissue edema volumes peaked at 3 hours in the subcutaneous implants and 2 days for the IM implants. Regarding orthotopic delivery of BMP-2, a dog model of critically sized radial defects treated with up to 2.4 mg of BMP-2 resulted in regenerated bone with cyst-like voids and impaired mechanical properties compared to bone formed with the lowest dose of BMP-2 (150 μg) [25]. Zara et al. determined a minimum threshold dose of BMP-2—11.25 μg in a critically sized rat bone defect model—at and above which poor bone quality and heterotopic mineralization were observed [109]. Likewise in a similar rat bone defect model, 10 μg BMP-2 resulted in improved bone healing compared to higher and lower doses [110]. The osteogenic effects of other growth factors (e.g., TGF-β, fibroblast growth factor-2) have also followed a biphasic dose response, whereby osteoinductive activity and bone healing peaked at mid-range concentrations [111-113]. Nonetheless, despite progress regarding the effects of BMP-2 dose, our current understanding of these outcomes has primarily been based on gross, tissue level analyses. Notably, the majority of the literature describing the biomolecular factors that participate in the bone healing process have been determined using fracture models, not critically sized bone defects [114]. Recently, we delivered a high dose (30 μg) of BMP-2 in a well-established critically sized rat femoral segmental defect model (Aim 2A). This model recapitulated the heterotopic mineralization often observed with high dose BMP-2 and demonstrated that the total amount and pattern of BMP-mediated bone formation depend on delivery matrix. Thus, the objective of this study was to explore cellular and molecular

mechanisms of bone formation and inflammation in the context of critically sized bone defects as a function of BMP-2 dose. The hypothesis was high dose BMP-2 would elicit greater osteogenic and inflammatory gene expression in both the bone defect and muscle tissue compared to low dose BMP-2.

5.3 Materials and Methods

Surgical procedure and tissue harvesting

All procedures were approved by the Georgia Institute of Technology Institutional Animal Care and Use Committee (IACUC). Prior to surgery, slow-release buprenorphine (Wildlife Pharmaceuticals) was administered subcutaneously for analgesia. Unilateral critically sized (8 mm) femoral segmental defects were created in 13-week-old female SASCO Sprague-Dawley rats (Charles River Laboratories) as previously described [38, 41]. Defects were treated with 2.5 μg (low dose) or 30 μg (high dose) recombinant human BMP-2 (rhBMP-2; Pfizer, Inc.) in irradiated RGD-alginate hydrogel (FMC Biopolymer) injected into a poly(ε-caprolactone) (PCL) nanofiber mesh.

Animals were euthanized by CO_2 inhalation. Bone defect samples and muscle samples from operated limbs and contralateral, unoperated control limbs were harvested at 3, 7, 14, and 21 days post-surgery for subsequent PCR analyses (n=3-5) and stored in RNAlater (Ambion) at 4°C. Bone defect tissue was harvested from within the nanofiber mesh, which fully enclosed the defect space, while intact femora served as control bone tissue. Additionally, historical micro-CT analyses had revealed that a significant portion of the heterotopic mineralization was located in the region of the adductor muscles adjacent to the defect, so a 5 mm biopsy of the adductor muscles from both limbs was collected for analysis.

RNA isolation and PCR analyses

RNA was extracted using a QIAzol (Qiagen) lysis reagent and QIAshredder (Qiagen) tissue homogenizer, and purified using an RNeasy Plus Mini Kit (Qiagen). RNA from bone defect samples was concentrated with an RNeasy MinElute Cleanup Kit (Qiagen). RNA quality and concentration were determined by spectrophotometry (NanoDrop ND-1000, Thermo Scientific). Samples were stored at -80°C until conversion to cDNA. Up to 120 ng (15 ng/μL) RNA was converted into cDNA using an RT^2 First Strand Kit (SABiosciences). TaqMan® primers (Invitrogen, Table 3) for genes encoding osteogenic, myogenic, and inflammatory factors and chemokines (Table 4) were used to design custom gene arrays. Two housekeeping genes, Hprt1 and Rplp1, were included in the analyses due to their stable expression in previous qPCR studies of bone defect tissue [205]. Gene expression was quantified by real-time PCR on a Biomark HD (Fluidigm) microfluidic PCR system. To evaluate the quality of the primers and the reactions, AccuRef Rat Universal cDNA from minced rat tissues (Gene Scientific) and distilled water were used as positive and negative controls, respectively. Based on these controls, only one primer (Interleukin-4) demonstrated poor quality, and all data obtained with this primer were removed from subsequent analyses.

Table 3. Target genes for qPCR analyses.

Gene symbol	Gene name	Product #
RUNX2	Runt-related transcription factor 2	Rn01512298_m1
OSX/SP7	Osterix	Rn02769744_s1
BMP2	Bone morphogenetic protein 2	Rn00567818_m1
COL1A1	Collagen, type I, alpha 1	Rn01463848_m1
OCN/BGLAP	Osteocalcin	Rn00566386_g1
OPN/SPP1	Osteopontin	Rn01449972_m1
ON/SPARC	Osteonectin	Rn01470624_m1
RANKL/Tnfsf11	Receptor activator of nuclear factor kappa-B ligand	Rn00589289_m1
CSF1	Colony stimulating factor 1 (macrophage)	Rn00696122_m1
OPG/Tnfrsf11b	Osteoprotegerin	Rn00563499_m1
IFNG	Interferon gamma	Rn00594078_m1
TNF	Tumor necrosis factor-alpha	Rn01525859_g1
IL1A	Interleukin 1 alpha	Rn00566700_m1
CCR7	Chemokine (C-C motif) receptor 7	Rn02758813_s1
IL4	Interleukin 4	Rn99999010_m1
IL6	Interleukin 6	Rn01410330_m1
IL10	Interleukin 10	Rn00563409_m1
PAX7	Paired box 7	Rn01518732_m1
MYF5	Myogenic factor 5	Rn01502779_g1
SDF1/CXCL12	Stromal cell-derived factor 1	Rn00573260_m1
CCL3	Chemokine (C-C motif) ligand 3	Rn01464736_g1
MCP1/CCL2	Monocyte chemoattractant protein 1	Rn00580555_m1
Rplp1	Ribosomal protein, large, P1	Rn03467157_gH
Hprt1	Hypoxanthine phosphoribosyltransferase 1	Rn01527840_m1

Table 4. Classification of target genes for qPCR analyses.

Role in bone healing	Target genes
Osteogenesis	RUNX2 OSX/SP7 BMP2 COL1A1
Mineralization	OCN/BGLAP OPN/SPP1 ON/SPARC
Osteoclast differentiation	RANKL CSF1 OPG
Inflammation	TNF IFNG IL1A IL6 IL10
Chemokines/Receptors	SDF1/CXCL12 MCP1/CCL2 CCL3 CCR7
Muscle progenitors	PAX7 MYF5
Housekeeping	Rplp1 Hprt1

Statistical analyses

Target cycle threshold (Ct) values were used for subsequent analyses with the basic gene expression workflow in JMP Genomics (SAS Institute). The Ct value of a gene in a

single sample was normalized to the mean Ct value of that gene over all samples. Data were analyzed by three-way analysis of variance (ANOVA) with post-hoc pairwise comparisons. Significance level was determined using a false discovery rate (FDR) [206] with an α of 0.05. In other words, the probability of finding a false positive (type I error) among all the differentially expressed genes was 0.05.

5.4 Results

Gene expression relative to intact controls

Volcano plots allowed for visualization of genes differentially expressed between groups of interest (Figure 20). The dashed line was set based on an FDR of 0.05, so all genes above the line were considered significantly different between groups, here low dose BMP-2 treated bone defects versus intact contralateral control bone at day 3. Because a lower Ct value means higher expression of a gene, negative values on the x-axis correspond to higher expression.

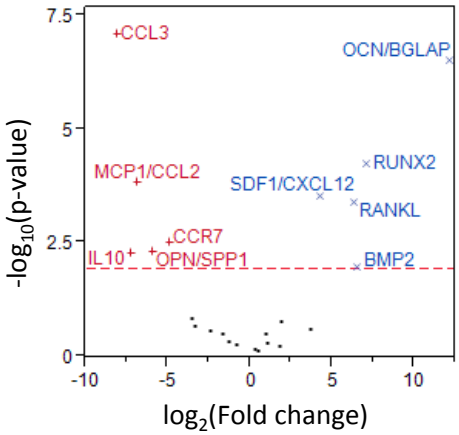

Figure 20. Representative volcano plot. Volcano plots display significance on the y-axis ($-\log_{10}$(p-value)) versus differential expression on the x-axis ($\log_2$ scale). The dashed line corresponds to an FDR of 5%, so genes above the line were considered significantly different between groups. Because a lower Ct value means higher expression of a gene, negative values on the x-axis correspond to higher expression. +Significantly greater expression for operated legs compared to control legs at Day 3 with low dose BMP-2. xSignificantly lower expression for operated legs compared to control legs at Day 3 with low dose BMP-2.

As expected, many differences in gene expression were observed between operated legs and intact control legs, particularly for bone tissue (Figure 21A). For bone defects treated with low dose BMP-2, at day 3, more inflammatory genes had higher expression, and more osteogenic genes had lower expression, while few genes were differentially expressed for high dose BMP-2 at the same time point. By day 14, low dose BMP-2 had lower inflammatory gene expression compared to intact bone, and again, more genes were differentially expressed than for high dose BMP-2 at 14 days.

Fewer differences were observed between operated leg and control muscle tissues (Figure 21B). At day 14, muscle adjacent to defects treated with low dose BMP-2 displayed greater osteogenic and lower inflammatory gene expression. For muscle adjacent to high dose BMP-2, a decrease in genes regulating progenitor cell mobilization and

osteoclastogenesis (SDF1, MCP1, and CSF1) compared to intact muscle was observed across time.

Of the two housekeeping genes, Rplp1 was found to have stable expression across tissues. As expected, no differences between control bone/muscle of low dose animals and control bone/muscle of high dose animals were found (data not shown). For reference, the expression values of intact, contralateral bone and muscle tissues used as controls in this study were also compared to those of intact, age-matched naïve bone and muscle, respectively. Minimal differences were observed between naïve samples and Day 3 and Day 7 tissues (data not shown).

A

	Low dose BMP-2	High dose BMP-2
Day 3	↑ CCL3, MCP1, IL10, CCR7, OPN ↓ SDF1, RUNX2, BMP2, RANKL, OCN	↑ CCL3, MCP1, OPN ↓ SDF1
Day 7	↑ MCP1 ↓ SDF1, OCN	↑ MCP1, IL6, OPN ↓ SDF1, BMP2, OCN
Day 14	↑ MCP1, IL6, COL1A1, OPN, ON, OSX ↓ SDF1, CCL3, IL1A, CCR7, IL10, CSF1	↑ MCP1, COL1A1, BMP2, OPN, OCN ↓ SDF1, CCL3, CSF1
Day 21	↑ MCP1, IL6, COL1A1, OPN, ON, BMP2 ↓ SDF1, CCL3, IL1A, CCR7, CSF1, OPG, PAX7	↑ MCP1, COL1A1, BMP2, OPN, ON ↓ SDF1, CCL3, IL1A, CCR7, IL10, OPG, MYF5

B

	Low dose BMP-2	High dose BMP-2
Day 3	↑ OPN —	↑ OPN ↓ SDF1
Day 7	— —	— —
Day 14	↑ COL1A1, OPN, OCN ↓ IFNG, IL6, CSF1	— ↓ MCP1, PAX7
Day 21	↑ OPN, ON —	↑ ON ↓ CSF1

Figure 21. Gene expression relative to intact controls. Arrows indicate significant differences in operated legs compared to intact controls. (A) As expected, many differences were measured between bone defects and intact control bone tissue. In both tissue types, more genes were differentially expressed with low dose BMP-2. In particular, at day 3, bone defects treated with low dose BMP-2 showed many inflammatory genes with higher expression, and many osteogenic genes with lower expression. (B) Muscle tissue adjacent to bone defects treated with high dose BMP-2 had lower expression of chemokine and osteoclastogenic genes (SDF1, MCP1, and CSF1) across time.

Temporal changes in gene expression

Temporal patterns of gene expression in bone defect tissue treated with either low dose or high dose BMP-2 were analyzed across 3, 7, 14, and 21 days post-injury (Figure 22). In general, osteogenic gene expression increased over time for low dose and high dose treated defects. However, these levels began to plateau over time for the low dose group, while steady increases in osteogenic gene expression were observed for the high dose group through 21 days. In bone defects treated with low dose BMP-2, peak expression of both pro- and anti-inflammatory factors occurred at day 3, whereas for high dose BMP-2, two pro-inflammatory factors (CCR7, IFNG) remained highly expressed through day 21. Chemokine expression was similar for low and high dose BMP-2 treated defects, with expression of MCP1 and CCL3 highest at day 3, and SDF1 expression highest at day 21. Additionally, expression of myogenic markers decreased over time in both groups.

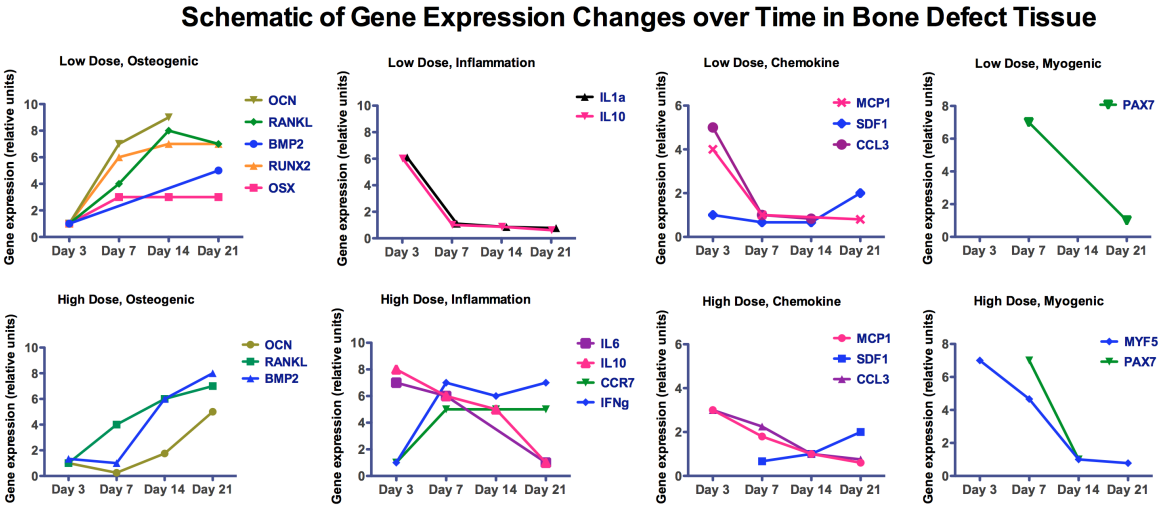

Figure 22. Schematic of changes in gene expression over time. Bone defects treated with high dose BMP-2 exhibited increasing expression of osteogenic factors through 21 days. However, these levels began to plateau for the low dose group by day 14. Inflammatory gene expression peaked at day 3 for the low dose group, while two pro-inflammatory genes (CCR7, IFNG) remained elevated through 21 days in high dose BMP-2 treated defects. For both groups, expression of chemokines and myogenic genes was reduced over time, except SDF1 expression, which peaked at day 21.

Effects of BMP-2 dose on gene expression

Bone defects treated with low dose BMP-2 resulted in heightened expression of inflammatory genes IL1A and CCR7 at day 3 compared to the high dose BMP-2 group (Figure 23A). In contrast, defects augmented with high dose BMP-2 led to greater expression of osteogenic factors RUNX2 and OCN at day 3. Muscle tissue adjacent to bone defects treated with low dose BMP-2 had higher expression of MCP1 (chemokine) at day 14 and OPN (multifunctional effector) at day 21 (Figure 23B). High dose BMP-2 resulted in greater expression of IFNG (inflammatory) at day 14.

No differences in intact bone were observed at any time point (Figure 23C). In intact muscle, while no genes had higher expression for the low dose group, high dose BMP-2 elicited greater expression of inflammatory genes IL1A and IFNG at day 7 and greater expression of the early osteogenic gene COL1A1 at day 14 compared to the low dose group (Figure 23D).

A Bone Tissue: Operated Leg

	Low dose BMP-2	High dose BMP-2
Day 3	↑ IL1A, CCR7	↑ RUNX2, OCN
Day 7	—	—
Day 14	—	—
Day 21	—	—

B Muscle Tissue: Operated Leg

	Low dose BMP-2	High dose BMP-2
Day 3	—	—
Day 7	—	—
Day 14	↑ MCP1	↑ IFNG
Day 21	↑ OPN	—

C Bone Tissue: Intact Leg

	Low dose BMP-2	High dose BMP-2
Day 3	—	—
Day 7	—	—
Day 14	—	—
Day 21	—	—

D Muscle Tissue: Intact Leg

	Low dose BMP-2	High dose BMP-2
Day 3	—	—
Day 7	—	↑ IL1A, IFNG
Day 14	—	↑ COL1A1
Day 21	—	—

Figure 23. Effects of BMP-2 dose on gene expression. Arrows indicate significant differences compared to alternate BMP-2 dose. (A) In bone defect tissue, increased expression of inflammatory (IL1A, CCR7) and osteogenic (RUNX2, OCN) factors was observed at day 3 with low and high dose BMP-2, respectively. (B) In muscle tissue of operated legs, both low dose and high dose groups resulted in increased expression of chemokine/inflammatory genes at days 14 and 21. (C) No differences were observed in intact bone tissue. (D) Intact muscle in the high dose BMP-2 group exhibited increased inflammatory gene expression at day 7 (IL1A, IFNG) and higher expression of an early osteogenic marker (COL1A1) at day 14.

Principal component analysis (PCA)

Principal component analysis (PCA) allowed for a global perspective of differential gene expression based on each factor analyzed (i.e., leg, time, and BMP-2 dose). This provided a clear visualization of the distinct separation of defect bone samples and intact control bone samples (Figure 24). Further, bone samples clustered according to time point, with day 3 and 7 samples together and day 14 and 21 samples together. No clear separation based on BMP-2 dose was observed.

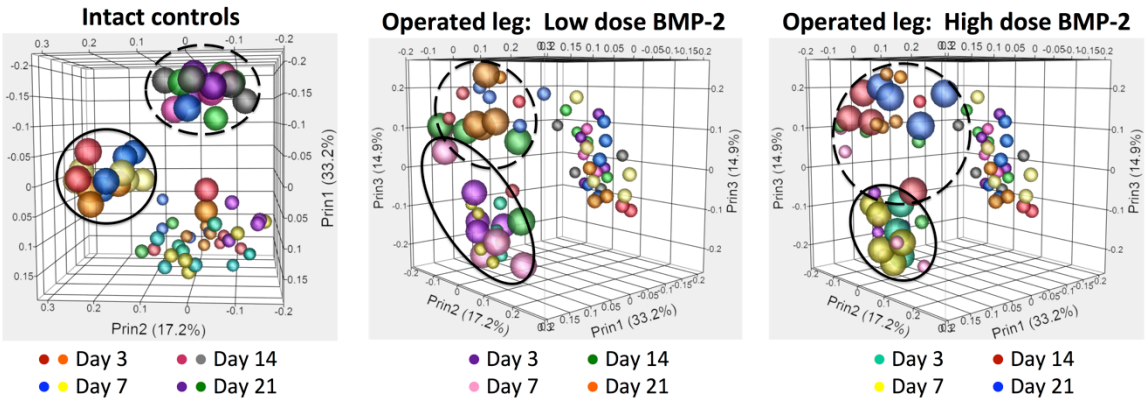

Figure 24. Principal component analysis of bone tissue. Samples of interest are enlarged. Overall, bone samples clustered according to time point (Solid circles: Day 3 and 7; Dashed circles: Day 14 and 21). Left: Intact control bone samples (enlarged) are clearly distinct from treated bone defect samples (small). Middle and right: The co-localization of low dose (enlarged in middle) and high dose (enlarged at right) samples indicated there was no clear separation of samples as a function of BMP-2 dose.

In contrast to the PCA of bone samples, PCA of muscle samples displayed no clear distinction between operated leg and control leg muscle samples (Figure 25). Similarly to bone tissues, however, muscle samples clustered according to time point, with day 3 and 7 samples together and day 14 and 21 samples together. Again, no clear separation of samples based on BMP-2 dose was observed.

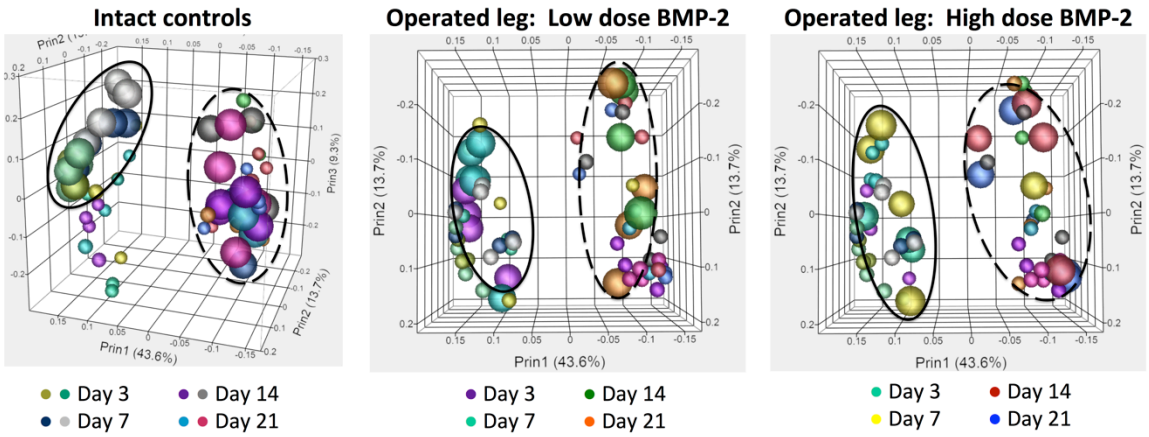

Figure 25. Principal component analysis of muscle tissue. Samples of interest are enlarged. Overall, muscle samples clustered according to time point (Solid circles: Days 3 and 7; Dashed circles: Days 14 and 21). Left: Intact control muscle samples (enlarged) are not clearly separated from operated leg muscle samples (small), especially at the 14 and 21 day time points (dashed circle). Middle and right: The co-localization of low dose (enlarged in middle) and high dose (enlarged at right) samples indicated there was no clear separation of samples as a function of BMP-2 dose.

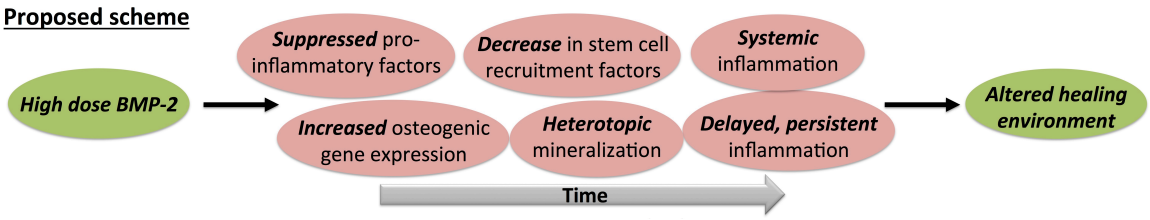

Figure 26. Proposed altered healing scheme. Low dose BMP-2 was thought to elicit healing via higher expression of inflammatory genes in bone defects early that was resolved over time. In contrast, high dose BMP-2 resulted in higher osteogenic gene expression early, which continued to increase over time. Systemic effects in intact muscle tissue were also observed with high dose BMP-2, including increased inflammatory and osteogenic gene expression.

5.5 Discussion

In Aim 2A, alginate hydrogel and collagen sponge were used to deliver high dose BMP-2 in our rat segmental bone defect model. Although the alginate delivery system facilitated significantly more bone deposition in the defect center, it did not reduce the volume of heterotopic bone compared to that of the collagen sponge. In contrast, an abundance of historical studies using low dose BMP-2 in this model did not elicit

heterotopic bone formation [38-41, 165, 188-190]. We believe that understanding cellular and molecular level changes associated with the use of high dose BMP-2 is crucial for developing therapeutics to minimize adverse effects (e.g., heterotopic mineralization, inflammation). The objective of this work was to determine the gene expression profiles in the bone defect space and adjacent muscle tissue in high dose and low dose BMP-2-mediated bone regeneration.

It is well understood that the initial inflammatory response is crucial for subsequent repair processes. In a rat fracture model, removal of the hematoma (especially days post-injury) led to impaired fracture healing [115]. Although results on their use are conflicting, nonsteroidal anti-inflammatory drugs (NSAIDs), a class of drugs commonly prescribed for pain relief, have been associated with impaired fracture healing and delayed bony union [207-209]. NSAIDs have demonstrated inhibitory effects on the proliferation and osteogenic differentiation of mesenchymal stem cells (MSCs) [210, 211], which have, themselves, been known to exhibit immunomodulatory properties during fracture healing [128]. Although the mechanism of action of NSAIDs on inflammatory cells remains unclear, these drugs are contraindicated for high-risk patient populations.

Based on the results of Aim 2A where heterotopic mineralization was observed as early as 14 days after high dose BMP-2 treatment of segmental bone defects, we explored gene expression in bone and muscle tissue at 3, 7, 14, and 21 days post-injury. We recognize that our analyses provide a snapshot of the cells only at the discrete time points chosen. Thus, additional differences in gene expression at alternate time points may have occurred but were undetected by our analyses. Additionally, although the target genes were chosen due to their known roles in inflammation, osteogenesis, and myogenesis, the custom arrays

were not an exhaustive list of the genes that invariably contribute to the complex healing process of these large bone defects.

The comparison of bone defect tissue to intact control bone revealed an increase in MCP1 expression and a decrease in SDF1 expression for both low and high dose BMP-2 treated defects at all time points. The chemokine MCP-1 functions in the recruitment of monocytes and macrophages, among other immune cells, and promotes osteoclastic differentiation. Mice lacking the gene for the MCP-1 receptor had reduced macrophage migration, impaired osteoclast function, and delayed bone healing [212, 213]. Since both BMP-2 doses used here have previously been shown to lead to functional bone regeneration in this model [39, 189], it is not surprising that MCP1 was highly expressed in bone defect tissue compared to intact bone tissue. The chemokine SDF-1 is strongly chemotactic for lymphocytes [214] and is present in high levels in the bone marrow where B cells are produced [215]; thus, the higher SDF1 expression observed in intact bone was also an expected result. Many osteogenic genes were more highly expressed in bone defects compared to intact bone tissue, except for their minimal expression levels at day 3. In particular, OPN was more highly expressed for both low and high dose BMP-2 treated defects at all time points (expect low dose at day 7). Osteopontin (OPN) is a primary component of native bone ECM, and in a fracture model of OPN knockout mice, OPN-deficient mice exhibited impaired angiogenesis and reduced late-stage bone remodeling [216].

Temporal patterns of gene expression in bone defect tissue showed two interesting differences between low dose and high dose BMP-2 treated defects. First, osteogenic gene expression levels began to plateau by day 14 for low dose BMP-2, but high dose BMP-2 resulted in steady increases in osteogenic gene expression through 21 days. In a similar result

following trauma in military personnel, osteogenic genes were upregulated in wounds that subsequently formed heterotopic mineralization [147]. Secondly, inflammatory gene expression in bone defects treated with low dose BMP-2 peaked at day 3, while for high dose BMP-2, the pro-inflammatory factors CCR7 and IFNG remained highly expressed through day 21. This suggests the bone defect microenvironment following treatment with low dose BMP-2 may allow for an earlier resolution of inflammation. Despite these differences, chemokine expression was similar for low and high dose BMP-2 treated defects, with expression of MCP1 and CCL3 highest at day 3, and SDF1 expression highest at day 21. SDF-1 is important for recruiting not only lymphocytes but also hematopoietic stem and progenitor cells [217], as well as promoting the homing of circulating osteoprogenitor cells to the site of bone injury [218, 219]. Thus, SDF-1 may serve as a compensatory mechanism to mitigate the persistent pro-inflammatory stimulus in the case of high dose BMP-2. Nonetheless, these findings are interpreted with caution until protein expression can corroborate these changes in gene expression, and this work is underway.

Although few genes were differentially expressed in the direct comparison between the two groups, low dose BMP-2 elicited higher inflammatory gene expression in bone defects at day 3, while high dose BMP-2 resulted in greater osteogenic gene expression at day 3. Notably, a heightened inflammatory response with low dose BMP-2 compared to high dose BMP-2 was contrary to our hypothesis. Nonetheless, this peak in inflammatory gene expression occurred at day 3, further supporting the theory of a more classical healing cascade with low dose BMP-2, compared to the response to high dose BMP-2, which involved persistent high expression of inflammatory genes over time (Figure 26). Just as early inflammation is necessary for healing, a significant contributor to delayed bone healing or eventual non-union is an unresolved (local or systemic) inflammatory response [114]. In a

sheep osteotomy model, inflammation was heightened and prolonged in sheep with mechanically-induced delayed bone healing [131]. Since heterotopic mineralization is believed to be stimulated by inflammation [146], the prolonged inflammation observed with high dose BMP-2 may have contributed to the initiation of this pathology.

Muscle in operated legs of both low dose and high dose BMP-2 groups exhibited increased expression of inflammatory/chemokine factors at later time points. These factors—MCP1 and OPN for low dose, and IFNG for high dose—are known to stimulate the mobilization of inflammatory cells. Interestingly, compared to intact muscle, muscle tissue adjacent to defects treated with low dose BMP-2 also displayed higher OPN expression at days 3, 14, and 21, while OPN had greater expression only at day 3 for high dose muscle. Besides modulating osteoclast recruitment and function during bone remodeling [220-222], OPN serves a variety of other crucial roles including inflammation, angiogenesis, and wound repair. OPN is important for inflammation and myogenesis during early muscle repair, and myoblasts in injured muscle have been shown to secrete osteopontin [223, 224]. Although the increase in OPN expression in injured muscle was not surprising, it is interesting to note that the differences in high dose muscle do not continue past day 3.

Although largely understudied, the systemic inflammatory response resulting from trauma such as critically sized bone defects cannot be ignored, as it too plays a role in the healing outcome. In two mouse muscle injury models, both dysregulation of BMP signaling and an inflammatory environment were necessary for heterotopic ossification to occur [150]. Inflammatory cells of hematopoietic origin have been shown to contribute to heterotopic ossification [151, 152]. Moreover, elevated levels of inflammatory cytokines both locally and systemically were associated with the development of heterotopic mineralization following combat injury [153], suggesting that local and circulating factors play a role in heterotopic

bone deposition. Furthermore, in a mouse model of polytrauma that involved either injection of bone fragments, induction of a muscle injury, or a combination of the two, the immediate (6 hours post-injury) systemic inflammatory response—IL-6 and IL-10 serum levels—were heightened as a result of the composite injury [225]. From combat operations, traumas such as blast injuries are known to elicit a higher and dysregulated inflammatory response [226, 227], and many of these patients subsequently develop heterotopic bone [228]. In this study, high dose BMP-2 led to delayed expression of inflammatory (IL1A, IFNG at day 7) and osteogenic (COL1A1 at day 14) markers in intact muscle compared to intact muscle in animals treated with low dose BMP-2. An increase in inflammatory and osteogenic genes in intact muscle suggests possible systemic effects resulting from the use of high dose BMP-2.

In general, the effects of BMP-2 dose in muscle tissue—whether operated or control muscle—were apparent at later time points than the differences observed in bone defect tissue. This is thought to be due to the time required for BMP-2 released from the alginate system to initiate chemotaxis and/or differentiation of muscle derived progenitor cells. Due to the proximity of muscle progenitors/myoblasts to bone and their ability to differentiate down the osteogenic lineage when exposed to BMP-2 [148], these cells may contribute directly to heterotopic bone formation. Muscle-derived progenitor cells from wounds that subsequently developed heterotopic bone were present in greater numbers and exhibited increased osteogenic differentiation compared to cells from wounds that did not form heterotopic bone [149]. No differences were observed in intact bone tissue as a function of BMP-2 dose, but a later time point than those chosen for this study may allow for detection of changes in the contralateral bone.

One limitation of this study was that the baseline inflammatory response to the surgery alone was not explored, and we further acknowledge that the muscle incurred significant damage in the creation of the bone defects. Though a scaffold-only group (i.e., no BMP-2) would have been an informative control, we believed the more interesting comparison for high dose BMP-2 treatment was low dose BMP-2, which has led to consistent, functional bridging of the bone defect in this model [38-41, 165, 188-190]. Previously, defects treated with alginate+mesh only (no BMP-2) had diminished osteogenic gene expression (e.g., RUNX2, OSX, BMP2, and OPN) compared to those given BMP-2 [205]. Furthermore, when only a mesh was implanted (no alginate or BMP-2), cellular infiltration into the defect was minimal at 3 days, with few macrophages and neutrophils present [229]. Although we anticipated cell number (and thus RNA yield) to be higher with chemotactic BMP-2 in this study, low amounts of RNA were obtained from bone defect samples at days 3 and 7. Despite low RNA yield, the Fluidigm system was successful in evaluating gene expression from these samples due to its pre-amplification process and sensitivity to small amounts of cDNA. Importantly, not only did the number of cells increase over the course of this study [229], but also the population/phenotype of cells likely changed over time. Therefore, the conclusions made herein were not based on changes in identical cell populations but were instead a comparison among very heterogeneous, dynamic cell populations in each tissue type as a function of BMP-2 dose. Furthermore, the large volume of (heterogeneous) tissue included in the analysis may have limited our ability to detect differences in gene expression. Particularly at the earlier time points at which the bone defect comprises primarily granulation tissue, the likelihood of measuring differential gene expression in osteoprogenitor cells (a minority of the cell population) was likely reduced. Nonetheless, increasing the sample size may have allowed for detection of

additional differences in gene expression (i.e., significant differences in more genes of a gene family), which would strengthen our conclusions.

Exploration of the gene expression profiles of tissue from bone defects and the adjacent soft tissue as a function of BMP-2 dose provided a crucial first step towards elucidating the pathological mechanisms associated with inflammation and heterotopic mineralization often observed with high dose BMP-2. By characterizing the complex bone defect environment during BMP-2 mediated bone regeneration, we may more effectively mitigate these adverse effects to promote successful bone regeneration. Modulating growth factor delivery and inflammation to better utilize endogenous repair mechanisms may allow for an improved healing response over currently used strategies.

VI. THE USE OF AMNION IN HIGH DOSE BMP-2 DELIVERY

6.1 Abstract

Due to their rich structural and biological content—extracellular matrix (ECM) proteins, immunomodulatory molecules, and a cocktail of growth factors—as well as availability for use clinically, natural ECM materials such as amniotic membrane may hold vast potential in tissue engineering applications. The treatment of large bone defects with supraphysiological doses of bone morphogenetic protein-2 (BMP-2) has been associated with clinical complications including heterotopic mineralization and inflammation, often causing pain and impaired mobility. With our rat critically sized segmental bone defect model, we have also observed heterotopic mineralization surrounding bone defects treated with high dose BMP-2, as well as local and systemic inflammatory effects. The objective of this study was to investigate the ability of amniotic membrane to attenuate heterotopic mineralization in critically sized bone defects treated with high dose BMP-2. We hypothesized that amniotic membrane surrounding collagen sponge would result in less heterotopic mineralization compared to collagen sponge alone. Amniotic membrane functioned as a reservoir for BMP-2, retaining more than PCL mesh through 21 days *in vitro*. As hypothesized, the collagen+amnion delivery system facilitated significantly less heterotopic bone deposition, which also resulted in less total bone volume compared to collagen sponge alone. Although bone formation in the defect was delayed by the presence of amniotic membrane around the defect, by 12 weeks, defect bone volumes were equivalent. Torsional stiffness was significantly reduced with amnion but was equivalent to the stiffness of intact bone. Heterogeneous cell infiltrate was observed with amnion, while the collagen group had mainly mineralized tissue present. In summary, amniotic membrane

retained significant amounts of BMP-2 *in vitro*, and amniotic membrane surrounding collagen sponge loaded with high dose BMP-2 enhanced the localization of bone formation in segmental bone defects.

6.2 Introduction

Native ECM materials such as amniotic membrane and small intestinal submucosa (SIS) represent a class of naturally derived biomaterials already employed in the clinic for tissue healing applications. With their intrinsic structural properties (proteins, glycosaminoglycans (GAGs), adhesive ligands, etc.) and ability to bind growth factors, these natural scaffolds provide an environment beneficial for resident and recruited cells [50, 51].

Amniotic membrane was used as early as 1910 for skin grafting [52] and has been used successfully for the regeneration of many tissues, including cornea [53, 54], tendon [20], and cartilage [55]. The amniotic membrane is a bioactive ECM composed of an epithelial layer, a basement membrane, a thick fibrous layer (fibroblasts within loosely crosslinked collagen, glycoproteins, and proteoglycans), and avascular connective tissue [56, 57]. Amniotic membrane contains large amounts of collagens type I and III and hyaluronan [58-60], as well as many growth factors, inflammatory mediators [51, 61], and angiogenic cytokines [62]. Although amniotic membrane materials are being increasingly used clinically, few studies have investigated the mechanisms behind the positive effects that result from their use. Furthermore, processing of the graft materials varies and is often not standardized. One patented procedure (PURION®) for amnion/chorion involves gentle cleansing, lamination of the amnion and chorion, dehydration, and devitalization (leaving cellular debris) [65]. Recently, amniotic membrane sheets processed by this method greatly improved the healing of diabetic foot ulcers compared to the clinical standard treatment [66], and micronized, injectable amniotic membrane slowed the progression of osteoarthritis in a rat

model [67]. By better understanding the mode of action and effects of ECM presentation on the cellular and healing response, we can effectively harness the endogenous repair mechanisms inherent in native tissues such as these.

SIS is one of the most commonly used ECM materials, comprising a dense collagen network (mainly types I, III, and VI) [68], glycoproteins, GAGs, and a cocktail of bioactive growth factors [69] that contribute to the scaffold's angiogenic [70], chemotactic [71], and immunosuppressive [72, 73] roles. Typically, SIS processing involves physical removal of the outer layers (leaving the submucosa and adjoining layers) followed by decellularization [74]. SIS was first used clinically in the 1960s as autograft or allograft tissue to replace dysfunctional vasculature [75]. Today, SIS grafts are primarily decellularized, porcine-derived materials, many of which are approved for clinical use and have had successful outcomes in the treatment of a variety of damaged tissues and diseases. For example, although limited mostly to case studies, CorMatrix© has been shown to function in the repair of cardiac tissues [76, 77]. In some cases, however, augmentation of diseased tissue with SIS had no benefit, or resulted in deleterious effects. For an in-depth review of SIS, see Andree et al. [50].

Similarly to amniotic membrane, SIS formulations have been tailored for different uses, including micronized SIS for cell delivery in a murine wound healing model, [78] and SIS gel for cardiac repair after myocardial infarction in the mouse [79]. Despite progress towards the characterization of SIS materials, the large degree of biological variability of native matrices such as these warrants improvements of standardized processing methods. Evaluating the biocompatibility, as well as biological and mechanical function of ECM materials post-processing is crucial for improving the biointegration and remodeling of these scaffolds. In particular, few studies have examined the host response to ECM-derived

biological materials. Allogenic and xenogenic ECM materials, even after decellularization, are capable of eliciting an immune response due to the presence of ECM proteins, which have been shown to stimulate the migration of neutrophils and macrophages [80-82]. Differences in the inflammatory profiles of noncrosslinked Restore™ SIS (pro-healing M2 macrophages) and crosslinked CuffPatch™ SIS (pro-inflammatory M1 macrophages) have been observed in a rat abdominal wall defect model [83].

Due to their rich biological content—a cocktail of growth factors and cytokines, including immunomodulatory molecules—as well as structural integrity afforded by the abundance of collagens and proteoglycans, ECM materials such as amniotic membrane may hold vast potential for tissue engineering. Effectively harnessing BMP-2, particularly via a clinically available material such as amniotic membrane that may function to retain BMP-2 and localize bone formation, could improve the current treatment paradigm for large bone defects. Accordingly, our *objective* was to investigate the ability of amniotic membrane to attenuate heterotopic mineralization in critically sized bone defects. We *hypothesized* that amniotic membrane surrounding collagen sponge would result in less heterotopic mineralization compared to collagen sponge alone.

6.3 Materials and Methods

rhBMP-2 release kinetics

To evaluate BMP-2 binding and release, 8-mm diameter disk-shaped samples (n=6) of dehydrated human amnion/chorion membrane (dHACM, MiMedx Group, Inc.) and poly(ε-caprolactone) (PCL) nanofiber mesh fabricated as described previously [40] were prepared using a biopsy punch. The specific amnion membrane product used was AmnioFix®; during processing, the epithelial layer was removed prior to dehydration. For BMP-2 binding, samples were incubated in 1 mL PBS containing 0.1% (w/v) bovine serum

albumin (BSA, Millipore Corporation) and 350 ng recombinant human BMP-2 (rhBMP-2, Pfizer, Inc.) for 18 h at 37°C. Construct-free wells served as controls, and the amount of BMP-2 remaining in construct-containing wells was subtracted from BMP-2 remaining in construct-free wells to determine the amount of BMP-2 initially bound [230]. For the release assay, samples were transferred to new wells, and the PBS solution was collected and replaced at 6 h, and at 1, 2, 4, 7, 14, and 21 days. Initial BMP-2 remaining in solution (unbound) and BMP-2 released over time were measured via an enzyme-linked immunosorbent assay (ELISA, R&D Systems).

Surgical procedure

Unilateral 8-mm (critically sized) femoral segmental defects were created in 13-week-old female SASCO Sprague-Dawley rats (Charles River Laboratories) as described previously [41]. A radiolucent polysulfone plate served as the internal fixation device, and the defects were created in the mid-diaphysis of the femur with an oscillating saw. The defects were treated with 30 μg recombinant human BMP-2 (rhBMP-2) (Pfizer, Inc.) in bovine type I collagen sponge (Kensey-Nash Corp.) alone or collagen sponge surrounded by amnion (dHACM, MiMedx Group, Inc.) (n=11). 150 μL of 0.1% (w/v) rat serum albumin (RSA, Sigma) in 4 mM HCl containing 30 μg of rhBMP-2 was added drop wise to the collagen sponge and allowed to adsorb for 10 minutes before implantation. For the amnion group, amnion was cut into 1.5 x 2.0 cm rectangle pieces and wrapped around the hydrated collagen sponge with the amnion layer facing outwards. During implantation, the collagen was press-fit into the defect, and for constructs containing amnion, the ends of the amnion were placed around the native bone ends. For analgesia, slow-release buprenorphine (Wildlife Pharmaceuticals) was administered prior to surgery. Animals were euthanized by CO_2

inhalation at 12 weeks post-surgery. All procedures were approved by the Georgia Institute of Technology Institutional Animal Care and Use Committee (IACUC).

Radiography and micro-computed tomography

Bone regeneration was assessed via radiography and micro-CT through 12 weeks. For micro-computed tomography (micro-CT) analyses to quantify bone volume (BV), two volumes of interest (VOIs) were used: a 6-mm diameter to characterize mineralization inside and bordering the defect (defect BV), and a large diameter including all bone formation within the thigh (total BV). Heterotopic bone volume was defined as the difference between these two VOIs.

Biomechanical testing

Ex vivo torsional testing to failure of femora (n=8) at 12 weeks provided a functional measure of the regenerated bone. For detailed methods, see [41]. After removal of the fixation plate and soft tissue, native bone ends were placed in Wood's metal (Alfa Aesar). Torsional testing to failure was performed at 3° per second (ELF 3200; Bose ElectroForce Systems Group). Maximum torque to failure and torsional stiffness were calculated from the resultant torque-rotation curves.

Histology

Histology was used to further characterize the distribution and maturation of newly formed bone within and surrounding the bone defect space (n=3). Samples were harvested at 12 weeks, fixed in 10% neutral buffered formalin for 48 h, and decalcified in a mild formic acid solution (Immunocal, Decal Chemical Corp.), which was changed three times a week for two weeks. After paraffin embedding, samples were sectioned by a tape transfer technique (Section Labs, Hiroshima, Japan) to obtain 5 μm mid-sagittal sections. Sections were stained with hematoxylin and eosin (H&E) to visualize the global cellular response,

residual collagen sponge and amnion materials, and spatial extent of mineralization. Mallory's modified aniline blue stain was used to distinguish mature and immature osteoid as described previously [9, 22-25].

Statistical Analyses

All data are reported as mean ± standard error of the mean (SEM). Data were analyzed using GraphPad Prism 5 (GraphPad Software, Inc.). BMP-2 release kinetics and bone volumes from micro-CT were analyzed by two-way repeated measures analysis of variance (ANOVA), with Bonferroni post hoc tests for pairwise comparisons. Biomechanical testing data was evaluated by t-tests. A p-value less than 0.05 was considered statistically significant.

6.4 Results

rhBMP-2 release kinetics

After 18 hours incubation in BMP-2 solution, both amnion and PCL mesh disk-shaped samples bound approximately 100 ng of BMP-2 (Figure 27A). As a percentage of bound BMP-2, significantly more BMP-2 was released over 21 days from PCL mesh compared to amnion ($p<0.001$, Figure 27B).

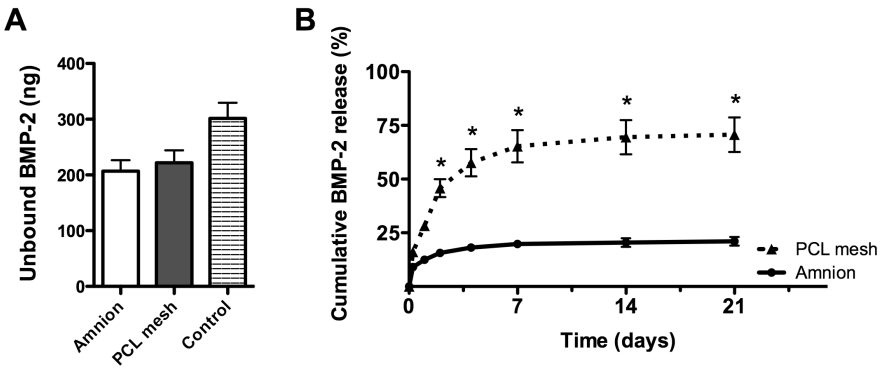

Figure 27. BMP-2 binding and release. (A) Both amnion and PCL mesh samples bound approximately 100 ng of BMP-2 after 18 h. (B) Significantly more of this bound BMP-2 was released over 21 days from PCL mesh compared to amnion (*$p<0.001$).

Radiography and micro-computed tomography

Representative radiographs of defects treated with high dose BMP-2 in collagen sponge alone (top) or with amnion (bottom) at 2, 4, 8, and 12 weeks post-operatively allowed for qualitative comparison of new bone formation (Figure 28). The total amount of mineralization, and especially the heterotopic mineralization located outside the bone defect area, appeared to be attenuated in the amnion group.

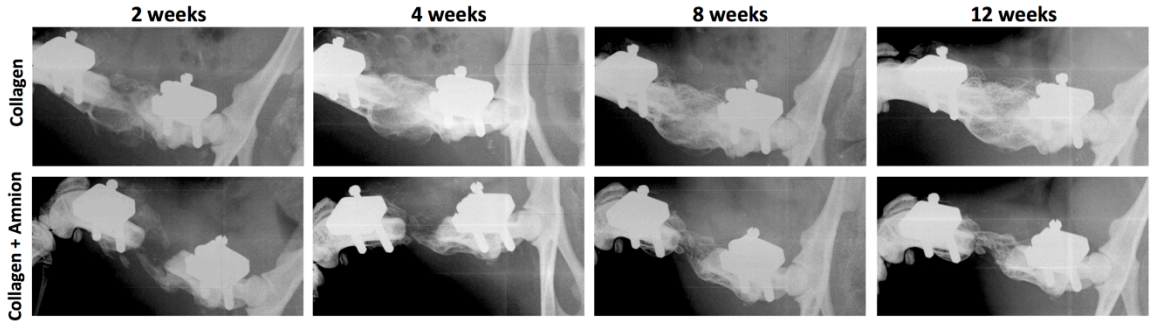

Figure 28. Radiographs of bone defects through 12 weeks. Representative radiographs of defects treated with high dose BMP-2 in collagen sponge alone (top) or collagen sponge with amnion (bottom) at 2, 4, 8, and 12 weeks post-operatively. Mineralization—in particular, heterotopic mineralization—appeared to be reduced in the amnion group.

Micro-CT analyses provided spatially distinct measurements of bone volume. Total bone volume (BV) increased over time and was significantly higher in the collagen group at 4, 8, and 12 weeks ($p<0.05$, Figure 29A). Bone volume within the defect region was also significantly higher in the collagen group at 4 and 8 weeks ($p<0.05$, Figure 29B). Although defect mineralization was delayed in the amnion group, defect BVs were equivalent between groups by 12 weeks. As hypothesized, heterotopic BV was significantly reduced at 8 and 12 weeks in the presence of amnion ($p<0.05$, Figure 29C). Bone density maps of the total bone volume (Figure 29D, top) and a mid-sagittal cross-section through the volume (bottom) allowed for visualization of a dense heterotopic shell and an inner sparse trabecular structure in the collagen group. In contrast, the majority of mineralization in the collagen+amnion group was present in the defect region.

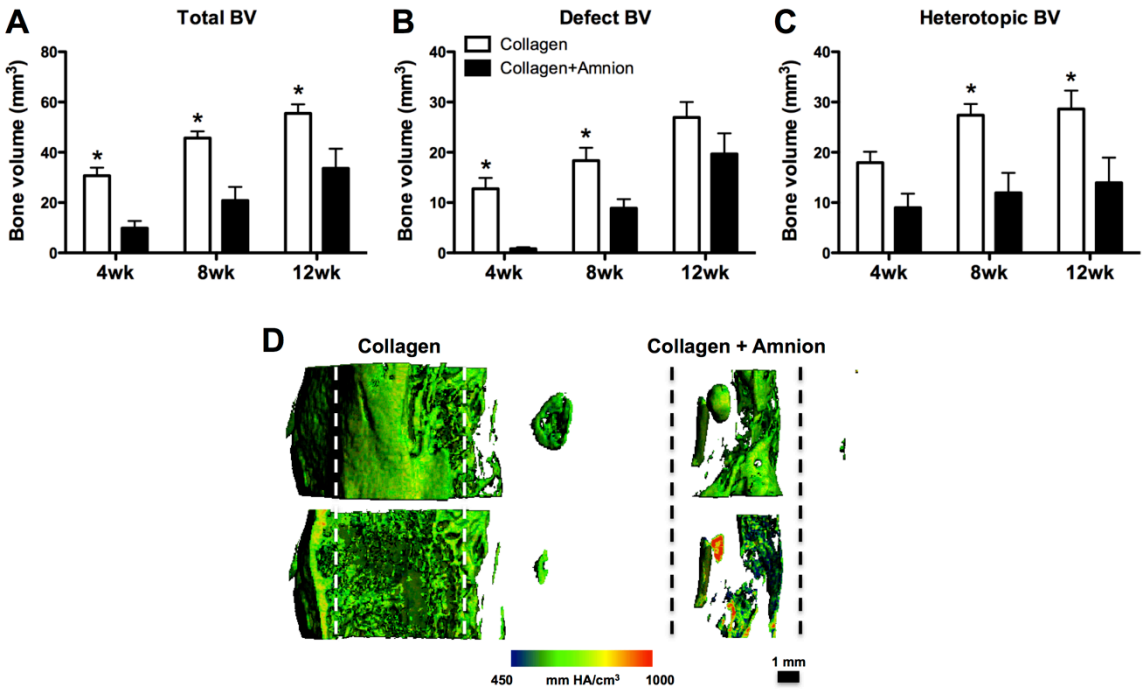

Figure 29. Spatial distribution of bone volume and bone mineral density maps. (A) Total bone volume (BV) increased over time and was significantly higher in the collagen group at 4, 8, and 12 weeks (*$p<0.05$). (B) Defect BV was delayed in the collagen+amnion group but by 12 weeks was not significantly different from the collagen group. (C) Heterotopic BV was significantly reduced at 8 and 12 weeks in the presence of amnion (*$p<0.05$). (D) Bone density maps of total BV. Top: entire volume. Bottom: mid-sagittal cross-section through volume. Dashed lines indicate the borders of the defect region. Dense heterotopic bone and a sparse inner trabecular structure were visible in the collagen group. Minimal heterotopic bone was observed in the collagen+amnion group.

Biomechanical testing

Biomechanical testing of the regenerated bone at 12 weeks was used as a measure of the functional recovery of the tissue. Maximum torque to failure was similar between groups (Figure 30A). However, torsional stiffness was significantly attenuated with amnion, likely due to the minimal heterotopic bone present (Figure 30B, $p<0.05$). Nonetheless, stiffness for amnion was similar to that of intact bone.

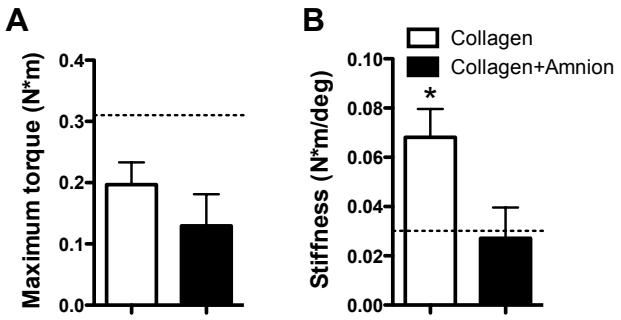

Figure 30. Functional assessment of the regenerated bone at 12 weeks. Dashed lines indicate mean values for historical intact control bone [40]. (A) Maximum torque to failure was similar between groups. (B) Torsional stiffness was significantly attenuated with amnion (*$p<0.05$), but stiffness for amnion was similar to that of intact bone.

Histology

Mid-sagittal histological sections were used to observe regenerating bone tissue at 12 weeks. With amnion, heterogeneous cell infiltrate was observed throughout the dense tissue in the defect space, and this hypercellularity appeared adjacent to the residual amnion tissue (Figure 31A, C). Orange staining of the amnion with Mallory's staining suggested early mineralization of the tissue (Figure 31C). In addition to the remaining amnion, a significant portion of collagen sponge was present at 12 weeks. In contrast to the collagen+amnion group, the collagen only group had predominantly mineralized tissue in the defect (Figure 31B, D). This bone tissue had a highly trabecular-like structure and was surrounded by small amounts of marrow tissue.

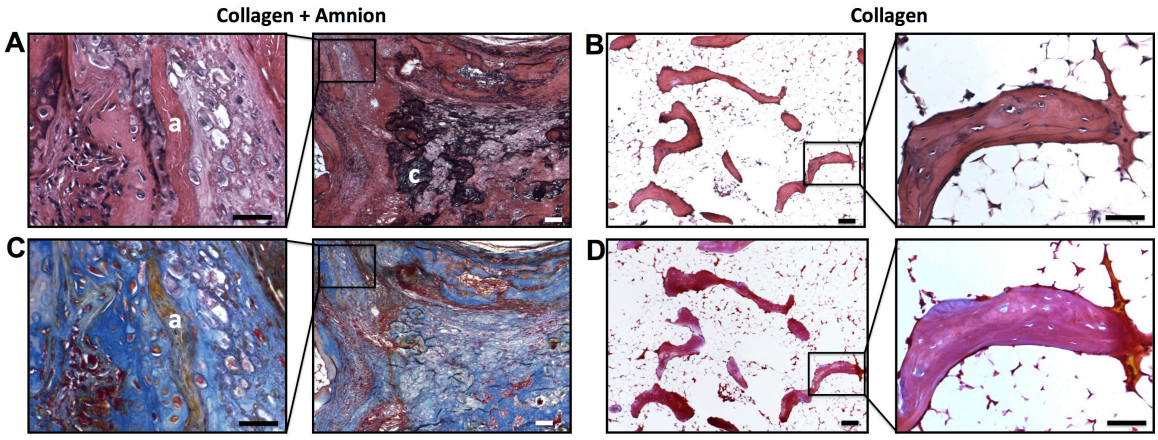

Figure 31. Bone defect tissue at 12 weeks. (A-B) H&E and (C-D) Mallory's aniline blue staining (mineral: orange-red). (A, C) In collagen+amnion treated defects, residual amnion (a) and collagen sponge (c) were visible. More cell infiltrate was present in the amnion group. (C) Orange staining of the amnion suggested early mineralization. (B, D) In the absence of amnion, the collagen sponge was resorbed. The lamellar structure and orange-red staining of the bony spicules was indicative of highly mineralized tissue. 4x scale bar = 100 μm. Insets: 20x scale bar = 50 μm.

6.5 Discussion

Traumatic bone injuries, and particularly critically sized defects, necessitate surgical intervention for repair, often involving augmentation with supraphysiological amounts of BMP-2. Adverse effects such as heterotopic mineralization and inflammation observed with high dose BMP-2 can be compounded by the delivery of high dose BMP-2 within collagen sponge, which has limited ability to retain growth factor. Therefore, if high doses of growth factors must be used, a crucial need exists for biomaterials capable of localizing and retaining these growth factors to the site of injury. Following upon Aim 2 where we modeled adverse effects of high dose BMP-2 (e.g., heterotopic mineralization, altered inflammatory response) in a rat segmental bone defect model, the objective of this study was to evaluate the efficacy of amniotic membrane to attenuate heterotopic bone formation with high dose BMP-2 treatment.

Amniotic membrane functioned as a reservoir for BMP-2, retaining more BMP-2 than PCL mesh scaffolds through 21 days *in vitro*. As hypothesized, heterotopic mineralization was reduced with amnion surrounding collagen sponge compared to collagen sponge alone. The attenuated heterotopic mineralization may be attributed to amnion functioning as a biological sink to retain BMP-2, as amniotic membrane is known to harbor a wide array of growth factors and cytokines [51, 61, 62, 231, 232]. Furthermore, the patented PURION® process has been shown to maintain the biological activity of the amnion [51], so it is likely the amnion bound (possibly permanently) a portion of the BMP-2 following release from the collagen scaffold. Additionally, the immunomodulatory factors present in the amnion [51, 61] may have tempered the inflammatory response such that the subsequent pathogenesis of heterotopic ossification was minimized.

The reduction in heterotopic bone deposition with collagen+amnion contributed to the lower total bone volume present in this group compared to collagen alone. Although bone formation in the defect was delayed by the presence of amnion around the defect, by 12 weeks, defect bone volumes were equivalent. This phenomenon of delayed healing in defects surrounded by a scaffold lacking macropores was observed previously with this rat model, where bone healing was accelerated in the presence of macroporous PCL mesh surrounding the defect [40]. Similarly, in a critically sized sheep tibial defect model, membrane perforations were necessary for successful bone regeneration [233, 234]. In a composite bone and muscle injury model, early vasculature was impaired compared to bone injury alone, and a significant amount of vessel ingrowth into the defect region occurred through the holes in the PCL mesh [235]. Collectively, these findings underscore the importance of sufficient interaction of the bone defect space with the surrounding muscle tissue, which is thought to provide an excellent source osteoprogenitor cells, growth factors,

and vasculature. In a pilot study of amnion surrounding defects treated with low dose BMP-2, no differences in vascular volume were observed at 12 weeks (data not shown). However, the 12 week time point is most likely too late to measure any differences that may have been present around weeks 2 to 4 when vascularization plays a crucial role in initiating the bone healing process [236].

In the present study, amnion tissue was still present at 12 weeks and may have impaired cellular infiltration into the defect space, thus contributing to the delayed bone formation in the defect. Prior analyses determined that amnion tissue had an effective pore size on the order of nanometers and was capable of supporting cell attachment on the surface but limited the invasion of cells into the scaffold [237]. Primarily composed of dense connective tissue, the amnion/chorion membrane used here is ~100 μm thick [61] and contains an abundance of collagens and proteoglycans [58-60]. Physiologically, amnion plays a major structural role *in situ* by containing the developing fetus and amniotic fluid throughout pregnancy [238]. Thus, in addition to playing a biological role, the amnion may be a physical barrier to contain BMP-2 within the defect space, while adversely limiting cell invasion into the defect. Likely, both the structural and biological properties of the amniotic membrane contributed to the reduced heterotopic mineralization, though more investigation into the mechanisms of their efficacy is necessary. Future work with macroporous amniotic membrane may be able to tease out whether the biological or physical role of the membrane is more crucial in its ability to minimize heterotopic bone deposition.

Although *ex vivo* torsional testing resulted in reduced torsional stiffness in the collagen+amnion group, it was equivalent to the stiffness of intact bone. From micro-CT analyses of bone volumes, amniotic membrane delayed bone healing inside the defect space through 8 weeks. However, in parallel to the equivalent defect bone volumes at 12 weeks,

torsional testing at 12 weeks indicated the functional recovery to intact bone properties of bone defect tissue treated with collagen+amnion was not impaired. In contrast, the average torsional stiffness for the collagen group was approximately double that of intact bone. These results are similar to the findings in Aim 2A, where the alginate+mesh and collagen+mesh delivery systems resulted in torsional stiffness values double that of intact bone, and both also had a significant amount of heterotopic bone present. Based on the equation for torsional stiffness,

$$k_t = \frac{G \text{ x } J_{avg}}{L}$$

where G is the elastic shear modulus, J_{avg} is the average polar moment of inertia (pMOI), and L is the gauge length, an increase in average pMOI resulting from a widely distributed pattern of bone formation (i.e., heterotopic bone) would cause a proportionate increase in torsional stiffness. Here, heterotopic bone is believed to be the primary contributor to the increased torsional stiffness observed in the collagen only group.

One limitation of this study was the evaluation of human amnion tissue (xenograft) in immunocompetent rats. Histology at 12 weeks revealed a large amount of heterogeneous cell infiltrate in the collagen+amnion group, while the collagen group had mainly trabecular-like mineralized tissue present. The delayed/incomplete degradation of the amnion may have elicited a heightened (inflammatory) cellular response, leading to the formation of a fibrous capsule. This hypercellularity, however, was not present adjacent the nanofiber mesh (surrounding alginate or collagen sponge) with high dose BMP-2 delivery at 12 weeks (Aim 2A), or in historical studies in these delivery systems with low dose BMP-2 [39, 165]. Further exploration is needed to determine specific phenotypes of inflammatory cells that likely invaded in response to amnion implantation, and development of IHC protocols is ongoing. In particular, at this late time point of 12 weeks, examination of T cell phenotypes of the

adaptive immune response would be interesting to explore. Nonetheless, a similar hypercellular response to human micronized amnion was observed in the joint space in a rat osteoarthritis model [67]. In that study, the cells, believed to be mononuclear cells, were adjacent to amnion particles, and the response persisted throughout the study to 21 days. In our case, the delivery of amnion in the bone defect region would be expected to further exacerbate the inflammatory/immune response beyond that seen in an immunoprivileged location such as the joint space. Despite the cleansing and devitalization that occurs during processing of the tissue, a portion of the cellular debris persists, and the immunogenicity of this cellular debris remains unknown [239]. We observed moderate inflammatory infiltrate mostly in the area of residual amnion tissue, and this response may have contributed to the delay in bone healing. Nonetheless, the clinical use of these grafts, which are allogeneic in nature, may result in attenuated inflammatory/immune responses compared to the heightened response observed in the current rat model.

In summary, amniotic membrane retained significant amounts of BMP-2 *in vitro*, and amniotic membrane surrounding collagen sponge loaded with high dose BMP-2 enhanced the localization of bone formation in segmental bone defects. One major advantage of the materials used in this study is their availability for use clinically, which would drastically accelerate the translation of amnion for bone regeneration applications. Although heterotopic bone was minimized, future studies are needed to elucidate mechanisms behind the initial delayed healing response observed with amniotic membrane.

VII. SUMMARY AND CONCLUSIONS[4] [5]

7.1 Overall Summary

Large bone defects resulting from trauma or tumor resection require augmentation of the tissue with allograft, autograft, or other bone substitute to heal these challenging injuries. As such, half a million bone grafting procedures take place every year in the United States alone, accounting for approximately $2.5 billion in medical expenses [17]. Thus, tissue engineering strategies based on osteoinductive cell and/or growth factor delivery provide much promise for improving therapies for bone regeneration. In particular, taking advantage of clinically approved biomaterials and growth factors by harnessing their healing efficacy for bone tissue engineering may accelerate the time line for translation of these therapeutics.

Growth factors approved by the FDA for osteoinduction are recombinant human bone morphogenetic protein-2 (rhBMP-2) and rhBMP-7 delivered via bovine collagen sponge, for use in spinal fusion, open tibial fractures, and non-unions [25, 26]. To date, however, these strategies remain inferior to autograft treatment, mainly due to the limited knowledge regarding efficacious dose, delivery method, and spatial and temporal distribution of the factor(s), as well as possible complications in the surrounding soft tissues (e.g., inflammation). These and other limiting factors necessitate the development of improved

---

[4] Portions of this chapter were adapted from Allen A B, Priddy L B, Li M T, Guldberg R E. Functional augmentation of naturally-derived materials for tissue regeneration. *Ann Biomed Eng*, 43(3), 555-567, 2015. License No. 3630480316395

[5] Portions of this chapter were adapted from Priddy L B, Chaudhuri O, Stevens H Y, Krishnan L, Uhrig B A, Willett N J, Guldberg R E. Oxidized alginate hydrogels for bone morphogenetic protein-2 delivery in long bone defects. *Acta Biomaterialia*, 10(10), 4390-4399, 2014. License No. 3603720780456

delivery systems [240], particularly for such potent growth factors, to maximize their healing potential while mitigating harmful side effects often associated with their use [29, 30].

Growth factor delivery has shown promise for healing large bone defects, albeit with limitations at present. Thus the goal of this thesis was to investigate hybrid biomaterial systems with controlled strategies for BMP-2 delivery to promote structural and functional restoration of segmental bone defects. Design of an effective biomaterial carrier must include careful consideration of a number of factors, including biomaterial degradability or ability to allow tissue ingrowth, and localization of growth factors to the site of injury to promote efficient healing and minimize negative effects. In particular, developing strategies to mitigate adverse effects associated with the use of high dose BMP-2 (e.g., heterotopic ossification, chronic inflammation) may improve the healing of large bone defects. Finally, understanding the role that specific cells and cytokines play in the processes of inflammation and bone healing, particularly in the context of large bone defects, is crucial for improving regenerative strategies.

Bone tissue regeneration may be impeded by the presence of residual biomaterials at the injury site. Therefore, understanding the timelines of protein release and the impact of timing of biomaterial degradation on bone healing is crucial for complete restoration of the form and function of bone tissue. In Chapter 3, we utilized an alginate modified by both irradiation and oxidation, thus a lower molecular weight and more degradable hydrogel. As a biomaterial, alginate is practical and easy to use due to its amenability to gentle crosslinking and injection. Previous studies in our lab have shown slower BMP-2 release and improved bone regeneration with irradiated alginate hydrogel+mesh compared to the clinically used collagen sponge [39, 165]. Therefore, in introducing an additional structural modification into the alginate, the goal was to maintain the appropriate BMP-2 release profile and ease of

use of the irradiated alginate, while accelerating alginate degradation to augment bone tissue interconnectivity and formation/maturation.

The release of BMP-2 from oxidized-irradiated alginate was accelerated compared to that from irradiated alginate. Although this accelerated BMP-2 release from oxidized-irradiated alginate did not lead to an increase in osteoblastic differentiation, both constructs contained bioactive BMP-2 after 26 days *in vitro*. *In vivo* bone mineral density was significantly greater at 8 weeks in the oxidized-irradiated group. Histological analyses at 12 weeks revealed enhanced degradation of oxidized-irradiated alginate and the appearance of more organized, lamellar bone. The difference in size distribution of residual alginate suggested that oxidation of irradiated alginate increased the degree of hydrolytic degradation. The more diffuse and fragmented oxidized-irradiated alginate may have allowed for an increase in cellular infiltration into the defect space, thereby promoting more rapid formation of organized, lamellar bone. Moreover, the breakdown of the oxidized-irradiated alginate may have been accelerated as the material degraded due to greater cellular invasion into the defect space. However, enhanced fragmentation of oxidized-irradiated alginate did not translate into augmented bone repair, as no differences in bone volume or mechanical properties were observed. Nonetheless, scaffold degradation remains a critical design parameter for evaluating the efficacy of growth factor delivery vehicles in tissue engineering.

Traumatic bone injuries, and particularly critically sized defects, necessitate surgical intervention for repair, often involving augmentation with BMP-2. However, the selection of BMP-2 dose is frequently empirical in nature, leading to the use of doses higher than necessary [30]. Supraphysiological doses of BMP-2 are known to elicit adverse effects such as heterotopic mineralization, inflammation, and impaired bone quality [29, 30, 108, 109]. Because the hybrid irradiated alginate+mesh delivery system had demonstrated efficacy in

slowing the release of low dose BMP-2 compared to collagen sponge [39], we hypothesized that the alginate+mesh would reduce heterotopic mineralization when loaded with a high dose of BMP-2 (Chapter 4, Aim 2A). Since oxidized-irradiated alginate showed limited improvements over irradiated alginate (Chapter 3, [189]), the irradiated alginate was chosen for Aim 2 studies.

The burst release of BMP-2 from the alginate+mesh was dampened compared to collagen sponge+/-mesh *in vitro*. In the rat segmental defect model, the alginate delivery system facilitated significantly more bone deposition in the central defect region (8 and 12 weeks) as well as greater total bone volume (12 weeks). Surprisingly, the total bone volume in this study was comparable to that seen with lower doses of BMP-2 in alginate hydrogel [189, 190]. The higher defect bone volume was likely due in part to delayed degradation and increased retention of BMP-2 in the alginate compared to the faster degrading collagen sponge [197]. However, contrary to our hypothesis, the alginate+mesh did not reduce the volume of heterotopic bone. The burst release of a large portion (>25%) of the delivered BMP-2 within the first 5 days from both delivery systems may have resulted in the large heterotopic bone formation seen in both groups. Moreover, the initial delay in burst release from the alginate group was insufficient in significantly reducing the heterotopic bone formation in the surrounding soft tissue. The heightened early cellular infiltration seen in the collagen sponge treated defects may be a result of the accelerated release of BMP-2 or the presence of the (bovine) collagen sponge itself.

The lack of significant differences between the two scaffolds in their functional biomechanical properties, as evaluated by failure in torsion, was as expected based on the extent of heterotopic bone formation, both in its volume and spatial extent (pMOI) for both scaffold groups. Though better central bone formation was seen with alginate group, the

comparable functional mechanics obtained even from the more heterotopically distributed bone in the collagen scaffolds provided insights into the continued use of these scaffolds in clinical care, especially since the torsional stiffness values were more than twice that of intact bone. Nonetheless, these stark differences in amount and distribution of *de novo* bone suggest the alginate hybrid delivery system may be superior to clinically used collagen sponge for high dose BMP-2 treatment of large bone defects. Contributions of this work include: (i) characterization of an orthotopic model that recapitulates adverse effects associated with high dose BMP-2 delivery and investigation of the factors contributing to these consequences, and (ii) evaluation of the hybrid alginate-PCL mesh delivery system for enhanced localized bone formation with high dose BMP-2 treatment.

It is thought that the pathway to healing versus chronic inflammation is determined soon after injury. Thus, advancing our understanding of the cellular and molecular factors that participate in the bone repair process in a critically sized bone defect model may allow for the development of improved tissue engineering strategies. Subsequently in Aim 2, we investigated variations in gene expression as a function of BMP-2 dose in the defect site and adjacent muscle during the inflammatory and early repair phases of our bone defect model (Chapter 5, Aim 2B). The irradiated alginate+mesh vehicle was used to deliver either a low (healing) dose of BMP-2 akin to that used in Aim 1, or the high dose used in Aim 2A. The hypothesis was that high dose BMP-2 would elicit greater osteogenic and inflammatory gene expression compared to low dose BMP-2.

Bone defects treated with high dose BMP-2 exhibited increasing expression of osteogenic genes through 21 days. However, these levels began to plateau for the low dose group by day 14. Similar findings following trauma in military personnel have been observed, whereby osteogenic genes were upregulated in wounds that subsequently formed heterotopic

mineralization [147]. Additionally, inflammatory gene expression peaked at day 3 for the low dose group, while two pro-inflammatory genes (CCR7, IFNG) remained elevated through 21 days in high dose BMP-2 treated defects. This suggested the bone defect microenvironment following treatment with low dose BMP-2 may allow for an earlier resolution of inflammation compared to the response following high dose BMP-2 treatment.

In the direct comparison between BMP-2 doses, contrary to our hypothesis, low dose BMP-2 elicited heightened inflammatory gene expression at day 3 in bone defect tissue. In contrast, high dose BMP-2 resulted in increased osteogenic gene expression in bone defects at day 3, and heightened expression of inflammatory and osteogenic genes in intact, unoperated limb muscle, indicating both local and systemic effects, respectively. The greater inflammatory gene expression at day 3 with low dose BMP-2 further supported the theory of a more classical healing cascade, since early inflammation is necessary for healing. Likewise, a significant contributor to impaired bone healing is an unresolved (local or systemic) inflammatory response. Since heterotopic mineralization is believed to be stimulated by inflammation [146], the prolonged and systemic inflammation observed with high dose BMP-2 may have contributed to the initiation of this pathology. Overall, the studies in Aim 2 provided insight into the effects of supraphysiological BMP-2 on the spatiotemporal patterns of bone formation, as well as the cells and signaling factors that play a role in this process. By characterizing the complex bone defect environment during BMP-2 mediated bone regeneration, we may more effectively mitigate these adverse effects to promote successful bone regeneration.

Due to their rich structural and biological content—ECM proteins, immunomodulatory molecules, and a cocktail of growth factors—as well as availability for use clinically, natural ECM materials such as amniotic membrane may hold vast potential in

tissue engineering applications. Despite the efficacy of BMP-2 for bone regeneration, the adverse effects of BMP-2 at supraphysiological doses (e.g., heterotopic bone formation, tissue swelling) warrant the investigation of strategies to attenuate these negative reactions. Since heterotopic mineralization was observed with a proportionately high dose of BMP-2 in our rat segmental bone defect model (Chapter 4), one subsequent objective was to evaluate the ability of amniotic membrane surrounding the bone defect space to attenuate heterotopic mineralization in critically sized bone defects treated with high dose BMP-2 (Chapter 6). Collagen sponge was chosen as the delivery vehicle for BMP-2 because it is an FDA-approved device. If successful in reducing heterotopic mineralization, the amniotic membrane (also clinically available) wrapped around collagen sponge could have an immediate impact in the clinic.

Amnion membrane retained more BMP-2 than PCL mesh did through 21 days *in vitro*. As hypothesized, the collagen+amnion delivery system reduced heterotopic bone deposition, which also resulted in less total bone volume compared to collagen sponge alone. Although bone formation in the defect was delayed by the presence of amnion membrane around the defect, by 12 weeks, defect bone volumes were equivalent. This phenomenon of delayed healing in defects surrounded by a scaffold lacking macropores was observed previously with this rat model, where bone healing was accelerated in the presence of macroporous PCL mesh surrounding the defect [40]. Similarly, in a critically sized sheep tibial defect model, membrane perforations were necessary for successful bone regeneration [233, 234]. These findings underscore the importance of sufficient interaction of the bone defect space with the surrounding muscle tissue, which is thought to provide an excellent source osteoprogenitor cells, growth factors, and vasculature. Likely, both the structural and

biological properties of the amniotic membrane contributed to the reduced heterotopic mineralization, though more investigation into these mechanisms is necessary.

Torsional stiffness was significantly reduced with amnion but was equivalent to the stiffness of intact bone. These results are similar to the findings in Aim 2A, where the alginate+mesh and collagen+mesh delivery systems (both containing a significant amount of heterotopic bone) resulted in torsional stiffness values double that of intact bone. Here, heterotopic bone was believed to be the primary contributor to the increased torsional stiffness observed in the collagen only group.

Heterogeneous cell infiltrate was observed with amnion, while the collagen group had mainly mineralized tissue present. The delayed/incomplete degradation of the amnion may have elicited a heightened (inflammatory) cellular response, leading to the formation of a fibrous capsule. A similar hypercellular response to human micronized amnion was observed in the joint space in a rat osteoarthritis model [67]. In that study, the cells, believed to be mononuclear cells, were adjacent to amnion particles, and the response persisted throughout the study to 21 days. In our case, the delivery of amnion in the bone defect region would be expected to further exacerbate the inflammatory/immune response beyond that seen in an immunoprivileged location such as the joint space. Despite the cleansing and devitalization that occurs during processing of the tissue, a portion of the cellular debris persists, and the immunogenicity of this cellular debris remains unknown [239]. Of note, this hypercellularity was not observed adjacent the nanofiber mesh (surrounding alginate or collagen sponge) with high dose BMP-2 delivery at 12 weeks (Aim 2A), or in historical studies in these delivery systems with low dose BMP-2 [39, 165]. Further exploration is needed to determine specific phenotypes of inflammatory cells that likely invaded in response to amnion implantation.

The significance of this work includes the evaluation of translational therapeutics that facilitated improved structural and functional repair of bone in a small animal model. Specifically, the efficacy of oxidized-irradiated alginate as a more degradable protein delivery system for BMP-2 was evaluated. Additionally, this work included characterization of a rodent model and development of associated techniques to elucidate the effects of a supraphysiological dose of BMP-2, akin to those used clinically, on bone healing and inflammation. Importantly, the effectiveness of the hybrid alginate+mesh delivery vehicle was compared to the clinically used collagen sponge. While gaining a better understanding of gene expression during bone healing with high and low dose BMP-2, this work evaluated the ability of ECM-derived amniotic membrane to reduce heterotopic mineralization in a critically sized bone defect model. Modulating growth factor delivery and inflammation to better utilize endogenous repair mechanisms may allow for an improved healing response over currently used strategies.

7.2 Biomaterial Degradability: Is It a Prerequisite for Functional Bone Healing?

Natural materials that function as the building blocks for tissues in the body serve as the basis for a variety of successful tissue engineering strategies. To date, however, biomaterials in the field of tissue engineering have been only moderately effective, due in part to the often-minimal degree to which they match the form and function of naturally occurring matrices [241]. Thus, the ability to tailor, e.g., mechanical properties, porosity, and degradation rate of a scaffold to ultimately match the structural properties of the native tissue can facilitate more complete integration of the biomaterial with the surrounding tissue.

Degradation is a key parameter regulated by both porosity and mechanical properties. Scaffold degradation concomitant with tissue formation is desirable for many tissue engineering applications. The effects of biomaterial degradation on BMP-2 release and

bioactivity, as well as bone regeneration *in vivo* were evaluated in Aim 1. The biomaterials studied were alginate hydrogels, which are capable of undergoing accelerated degradation via structural modifications. Alginate hydrogels derived from brown algae have been widely studied for many healthcare applications, including pharmaceutics, dental impressions, and wound dressings. As a biomaterial, alginate possesses advantages such as ease of gelling, biocompatibility, and low immunogenicity, but its inability to enzymatically degrade [20] hinders its use for regenerative medicine applications. For degradation, alginate is dependent on the often slow dissociation of ionic crosslinks [21]; however, modification of the polymer structure by techniques such as irradiation and oxidation can increase the degradation rate.

In our hands, the effects of alginate oxidation were minimal. Most notably, oxidized-irradiated alginate led to accelerated BMP-2 release *in vitro*, higher bone mineral density (albeit transiently) at 8 weeks, and fewer large fragments of residual alginate at 12 weeks. Additionally, oxidized-irradiated alginate resulted in the recovery of biomechanical properties to those of intact bone, while irradiated alginate led to lower max torque compared to intact bone. Nonetheless, because oxidation did not lead to significant improvements in bone regeneration, irradiated alginate was used for the studies in Aim 2. Of further concern was the faster release of BMP-2 from oxidized-irradiated alginate, which would be a disadvantage, especially with delivery of high doses of BMP-2.

Notably, much of the oxidized-irradiated alginate remained in the defect at 12 weeks, comprising ~30% of the total stained area (determined by histomorphometry), compared to ~40% of total area composed of irradiated alginate. Despite incomplete degradation of both alginates in the timeframe and species of this model, both facilitated robust, functional bone regeneration. Thus it is believed that integration of the biomaterial with host tissue (e.g.,

interactions that support the recruitment, attachment, and differentiation of progenitor cells) is more crucial to successful healing than complete degradation of the biomaterial itself.

Importantly, the evaluation of these biomaterials in a rat model may have limited our ability to measure differences between the groups, due to the limited capacity for bone remodeling in the rat species. In collaboration with Dr. Dietmar Hutmacher, the irradiated alginate delivery system (hydrogel + nanofiber mesh) was used for BMP-2 delivery in a sheep tibial defect model, resulting in a greater degree of bone remodeling than had been observed in the rat model.

7.3 Alginate-PCL Mesh Constructs for Improving BMP-2 Bioactivity and Localized Bone Regeneration

Improved bone healing and higher local retention of low dose BMP-2 at the defect site has been observed with the alginate-PCL mesh delivery system compared to both collagen sponge (with BMP-2) and autograft [39, 40, 165, 189, 190]. With low dose BMP-2 in alginate (Aim 1), a burst release through 5 days followed by minimal release of BMP-2 was observed from both alginates (as seen previously with irradiated alginate [40]). Nonetheless, approximately one-third of the loaded BMP-2 remained bound to the alginate-PCL nanofiber mesh constructs and was bioactive through 26 days [189]. While Jeon et al. measured an increase in bone volume from a slow, sustained release of BMP-2 [166], others reported improved bone healing when an initial burst release was followed by a smaller sustained release [39, 167, 168].

Similarly, in the delivery of high dose BMP-2 (Aim 2A), most of the BMP-2 was released by 5 days. However, compared to collagen sponge (with or without a mesh), the initial (within the first 48 hours) burst release from alginate was mitigated. Importantly, BMP-2 retained in the alginate constructs at 26 days *in vitro* demonstrated significantly higher

bioactivity. Although the alginate system did not reduce the amount of heterotopic bone *in vivo*, it resulted in significantly more total bone volume and bone volume in the defect space. The enhanced bioactivity of BMP-2 remaining in the alginate constructs at 26 days likely facilitated the increases in total bone volume and bone deposition in the defect center. Though not directly quantified, the presumed earlier collapse of the local chemotactic gradient for collagen sponge, as can be inferred by the high decay constant and the lower amount of BMP-2 recovered *in vitro* at day 26, could further explain the differences in bone formation patterns between the two delivery systems.

Regardless of BMP-2 dose, the bioactivity of the bound BMP-2 in the alginate constructs may have been prolonged due to the interaction of the protein with the biomaterial, which could have delayed/minimized protein denaturation. Maintenance, and even possible enhancement, of bioactivity of VEGF, another heparin-binding growth factor, has been observed in the presence of alginate [45, 169]. Furthermore, BMP-2 bioactivity has been sustained on the order of weeks using various delivery vehicles, including PCL [170]. However, to our knowledge, our Aim 1 studies were the first demonstration of prolonged bioactivity of BMP-2 retained within alginate hydrogels, specifically an alginate-PCL mesh carrier [189]. Likely, both the alginate hydrogel and the nanofiber mesh contributed to the binding of BMP-2, as BMP-2 retention was enhanced in the hybrid delivery system compared to both the mesh only and alginate only constructs. However, the precise roles of each are yet to be delineated. In Aim 2A with collagen sponge (+/- mesh), no effect of the nanofiber mesh on BMP-2 release, retention, or bioactivity was observed.

It is possible that both the initial burst release and the localized retention of BMP-2 in the alginate constructs in both Aim 1 (low dose) and Aim 2A (high dose) facilitated bone regeneration, the former by recruiting the initial wave of osteoprogenitor cells to the defect

site, and the latter by influencing the differentiation of osteoprogenitor cells once present within the defect space [168, 171]. Collectively, these findings suggest the bioavailability of BMP-2 for an extended time frame (~weeks) may be required for robust localized bone formation in critically sized bone defects.

7.4 Mechanistic Insight into Bone Healing with High Dose BMP-2

From Aim 1 and many additional studies with this bone defect model [38-41, 165, 188-190], it is well understood that a low dose of BMP-2 in our alginate delivery system is sufficient to heal the bone defect and does not elicit heterotopic mineralization. In contrast, in Aim 2A, high dose BMP-2 (regardless of delivery system) effectively recapitulated heterotopic bone formation using the same rat model, similar to that observed clinically with the use of high doses of BMP-2. Thus, in Aim 2B, we investigated the role of BMP-2 dose on gene expression in the defect site and adjacent muscle during the inflammatory and early repair phases of our bone defect model.

Temporal patterns of gene expression in bone defect tissue showed two interesting differences between low dose and high dose BMP-2 treated defects. First, osteogenic gene expression levels began to plateau by day 14 for low dose BMP-2, but high dose BMP-2 resulted in steady increases in osteogenic gene expression through 21 days. In a similar result following trauma in military personnel, osteogenic genes were more highly expressed in wounds that subsequently formed heterotopic mineralization [147]. Secondly, inflammatory gene expression in bone defects treated with low dose BMP-2 peaked at day 3, while for high dose BMP-2, the pro-inflammatory factors CCR7 and IFNG remained highly expressed through day 21. This suggests the bone defect microenvironment following treatment with low dose BMP-2 may allow for an earlier resolution of inflammation.

Although few genes were differentially expressed in the direct comparison between the two groups, low dose BMP-2 elicited higher inflammatory gene expression in bone defects at day 3, while high dose BMP-2 resulted in greater osteogenic gene expression at day 3. Notably, a heightened inflammatory response with low dose BMP-2 compared to high dose BMP-2 was contrary to our hypothesis. Nonetheless, this peak in inflammatory gene expression occurred at day 3, further supporting the theory of a more classical healing cascade with low dose BMP-2, compared to the response to high dose BMP-2, which involved persistent high expression of inflammatory genes over time. Just as early inflammation is necessary for healing, a significant contributor to delayed bone healing or eventual non-union is an unresolved (local or systemic) inflammatory response. In a sheep osteotomy model, inflammation was heightened and prolonged in sheep with mechanically-induced delayed bone healing [131]. Since heterotopic mineralization is believed to be stimulated by inflammation [146], the prolonged inflammation observed with high dose BMP-2 may have contributed to the initiation of this pathology. Besides prolonged inflammation, high dose BMP-2 led to delayed expression of inflammatory (IL1A, IFNG at day 7) and osteogenic (COL1A1 at day 14) markers in intact muscle compared to intact muscle in animals treated with low dose BMP-2. An increase in inflammatory and osteogenic genes in intact muscle suggested possible systemic effects resulting from the use of high dose BMP-2. Protein expression studies are underway with the goal of corroborating these changes in gene expression.

Exploration of the gene expression profiles of tissue from bone defects and the adjacent soft tissue as a function of BMP-2 dose provided a crucial first step towards elucidating the pathological mechanisms associated with inflammation and heterotopic mineralization often observed with high dose BMP-2 (and seen in Aim 2A of this work).

Advancing our understanding of the cellular and molecular factors that participate in the bone repair process in a critically sized bone defect model may allow for the development of improved tissue engineering therapies to restrict heterotopic bone formation.

7.5 Strategies to Mitigate Heterotopic Bone with High Dose BMP-2

Traumatic bone injuries, and particularly critically sized defects, necessitate surgical intervention for repair, often involving augmentation with supraphysiological amounts of BMP-2. Adverse effects such as heterotopic mineralization and inflammation observed with high dose BMP-2 can be compounded by the delivery of high dose BMP-2 within collagen sponge, which has limited ability to retain growth factor. Despite the efficacy of BMP-2 for bone regeneration, investigation into biomaterial strategies capable of attenuating these negative reactions is necessary. Since heterotopic mineralization was observed with a high dose of BMP-2 in our rat segmental bone defect model in Aim 2A, our subsequent objective was to evaluate the ability of ECM-derived amniotic membrane surrounding the bone defect space to attenuate heterotopic mineralization in critically sized bone defects treated with high dose BMP-2. One major advantage of the materials used in this study—collagen sponge and amniotic membrane—is their availability for use clinically, which would drastically accelerate the translation of amnion for bone regeneration applications.

Amniotic membrane functioned as a reservoir for BMP-2, retaining more BMP-2 than PCL mesh scaffolds through 21 days *in vitro*. As hypothesized, heterotopic mineralization was reduced with amnion surrounding collagen sponge compared to collagen sponge alone. The attenuated heterotopic mineralization may be attributed to amnion functioning as a biological sink to retain BMP-2, as amniotic membrane is known to harbor a wide array of growth factors and cytokines [51, 61, 62, 231, 232]. Furthermore, the patented PURION® process that the amnion undergoes has been shown to maintain the

biological activity of the tissue [51], so it was likely the amnion bound (possibly permanently) a portion of the BMP-2 following release from the collagen scaffold. Additionally, the immunomodulatory factors present in the amnion [51, 61] may have tempered the inflammatory response such that the subsequent pathogenesis of heterotopic ossification was minimized.

In the present study, amnion tissue was still present at 12 weeks and may have impaired cellular infiltration into the defect space, thus contributing to the delayed bone formation in the defect. Prior analyses determined that amnion tissue had an effective pore size on the order of nanometers and was capable of supporting cell attachment on the surface but limited the invasion of cells into the scaffold [237]. Thus, in addition to playing a biological role, the amnion may have been a physical barrier to contain BMP-2 within the defect space. Likely, both the structural and biological properties of the amniotic membrane contributed to the reduced heterotopic mineralization, though more investigation into these mechanisms is necessary. Future work exploring macroporous amniotic membrane and evaluating the bioactivity of the BMP-2 after interaction with amnion may allow for elucidation of whether the physical or biological role of the membrane was more crucial in its ability to minimize heterotopic bone deposition.

We observed moderate inflammatory infiltrate mostly in the area of residual amnion tissue, and this response may have exacerbated the delay in bone healing. Nonetheless, the clinical use of these grafts, which are allogeneic in nature, may result in attenuated inflammatory/immune responses compared to the heightened response observed in the current rat model.

7.6 Final Conclusions

In summary, this thesis evaluated novel translatable strategies for promoting biomaterial degradation and growth factor bioactivity and localization, as well as reducing heterotopic mineralization in a challenging segmental bone defect model. Of significance, our rat model recapitulated adverse effects associated with orthotopic high dose BMP-2 delivery, particularly heterotopic mineralization, prolonged local inflammation, and systemic inflammatory effects. The spatiotemporal differences in gene expression may, in part, explain the heterotopic mineralization and tissue swelling seen clinically with high doses of BMP-2. By providing insight into the complex process of bone healing as a function of BMP-2 dose, we have identified specific alterations in gene expression that are involved in the early healing of large bone defects. The findings here support the overall hypothesis that a biomaterial delivery vehicle that allows for localized growth factor availability and minimal heterotopic bone formation would facilitate structural and functional restoration of segmental bone defects. By considering these fundamental biomaterial parameters, we may more effectively harness endogenous repair mechanisms for successful bone regeneration.

APPENDIX A

A.1 Histomorphometry Protocol

For Safranin O stained sections, the red stained regions were considered alginate, and the blue stained regions were considered infiltrating tissue. The images were first converted from RGB (Red, Green, Blue) to HSV (Hue, Saturation, Value) color space and separated into red and blue colors by their hue values (0° to 360°) to allow separation of regions based on color [164]. All hue values (H – Hue channel) outside the 40°-275° segment (yellow, green, and blue colors) were considered as 'red' color encompassing the variation in red color seen in the images (Figure 32A). Using the Value channel (V), values greater than 90% were considered 'white' and assigned as the image background. This assumption agreed with the white spaces in the images that were neither red nor blue stained. An obvious caveat is the assumption of unstained areas as areas without tissue. The indices obtained from the color and background separations were used to generate binary images of the red stained alginate and blue stained tissue. These areas were normalized to total area. Additionally, a frequency distribution representing the relative area of the individual alginate regions normalized to total area was generated for every image to identify differences in the relative size distribution of alginate loci.

Similar techniques were used to evaluate the Picrosirius red stained images, with some important differences dictated by image composition. Imaging under polarized microscopy produced a dark background, green/yellow birefringence for organized collagen (lamellar bone), dark red color for disorganized collagen structures, and white color for unstained areas. The images were first converted from RGB to the YUV (luma and chrominance) color space to highlight the white areas and saved as 'tiff' format files. These

saved images were subsequently converted to HSV color space as described above to demarcate the white-colored birefringent non-collagenous areas (outside 0°-160°). The original RGB images were also converted to HSV color space to identify areas of green/yellow (7°-175°) (Figure 32B) and red colors (outside 7°-300°) within the image. Regions not defined as one of the three color cut-offs were considered background. Binary images of only green/yellow, red, and white colored areas of the images were generated for reference, and the relative areas measured. Additionally, a particle size filter (50-pixel connectivity) was applied to the binarized images to isolate large contiguous organized structures as expected in mature bone.

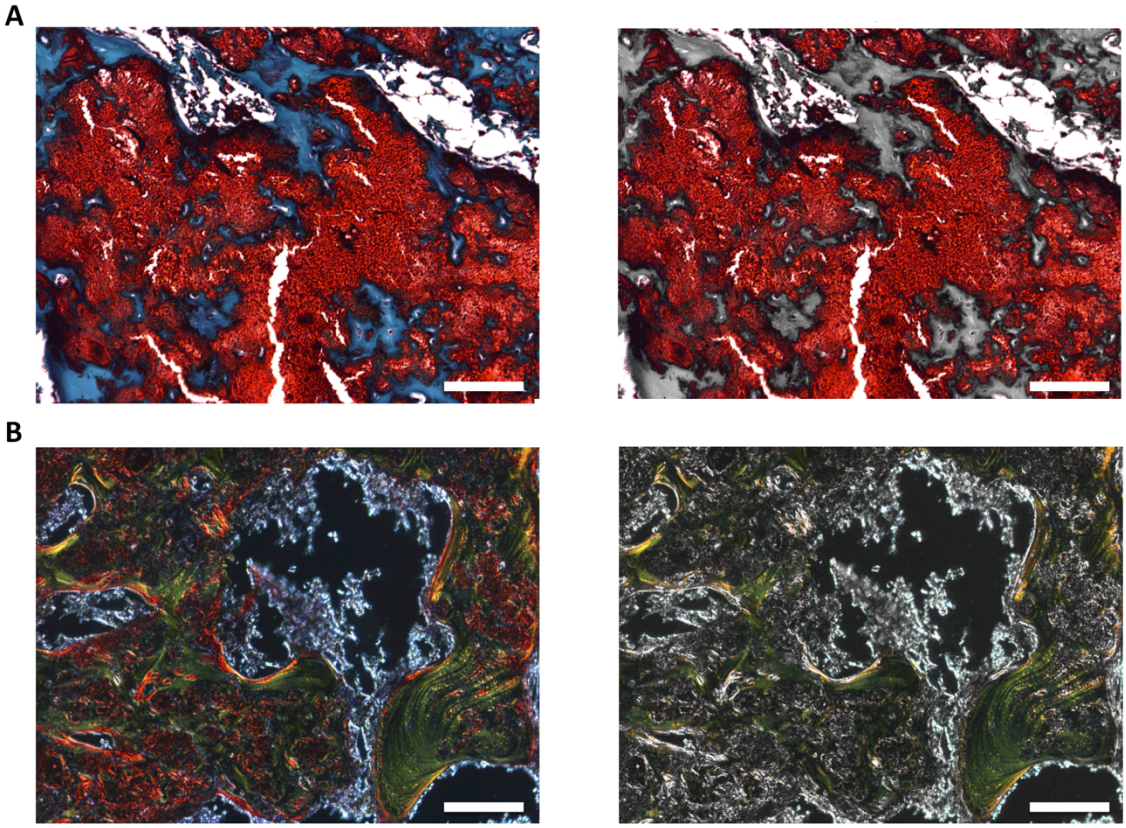

Figure 32. Color separation in histology images. (A) Red alginate areas from Safranin O staining were filtered for quantification. (B) Green/yellow lamellar bone from Picrosirius red staining was filtered for subsequent area analysis. Scale bar = 100 μm.

REFERENCES

1. Lee, N.K. and G. Karsenty, *Reciprocal regulation of bone and energy metabolism.* Trends Endocrinol Metab, 2008. **19**(5): p. 161-6.
2. Marks, S.C., Jr. and S.N. Popoff, *Bone cell biology: the regulation of development, structure, and function in the skeleton.* Am J Anat, 1988. **183**(1): p. 1-44.
3. Wolff, J., *Das Gesetz der Transformation der Knochen.* 1892, Berlin: Hirschwald.
4. Gerstenfeld, L.C., et al., *Fracture healing as a post-natal developmental process: Molecular, spatial, and temporal aspects of its regulation.* Journal of Cellular Biochemistry, 2003. **88**(5): p. 873-884.
5. Urist, M.R., *Bone: Formation by Autoinduction.* Science, 1965. **150**(3698): p. 893-899.
6. Buckwalter, J.A., et al., *Bone biology. II: Formation, form, modeling, remodeling, and regulation of cell function.* Instr Course Lect, 1996. **45**: p. 387-99.
7. Patino, M.G., et al., *Collagen: an overview.* Implant Dent, 2002. **11**(3): p. 280-5.
8. Schaffler, M.B. and O.D. Kennedy, *Osteocyte signaling in bone.* Curr Osteoporos Rep, 2012. **10**(2): p. 118-25.
9. Burger, E.H., et al., *Function of Osteocytes in Bone - Their Role in Mechanotransduction.* Journal of Nutrition, 1995. **125**(7): p. S2020-S2023.
10. Shapiro, F., *Bone development and its relation to fracture repair. The role of mesenchymal osteoblasts and surface osteoblasts.* Eur Cell Mater, 2008. **15**: p. 53-76.
11. Mackie, E.J., et al., *Endochondral ossification: How cartilage is converted into bone in the developing skeleton.* International Journal of Biochemistry & Cell Biology, 2008. **40**(1): p. 46-62.
12. Gonzalez, Y., M. Cerrolaza, and C. Gonzalez, *Poroelastic analysis of bone tissue differentiation by using the boundary element method.* Engineering Analysis with Boundary Elements, 2009. **33**(5): p. 731-740.
13. Manolagas, S.C., *Birth and death of bone cells: basic regulatory mechanisms and implications for the pathogenesis and treatment of osteoporosis.* Endocr Rev, 2000. **21**(2): p. 115-37.
14. Feng, X. and J.M. McDonald, *Disorders of bone remodeling.* Annu Rev Pathol, 2011. **6**: p. 121-45.
15. Finkelstein, E.A., P.S. Corso, and T.R. Miller, *Incidence and Economic Burden of Injuries in the United States.* 1 ed. 2006: Oxford University Press, USA. 208.
16. Praemer, A., S. Furner, and D.P. Rice, *Musculoskeletal Conditions in the United States.* 1 ed. 1999: Amer Acad of Orthopaedic Surgeons. 182.
17. Laurencin, C., Y. Khan, and S.F. El-Amin, *Bone graft substitutes.* Expert Rev Med Devices, 2006. **3**(1): p. 49-57.
18. Ziegler-Graham, K., et al., *Estimating the prevalence of limb loss in the United States: 2005 to 2050.* Arch Phys Med Rehabil, 2008. **89**(3): p. 422-9.
19. Sasso, R.C., J.C. LeHuec, and C. Shaffrey, *Iliac crest bone graft donor site pain after anterior lumbar interbody fusion: a prospective patient satisfaction outcome assessment.* J Spinal Disord Tech, 2005. **18**(Suppl.): p. S77-81.
20. Seeherman, H., J. Wozney, and R. Li, *Bone morphogenetic protein delivery systems.* Spine, 2002. **27**(16 Suppl. 1): p. S16-23.
21. Liu, R., A. Schindeler, and D.G. Little, *The potential role of muscle in bone repair.* J Musculoskelet Neuronal Interact, 2010. **10**(1): p. 71-6.

22. Lind, M., E.F. Eriksen, and C. Bunger, *Bone morphogenetic protein-2 but not bone morphogenetic protein-4 and -6 stimulates chemotactic migration of human osteoblasts, human marrow osteoblasts, and U2-OS cells.* Bone, 1996. **18**(1): p. 53-57.
23. Wang, E.A., et al., *Bone morphogenetic protein-2 causes commitment and differentiation in C3H10T1/2 and 3T3 cells.* Growth Factors, 1993. **9**(1): p. 57-71.
24. Wozney, J.M., *The bone morphogenetic protein family and osteogenesis.* Mol Reprod Dev, 2005. **32**(2): p. 160-167.
25. Lieberman, J.R., A. Daluiski, and T.A. Einhorn, *The role of growth factors in the repair of bone.* J Bone Joint Surg, 2002. **84**(6): p. 1032-1044.
26. Nauth, A., et al., *Growth factors and bone regeneration: how much bone can we expect?* Injury, 2011. **42**(6): p. 574-9.
27. Swiontkowski, M.F., et al., *Recombinant human bone morphogenetic protein-2 in open tibial fractures. A subgroup analysis of data combined from two prospective randomized studies.* J Bone Joint Surg, 2006. **88**(1258-1265).
28. Cahill, K.S., et al., *Prevalence, complications, and hospital charges associated with use of bone-morphogenetic proteins in spinal fusion procedures.* JAMA, 2009. **302**(1): p. 58-66.
29. Shields, L.B., et al., *Adverse effects associated with high-dose recombinant human bone morphogenetic protein-2 use in anterior cervical spine fusion.* Spine, 2006. **31**(5): p. 542-547.
30. Dickerman, R.D., et al., *rh-BMP-2 can be used safely in the cervical spine: dose and containment are the keys!* The Spine Journal, 2007. **7**(4): p. 508-509.
31. Augst, A.D., H.J. Kong, and D.J. Mooney, *Alginate Hydrogels as Biomaterials.* Macromolecular Bioscience, 2006. **6**(8): p. 623-633.
32. Gombotz, W.R. and S. Wee, *Protein release from alginate matrices.* Advanced Drug Delivery Reviews, 1998. **31**(3): p. 267-285.
33. Lee, K.Y., et al., *Controlled growth factor release from synthetic extracellular matrices.* Nature, 2000. **408**(6815): p. 998-1000.
34. Simmons, C.A., et al., *Dual growth factor delivery and controlled scaffold degradation enhance in vivo bone formation by transplanted bone marrow stromal cells.* Bone, 2004. **35**(2): p. 562-569.
35. Shoichet, M.S., et al., *Stability of Hydrogels Used in Cell Encapsulation: An In Vitro Comparison of Alginate and Agarose.* Biotechnology and Bioengineering, 1996. **50**: p. 374-381.
36. Silva, E.A. and D.J. Mooney, *Effects of VEGF temporal and spatial presentation on angiogenesis.* Biomaterials, 2010. **31**(6): p. 1235-1241.
37. Alsberg, E., et al., *Regulating bone formation via controlled scaffold degradation.* J Dent Res, 2003. **82**(11): p. 903-908.
38. Boerckel, J.D., et al., *In vivo model for evaluating the effects of mechanical stimulation on tissue-engineered bone repair.* J Biomech Eng, 2009. **131**(8): p. 084502.
39. Boerckel, J.D., et al., *Effects of protein dose and delivery system on BMP-mediated bone regeneration.* Biomaterials, 2011. **32**(22): p. 5241-5251.
40. Kolambkar, Y.M., et al., *An alginate-based hybrid system for growth factor delivery in the functional repair of large bone defects.* Biomaterials, 2011. **32**(1): p. 65-74.
41. Oest, M.E., et al., *Quantitative assessment of scaffold and growth factor-mediated repair of critically sized bone defects.* J Orthop Res, 2007. **25**(7): p. 941-50.
42. Boerckel, J.D., *Mechanical Regulation of Bone Regeneration and Vascular Growth in vivo*, in *George W. Woodruff School of Mechanical Engineering.* 2011, Georgia Institute of Technology. p. 205.

43. Boontheekul, T., H.J. Kong, and D.J. Mooney, *Controlling alginate gel degradation utilizing partial oxidation and bimodal molecular weight distribution.* Biomaterials, 2005. **26**(15): p. 2455-65.
44. Bouhadir, K.H., et al., *Degradation of partially oxidized alginate and its potential application for tissue engineering.* Biotechnol Prog, 2001. **17**: p. 945-950.
45. Silva, E.A. and D.J. Mooney, *Spatiotemporal control of vascular endothelial growth factor delivery from injectable hydrogels enhances angiogenesis.* J Thromb Haemost, 2007. **5**: p. 590-598.
46. Babensee, J.E., et al., *Host response to tissue engineered devices.* Adv Drug Delivery Rev, 1998. **33**: p. 111-139.
47. Harriger, M.D., et al., *Glutaraldehyde crosslinking of collagen substrates inhibits degradation in skin substitutes grafted to athymic mice.* J Biomed Mater Res, 1997. **35**(2): p. 137-45.
48. Weadock, K.S., et al., *Effect of physical crosslinking methods on collagen-fiber durability in proteolytic solutions.* J Biomed Mater Res, 1996. **32**(2): p. 221-6.
49. Uludag, H., et al., *Delivery systems for BMPs: factors contributing to protein retention at an application site.* J Bone Joint Surg Am, 2001. **83-A Suppl 1**(Pt 2): p. S128-35.
50. Andree, B., et al., *Small Intestinal Submucosa Segments as Matrix for Tissue Engineering: Review.* Tissue Eng: Part B, 2013. **19**(4): p. 279-291.
51. Koob, T.J., et al., *Biological properties of dehydrated human amnion/chorion composite graft: implications for chronic wound healing.* Int Wound J, 2013.
52. Davis, J.W., *Skin transplantation with a review of 550 cases at the Johns Hopkins Hospital.* Johns Hopkins Med J, 1910. **15**: p. 307.
53. De Rotth, A., *Plastic repair of conjunctival defects with fetal membrane.* Archives of Ophthalmology, 1940. **23**: p. 522.
54. Lee, S.H. and S.C. Tseng, *Amniotic membrane transplantation for persistent epithelial defects with ulceration.* American Journal of Ophthalmology, 1997. **123**(3): p. 303-312.
55. Jin, C.Z., et al., *Human amniotic membrane as a delivery matrix for articular cartilage repair.* Tissue Eng, 2007. **13**(4): p. 693-702.
56. Dua, H.S., et al., *The amniotic membrane in ophthalmology.* Survey of Ophthalmology, 2004. **49**(1): p. 51-77.
57. Parry, S. and J.F. Strauss, *Mechanisms of disease - Premature rupture of the fetal membranes.* New England Journal of Medicine, 1998. **338**(10): p. 663-670.
58. Helmig, R., et al., *Different biomechanical properties of human fetal membranes obtained before and after delivery.* Eur J Obstet Gynecol Reprod Biol, 1993. **48**(3): p. 183-189.
59. Malak, T.M., et al., *Confocal immunofluorescence localization of collagen types I, III, IV, V and VI and their ultrastructural organization in term human fetal membranes.* Placenta, 1993. **14**(4): p. 385-406.
60. Meinert, M., et al., *Proteoglycans and hyaluronan in human fetal membranes.* Am J Obstet Gynecol, 2001. **184**(4): p. 679-85.
61. Koob, T.J., et al., *Properties of dehydrated human amnion/chorion composite grafts: Implications for wound repair and soft tissue regeneration.* J Biomed Mater Res B Appl Biomater, 2014.
62. Koob, T.J., et al., *Angiogenic properties of dehydrated human amnion/chorion allografts: therapeutic potential for soft tissue repair and regeneration.* Vasc Cell, 2014. **6**: p. 10.
63. Hao, Y., et al., *Identification of antiangiogenic and antiinflammatory proteins in human amniotic membrane.* Cornea, 2000. **19**(348-352).
64. Lindenmair, A., et al., *Osteogenic differentiation of intact human amniotic membrane.* Biomaterials, 2010. **31**(33): p. 8659-65.
65. Daniel, J., et al., *Placental Tissue Grafts.* 2012, MiMedx Group, Inc.: USA.

66. Zelen, C.M., et al., *A prospective randomised comparative parallel study of amniotic membrane wound graft in the management of diabetic foot ulcers.* Int Wound J, 2013. **10**(5): p. 502-7.
67. Willett, N.J., et al., *Intra-articular injection of micronized dehydrated human amnion/chorion membrane attenuates osteoarthritis development.* Arthritis Res Ther, 2014. **16**(1): p. R47.
68. Hodde, J., *Naturally occurring scaffolds for soft tissue repair and regeneration.* Tissue Eng, 2002. **8**(2): p. 295-308.
69. Pu, L.L.Q. and P.S.E.F.D. Comm, *Small intestinal submucosa (Surgisis) as a bioactive prosthetic material for repair of abdominal wall fascial defect.* Plastic and Reconstructive Surgery, 2005. **115**(7): p. 2127-2131.
70. Azzarello, J., et al., *Assessment of angiogenic properties of biomaterials using the chicken embryo chorioallantoic membrane assay.* Biomedical Materials, 2007. **2**(2): p. 55-61.
71. Badylak, S., et al., *Strength over time of a resorbable bioscaffold for body wall repair in a dog model.* J Surg Res, 2001. **99**(2): p. 282-7.
72. Palmer, E.M., L.G. Baum, and G.A. van Seventer, *Small intestinal submucosa induces loss of mitochondrial integrity and caspase-dependent apoptosis in human T cells.* Tissue Eng, 2003. **9**(2): p. 307-14.
73. Palmer, E.M., et al., *Human helper T cell activation and differentiation is suppressed by porcine small intestinal submucosa.* Tissue Eng, 2002. **8**(5): p. 893-900.
74. Badylak, S., et al., *Endothelial cell adherence to small intestinal submucosa: an acellular bioscaffold.* Biomaterials, 1999. **20**(23-24): p. 2257-63.
75. Matsumoto, T., et al., *A study of inverted intestinal graft in the major veins.* Angiology, 1966. **17**(11): p. 842-50.
76. Wallen, J. and V. Rao, *Extensive Tricuspid Valve Repair After Endocarditis Using CorMatrix Extracellular Matrix.* Annals of Thoracic Surgery, 2014. **97**(3): p. 1048-1050.
77. Yanagawa, B., et al., *Potential myocardial regeneration with CorMatrix ECM: A case report.* Journal of Thoracic and Cardiovascular Surgery, 2014. **147**(4): p. E41-E43.
78. Zhou, Y.L., et al., *Expansion and Delivery of Adipose-Derived Mesenchymal Stem Cells on Three Microcarriers for Soft Tissue Regeneration.* Tissue Engineering Part A, 2011. **17**(23-24): p. 2981-2997.
79. Okada, M., et al., *Differential efficacy of gels derived from small intestinal submucosa as an injectable biomaterial for myocardial infarct repair.* Biomaterials, 2010. **31**(30): p. 7678-7683.
80. Adair-Kirk, T.L., et al., *A site on laminin alpha 5, AQARSAASKVKVSMKF, induces inflammatory cell production of matrix metalloproteinase-9 and chemotaxis.* Journal of Immunology, 2003. **171**(1): p. 398-406.
81. Houghton, A.M., et al., *Elastin fragments drive disease progression in a murine model of emphysema.* Journal of Clinical Investigation, 2006. **116**(3): p. 753-759.
82. Senior, R.M., et al., *Neutrophils Show Chemotaxis to Type-Iv Collagen and Its 7s Domain and Contain a 67-Kd Type-Iv Collagen Binding-Protein with Lectin Properties.* American Journal of Respiratory Cell and Molecular Biology, 1989. **1**(6): p. 479-487.
83. Badylak, S.F., et al., *Macrophage Phenotype as a Determinant of Biologic Scaffold Remodeling.* Tissue Engineering Part A, 2008. **14**(11): p. 1835-1842.
84. Allen, A.B., et al., *Functional Augmentation of Naturally-Derived Materials for Tissue Regeneration.* Annals of Biomedical Engineering, 2015. **43**(3): p. 555-567.
85. Schmoekel, H.G., et al., *Bone repair with a form of BMP-2 engineered for incorporation into fibrin cell ingrowth matrices.* Biotechnol Bioeng, 2005. **89**(3): p. 253-62.
86. Stabenfeldt, S.E., et al., *Engineering fibrin polymers through engagement of alternative polymerization mechanisms.* Biomaterials, 2012. **33**(2): p. 535-544.

87. Lutolf, M.R., et al., *Repair of bone defects using synthetic mimetics of collagenous extracellular matrices.* Nature Biotechnology, 2003. **21**(5): p. 513-518.
88. Mariner, P.D., et al., *Synthetic hydrogel scaffold is an effective vehicle for delivery of INFUSE (rhBMP2) to critical-sized calvaria bone defects in rats.* Journal of Orthopaedic Research, 2013. **31**(3): p. 401-406.
89. Shekaran, A., et al., *Bone regeneration using an alpha 2 beta 1 integrin-specific hydrogel as a BMP-2 delivery vehicle.* Biomaterials, 2014. **35**(21): p. 5453-5461.
90. Littenberg, B., et al., *Closed fractures of the tibial shaft. A meta-analysis of three methods of treatment.* J Bone Joint Surg Am, 1998. **80**(2): p. 174-83.
91. Zimmermann, G., et al., *Treatment of tibial shaft non-unions: bone morphogenetic proteins versus autologous bone graft.* Injury, 2009. **40 Suppl 3**: p. S50-3.
92. Kitaori, T., et al., *Stromal cell-derived factor 1/CXCR4 signaling is critical for the recruitment of mesenchymal stem cells to the fracture site during skeletal repair in a mouse model.* Arthritis Rheum, 2009. **60**(3): p. 813-23.
93. Boyce, A.S., et al., *Canine investigation of rhBMP-2, autogenous bone graft, and rhBMP-2 with autogenous bone graft for the healing of a large segmental tibial defect.* J Orthop Trauma, 2009. **23**(10): p. 685-92.
94. Jones, C.B., et al., *Improved healing efficacy in canine ulnar segmental defects with increasing recombinant human bone morphogenetic protein-2/allograft ratios.* J Orthop Trauma, 2008. **22**(8): p. 550-9.
95. Mehta, M., et al., *Biomaterial delivery of morphogens to mimic the natural healing cascade in bone.* Adv Drug Deliv Rev, 2012. **64**(12): p. 1257-76.
96. Bragdon, B., et al., *Bone morphogenetic proteins: a critical review.* Cell Signal, 2011. **23**(4): p. 609-20.
97. Wozney, J.M., *Overview of bone morphogenetic proteins.* Spine (Phila Pa 1976), 2002. **27**(16 Suppl 1): p. S2-8.
98. Kubler, N.R., et al., *Inductive properties of recombinant human BMP-2 produced in a bacterial expression system.* Int J Oral Maxillofac Surg, 1998. **27**(4): p. 305-9.
99. Wang, E.A., et al., *Recombinant human bone morphogenetic protein induces bone formation.* Proc Natl Acad Sci U S A, 1990. **87**(6): p. 2220-4.
100. Yamaguchi, A., et al., *Recombinant human bone morphogenetic protein-2 stimulates osteoblastic maturation and inhibits myogenic differentiation in vitro.* J Cell Biol, 1991. **113**(3): p. 681-7.
101. Tsuji, K., et al., *BMP2 activity, although dispensable for bone formation, is required for the initiation of fracture healing.* Nature Genetics, 2006. **38**(12): p. 1424-1429.
102. Wozney, J.M., *The bone morphogenetic protein family and osteogenesis.* Molecular Reproduction and Development, 2005. **32**(2): p. 160-167.
103. Service, R.F., *Tissue engineers build new bone.* Science, 2000. **289**(5484): p. 1498-500.
104. Groeneveld, E.H.J. and E.H. Burger, *Bone morphogenetic proteins in human bone regeneration.* European Journal of Endocrinology, 2000. **142**(1): p. 9-21.
105. Wang, E.A., et al., *Purification and Characterization of Other Distinct Bone-Inducing Factors.* Proceedings of the National Academy of Sciences of the United States of America, 1988. **85**(24): p. 9484-9488.
106. Swiontkowski, M.F., et al., *Recombinant human bone morphogenetic protein-2 in open tibial fractures. A subgroup analysis of data combined from two prospective randomized studies.* Journal of Bone and Joint Surgery, 2006. **88**(1258-1265).
107. Cahill, K.S., et al., *Prevalence, Complications, and Hospital Charges Associated With Use of Bone-Morphogenetic Proteins in Spinal Fusion Procedures.* The Journal of the American Medical Association, 2009. **302**(1): p. 58-66.

108. Lee, K.B., et al., *BMP induced inflammation: a comparison of rhBMP-7 and rhBMP-2.* J Orthop Res, 2012. **30**(12): p. 1985-94.
109. Zara, J.N., et al., *High doses of bone morphogenetic protein 2 induce structurally abnormal bone and inflammation in vivo.* Tissue Eng A, 2011. **17**: p. 1389-1399.
110. Angle, S.R., et al., *Healing of rat femoral segmental defect with bone morphogenetic protein-2: a dose response study.* J Musculoskelet Neuronal Interact, 2012. **12**(1): p. 28-37.
111. Centrella, M., T.L. Mccarthy, and E. Canalis, *Transforming Growth-Factor-Beta Is a Bifunctional Regulator of Replication and Collagen-Synthesis in Osteoblast-Enriched Cell-Cultures from Fetal-Rat Bone.* Journal of Biological Chemistry, 1987. **262**(6): p. 2869-2874.
112. Schliephake, H., *Bone growth factors in maxillofacial skeletal reconstruction.* International Journal of Oral and Maxillofacial Surgery, 2002. **31**(5): p. 469-484.
113. Zellin, G. and A. Linde, *Effects of recombinant human fibroblast growth factor-2 on osteogenic cell populations during orthopic osteogenesis in vivo.* Bone, 2000. **26**(2): p. 161-168.
114. Claes, L., S. Recknagel, and A. Ignatius, *Fracture healing under healthy and inflammatory conditions.* Nat Rev Rheumatol, 2012. **8**(3): p. 133-43.
115. Grundnes, O. and O. Reikeras, *The importance of the hematoma for fracture healing in rats.* Acta Orthop Scand, 1993. **64**(3): p. 340-2.
116. Kolar, P., et al., *The early fracture hematoma and its potential role in fracture healing.* Tissue Eng Part B Rev, 2010. **16**(4): p. 427-34.
117. Mountziaris, P.M. and A.G. Mikos, *Modulation of the inflammatory response for enhanced bone tissue regeneration.* Tissue Eng Part B Rev, 2008. **14**(2): p. 179-86.
118. Pape, H.-C., et al., *Trauma-induced inflammation and fracture healing.* Journal of Orthopaedic Trauma, 2010. **24**(9): p. 522-525.
119. Cho, T.-J., L.C. Gerstenfeld, and T.A. Einhorn, *Differential Temporal Expression of Members of the Transforming Growth Factor B Superfamily During Murine Fracture Healing.* Journal of Bone and Mineral Research, 2002. **17**(3): p. 513-520.
120. Kon, T., et al., *Expression of Osteoprotegerin, Receptor Activator of NF-κB Ligand (Osteoprotegerin Ligand) and Related Proinflammatory Cytokines During Fracture Healing.* Journal of Bone and Mineral Research, 2001. **16**(6): p. 1004-1014.
121. Rundle, C.H., et al., *Microarray analysis of gene expression during the inflammation and endochondral bone formation stages of rat femur fracture repair.* Bone, 2006. **38**(4): p. 521-9.
122. Bocker, W., et al., *IKK-2 is required for TNF-alpha-induced invasion and proliferation of human mesenchymal stem cells.* J Mol Med (Berl), 2008. **86**(10): p. 1183-92.
123. Glass, G.E., et al., *TNF-alpha promotes fracture repair by augmenting the recruitment and differentiation of muscle-derived stromal cells.* Proc Natl Acad Sci U S A, 2011. **108**(4): p. 1585-90.
124. Thevenot, P.T., et al., *The effect of incorporation of SDF-1alpha into PLGA scaffolds on stem cell recruitment and the inflammatory response.* Biomaterials, 2010. **31**(14): p. 3997-4008.
125. Barnes, G.L., et al., *Growth factor regulation of fracture repair.* Journal of Bone and Mineral Research, 1999. **14**(11): p. 1805-1815.
126. Dimitriou, R., E. Tsiridis, and P.V. Giannoudis, *Current concepts of molecular aspects of bone healing.* Injury, 2005. **36**(12): p. 1392-404.
127. Doll, B.A., et al., *Bone Regeneration and Repair.* 2005, Humana Press: Totowa, NJ. p. 337-358.
128. Granero-Molto, F., et al., *Regenerative effects of transplanted mesenchymal stem cells in fracture healing.* Stem Cells, 2009. **27**(8): p. 1887-98.

129. Schett, G. and J.-P. David, *The multiple faces of autoimmune-mediated bone loss.* Nature Reviews Endocrinology, 2010. **6**: p. 698-706.
130. Takayanagi, H., *Osteoimmunology and the effects of the immune system on bone.* Nat Rev Rheumatol, 2009. **5**(12): p. 667-76.
131. Schmidt-Bleek, K., et al., *Inflammatory phase of bone healing initiates the regenerative healing cascade.* Cell Tissue Res, 2012. **347**(3): p. 567-73.
132. Gerstenfeld, L., et al., *Impaired Fracture Healing in the Absence of TNF-α Signaling: The Role of TNF-α in Endochondral Cartilage Resorption.* Journal of Bone and Mineral Research, 2003. **18**(9): p. 1584-1592.
133. Yang, X., et al., *Callus mineralization and maturation are delayed during fracture healing in interleukin-6 knockout mice.* Bone, 2007. **41**(6): p. 928-36.
134. Guo, R., et al., *Ubiquitin ligase Smurf1 mediates tumor necrosis factor-induced systemic bone loss by promoting proteasomal degradation of bone morphogenetic signaling proteins.* J Biol Chem, 2008. **283**(34): p. 23084-92.
135. Miller, R.R., et al., *Persistent changes in interleukin-6 and lower extremity function following hip fracture.* J Gerontol A Biol Sci Med Sci, 2006. **61**(10): p. 1053-1058.
136. Pape, H.-C., et al., *Biochemical changes after trauma and skeletal surgery of the lower extremity: quantification of the operative burden.* Crit Care Med, 2000. **28**(10): p. 3441-3448.
137. Cunningham, N.S., V. Paralkar, and A.H. Reddi, *Osteogenin and recombinant bone morphogenetic protein 2B are chemotactic for human monocytes and stimulate transforming growth factor beta1 mRNA expression.* Proceedings of the National Academy of Sciences, 1992. **89**: p. 11740-11744.
138. Irie, K., et al., *Osteoclast differentiation in ectopic bone formation induced by recombinant human bone morphogenetic protein 2 (rhBMP-2).* J Bone Miner Metab, 2003. **21**(6): p. 363-9.
139. Itoh, K., et al., *Bone Morphogenetic Protein 2 Stimulates Osteoclast Differentiation and Survival Supported by Receptor Activator of Nuclear Factor-kB Ligand.* Endocrinology, 2001. **142**(8): p. 3656-3662.
140. Sanders, R.L., *Bone formation in upper abdominal scars.* Ann Surg, 1955. **141**(5): p. 621-6.
141. Ekelund, A., O. Brosjo, and O.S. Nilsson, *Experimental induction of heterotopic bone.* Clin Orthop Relat Res, 1991(263): p. 102-12.
142. Shore, E.M., et al., *A recurrent mutation in the BMP type I receptor ACVR1 causes inherited and sporadic fibrodysplasia ossificans progressiva.* Nat Genet, 2006. **38**(5): p. 525-7.
143. Kaplan, F.S., et al., *Heterotopic ossification.* J Am Acad Orthop Surg, 2004. **12**(2): p. 116-25.
144. Potter, B.K., et al., *Heterotopic ossification following combat-related trauma.* J Bone Joint Surg Am, 2010. **92 Suppl 2**: p. 74-89.
145. Forsberg, J.A., et al., *Heterotopic ossification in high-energy wartime extremity injuries: prevalence and risk factors.* J Bone Joint Surg Am, 2009. **91**(5): p. 1084-91.
146. Kaplan, F.S., et al., *Morphogen receptor genes and metamorphogenes: skeleton keys to metamorphosis.* Ann N Y Acad Sci, 2007. **1116**: p. 113-33.
147. Evans, K.N., et al., *Osteogenic gene expression correlates with development of heterotopic ossification in war wounds.* Clin Orthop Relat Res, 2014. **472**(2): p. 396-404.
148. Katagiri, T., et al., *Bone Morphogenetic Protein-2 Converts the Differentiation Pathway of C2c12 Myoblasts into the Osteoblast Lineage.* Journal of Cell Biology, 1994. **127**(6): p. 1755-1766.

149. Davis, T.A., et al., *Heterotopic ossification in complex orthopaedic combat wounds: quantification and characterization of osteogenic precursor cell activity in traumatized muscle.* J Bone Joint Surg Am, 2011. **93**(12): p. 1122-31.
150. Lounev, V.Y., et al., *Identification of Progenitor Cells That Contribute to Heterotopic Skeletogenesis.* Journal of Bone and Joint Surgery-American Volume, 2009. **91A**(3): p. 652-663.
151. Davis, T.A., et al., *Ectopic bone formation in severely combat-injured orthopedic patients -- a hematopoietic niche.* Bone, 2013. **56**(1): p. 119-26.
152. Kaplan, F.S., et al., *Hematopoietic stem-cell contribution to ectopic skeletogenesis.* J Bone Joint Surg Am, 2007. **89**(2): p. 347-57.
153. Evans, K.N., et al., *Inflammatory Cytokine and Chemokine Expression is Associated With Heterotopic Ossification in High-Energy Penetrating War Injuries.* Journal of Orthopaedic Trauma, 2012. **26**(11): p. E204-E213.
154. Augst, A.D., H.J. Kong, and D.J. Mooney, *Alginate hydrogels as biomaterials.* Macromol Biosci, 2006. **6**(8): p. 623-633.
155. Gombotz, W.R. and S. Wee, *Protein release from alginate matrices.* Adv Drug Delivery Rev, 1998. **31**(3): p. 267-285.
156. Rowley, J.A., G. Madlambayan, and D.J. Mooney, *Alginate hydrogels as synthetic extracellular matrix materials.* Biomaterials, 1999. **20**: p. 45-53.
157. Shoichet, M.S., et al., *Stability of hydrogels used in cell encapsulation: an in vitro comparison of alginate and agarose.* Biotechnol Bioeng, 1996. **50**: p. 374-381.
158. Kong, H.J., et al., *Controlling rigidity and degradation of alginate hydrogels via molecular weight distribution.* Biomacromolecules, 2004. **5**: p. 1720-1727.
159. Kim, W.S., et al., *Adipose tissue engineering using injectable, oxidized alginate hydrogels.* Tissue Eng A, 2012. **18**(7-8): p. 737-43.
160. Wiemann, M., et al., *The binding of rhBMP-2 to the receptors of viable MC3T3-E1 cells and the question of cooperativity.* Materialwiss Werkst, 2001. **32**(12): p. 931-936.
161. Patterson, J., et al., *Hyaluronic acid hydrogels with controlled degradation properties for oriented bone regeneration.* Biomaterials, 2010. **31**(26): p. 6772-81.
162. Chubinskaya, S., et al., *Gene expression by human articular chondrocytes cultured in alginate beads.* Journal of Histochemistry & Cytochemistry, 2001. **49**(10): p. 1211-1219.
163. You, J.O., et al., *Preparation of regular sized Ca-alginate microspheres using membrane emulsification method.* Journal of Microencapsulation, 2001. **18**(4): p. 521-532.
164. *How can I convert an RGB image to grayscale but keep one color?* ; Available from: http://stackoverflow.com/questions/4063965/how-can-i-convert-an-rgb-image-to-grayscale-but-keep-one-color.
165. Kolambkar, Y.M., et al., *Spatiotemporal delivery of bone morphogenetic protein enhances functional repair of segmental bone defects.* Bone, 2011. **49**(3): p. 485-92.
166. Jeon, O., et al., *Long-term delivery enhances in vivo osteogenic efficacy of bone morphogenetic protein-2 compared to short-term delivery.* Biochem Biophys Res Commun, 2008. **369**(2): p. 774-80.
167. Brown, K.V., et al., *Improving bone formation in a rat femur segmental defect by controlling bone morphogenetic protein-2 release.* Tissue Eng A, 2011. **17**(13-14): p. 1735-46.
168. Li, B., et al., *The effects of rhBMP-2 released from biodegradable polyurethane/microsphere composite scaffolds on new bone formation in rat femora.* Biomaterials, 2009. **30**(35): p. 6768-79.
169. Peters, M.C., et al., *Release from alginate enhances the biological activity of vascular endothelial growth factor.* J Biomater Sci, Polym Ed, 1998. **9**(12): p. 1267-1278.

170. Rai, B., et al., *Novel PCL-based honeycomb scaffolds as drug delivery systems for rhBMP-2.* Biomaterials, 2005. **26**(17): p. 3739-48.
171. Li, R.H. and J.M. Wozney, *Delivering on the promise of bone morphogenetic proteins.* Trends Biotechnol, 2001. **19**(7): p. 255-265.
172. Geiger, M., R.H. Li, and W. Friess, *Collagen sponges for bone regeneration with rhBMP-2.* Adv Drug Deliv Rev, 2003. **55**(12): p. 1613-29.
173. Kanakaris, N.K. and P.V. Giannoudis, *The health economics of the treatment of long-bone non-unions.* Injury, 2007. **38 Suppl 2**: p. S77-84.
174. *Summary of Safety and Effectiveness Data (SSED) for INFUSE Bone Graft.* 2004: Food and Drug Administration. p. 1-29.
175. Liu, F., et al., *A dose- and time-controllable syngeneic animal model of breast cancer microcalcification.* Breast Cancer Res Treat, 2010. **122**(1): p. 87-94.
176. Ruhe, P.Q., et al., *In vivo release of rhBMP-2 loaded porous calcium phosphate cement pretreated with albumin.* J Mater Sci Mater Med, 2006. **17**(10): p. 919-27.
177. Friess, W., et al., *Characterization of absorbable collagen sponges as rhBMP-2 carriers.* Int J Pharm, 1999. **187**(1): p. 91-9.
178. Brown, K.V., et al., *Improving bone formation in a rat femur segmental defect by controlling bone morphogenetic protein-2 release.* Tissue Eng Part A, 2011. **17**(13-14): p. 1735-46.
179. Bramono, D.S., et al., *Bone marrow-derived heparan sulfate potentiates the osteogenic activity of bone morphogenetic protein-2 (BMP-2).* Bone, 2012. **50**(4): p. 954-64.
180. Mulconrey, D.S., et al., *Bone morphogenetic protein (RhBMP-2) as a substitute for iliac crest bone graft in multilevel adult spinal deformity surgery: minimum two-year evaluation of fusion.* Spine (Phila Pa 1976), 2008. **33**(20): p. 2153-9.
181. Fu, R., et al., *Effectiveness and harms of recombinant human bone morphogenetic protein-2 in spine fusion: a systematic review and meta-analysis.* Ann Intern Med, 2013. **158**(12): p. 890-902.
182. Sandhu, H.S., et al., *Effective doses of recombinant human bone morphogenetic protein-2 in experimental spinal fusion.* Spine (Phila Pa 1976), 1996. **21**(18): p. 2115-22.
183. Sciadini, M.F. and K.D. Johnson, *Evaluation of recombinant human bone morphogenetic protein-2 as a bone-graft substitute in a canine segmental defect model.* J Orthop Res, 2000. **18**(2): p. 289-302.
184. La, W.G., et al., *The efficacy of bone morphogenetic protein-2 depends on its mode of delivery.* Artif Organs, 2010. **34**(12): p. 1150-3.
185. Zegzula, H.D., et al., *Bone formation with use of rhBMP-2 (recombinant human bone morphogenetic protein-2).* J Bone Joint Surg Am, 1997. **79**(12): p. 1778-90.
186. Arosarena, O. and W. Collins, *Comparison of BMP-2 and -4 for rat mandibular bone regeneration at various doses.* Orthod Craniofac Res, 2005. **8**(4): p. 267-76.
187. Lee, K.B., et al., *Inflammatory characteristics of rhBMP-2 in vitro and in an in vivo rodent model.* Spine (Phila Pa 1976), 2011. **36**(3): p. E149-54.
188. Boerckel, J.D., et al., *Effects of in vivo mechanical loading on large bone defect regeneration.* J Orthop Res, 2012. **30**(7): p. 1067-75.
189. Priddy, L.B., et al., *Oxidized alginate hydrogels for bone morphogenetic protein-2 delivery in long bone defects.* Acta Biomater, 2014. **10**(10): p. 4390-9.
190. Krishnan, L., et al., *Hydrogel-based Delivery of rhBMP-2 Improves Healing of Large Bone Defects Compared With Autograft.* Clin Orthop Relat Res, 2015.
191. Kawamoto, T. and K. Kawamoto, *Skeletal Development and Repair: Methods and Protocols.* Methods in Molecular Biology. Vol. 1130. 2013: Humana Press. 1-328.

192. Carragee, E.J., E.L. Hurwitz, and B.K. Weiner, *A critical review of recombinant human bone morphogenetic protein-2 trials in spinal surgery: emerging safety concerns and lessons learned.* Spine J, 2011. **11**(6): p. 471-91.
193. Samorezov, J.E. and E. Alsberg, *Spatial regulation of controlled bioactive factor delivery for bone tissue engineering.* Adv Drug Deliv Rev, 2014.
194. Visser, R., et al., *The effect of an rhBMP-2 absorbable collagen sponge-targeted system on bone formation in vivo.* Biomaterials, 2009. **30**(11): p. 2032-7.
195. Seeherman, H., *The influence of delivery vehicles and their properties on the repair of segmental defects and fractures with osteogenic factors.* J Bone Joint Surg Am, 2001. **83-A Suppl 1**(Pt 2): p. S79-81.
196. Ratko, T.A., et al., *Bone Morphogenetic Protein: The State of the Evidence of On-Label and Off-Label Use*. 2010, Blue Cross and Blue Shield EPC.
197. Puppi, D., et al., *Polymeric materials for bone and cartilage repair.* Progress in Polymer Science, 2010. **35**(4): p. 403-440.
198. Liu, R., et al., *Myogenic progenitors contribute to open but not closed fracture repair.* BMC Musculoskelet Disord, 2011. **12**: p. 288.
199. Schindeler, A., R. Liu, and D.G. Little, *The contribution of different cell lineages to bone repair: exploring a role for muscle stem cells.* Differentiation, 2009. **77**(1): p. 12-8.
200. Stein, H., et al., *The muscle bed--a crucial factor for fracture healing: a physiological concept.* Orthopedics, 2002. **25**(12): p. 1379-83.
201. Willett, N.J., et al., *Attenuated human bone morphogenetic protein-2-mediated bone regeneration in a rat model of composite bone and muscle injury.* Tissue Eng Part C Methods, 2013. **19**(4): p. 316-25.
202. Huard, J., B. Cao, and Z. Qu-Petersen, *Muscle-derived stem cells: potential for muscle regeneration.* Birth Defects Res C Embryo Today, 2003. **69**(3): p. 230-7.
203. Einhorn, T.A., *Clinical applications of recombinant human BMPs: early experience and future development.* J Bone Joint Surg Am, 2003. **85-A Suppl 3**: p. 82-8.
204. Mroz, T.E., et al., *Complications related to osteobiologics use in spine surgery: a systematic review.* Spine, 2010. **35**(9 Suppl): p. S86-104.
205. Uhrig, B.A., *Tissue Regeneration in Composite Injury Models of Limb Trauma*, in *BioEngineering*. 2013, Georgia Institute of Technology. p. 196.
206. Pawitan, Y., et al., *False discovery rate, sensitivity and sample size for microarray studies.* Bioinformatics, 2005. **21**(13): p. 3017-24.
207. Pountos, I., et al., *Pharmacological agents and impairment of fracture healing: what is the evidence?* Injury, 2008. **39**(4): p. 384-94.
208. Dimmen, S., et al., *Negative effect of parecoxib on bone mineral during fracture healing in rats.* Acta Orthop, 2008. **79**(3): p. 438-44.
209. Simon, A.M. and J.P. O'Connor, *Dose and time-dependent effects of cyclooxygenase-2 inhibition on fracture-healing.* J Bone Joint Surg Am, 2007. **89**(3): p. 500-11.
210. Chang, J.K., et al., *Effects of anti-inflammatory drugs on proliferation, cytotoxicity and osteogenesis in bone marrow mesenchymal stem cells.* Biochem Pharmacol, 2007. **74**(9): p. 1371-82.
211. Ito, S., et al., *Glucocorticoids induce the differentiation of a mesenchymal progenitor cell line, ROB-C26 into adipocytes and osteoblasts, but fail to induce terminal osteoblast differentiation.* Bone, 2007. **40**(1): p. 84-92.
212. Kuziel, W.A., et al., *Severe reduction in leukocyte adhesion and monocyte extravasation in mice deficient in CC chemokine receptor 2.* Proc Natl Acad Sci U S A, 1997. **94**(22): p. 12053-8.

213. Xing, Z., et al., *Multiple roles for CCR2 during fracture healing.* Dis Model Mech, 2010. **3**(7-8): p. 451-8.
214. Bleul, C.C., et al., *A highly efficacious lymphocyte chemoattractant, stromal cell-derived factor 1 (SDF-1).* J Exp Med, 1996. **184**(3): p. 1101-9.
215. Nagasawa, T., *Microenvironmental niches in the bone marrow required for B-cell development.* Nat Rev Immunol, 2006. **6**(2): p. 107-16.
216. Duvall, C.L., et al., *Impaired angiogenesis, early callus formation, and late stage remodeling in fracture healing of osteopontin-deficient mice.* J Bone Miner Res, 2007. **22**(2): p. 286-97.
217. Lau, T.T. and D.A. Wang, *Stromal cell-derived factor-1 (SDF-1): homing factor for engineered regenerative medicine.* Expert Opin Biol Ther, 2011. **11**(2): p. 189-97.
218. Das, A., et al., *Delivery of bioactive lipids from composite microgel-microsphere injectable scaffolds enhances stem cell recruitment and skeletal repair.* PLoS One, 2014. **9**(7): p. e101276.
219. Shinohara, K., et al., *Stromal cell-derived factor-1 and monocyte chemotactic protein-3 improve recruitment of osteogenic cells into sites of musculoskeletal repair.* J Orthop Res, 2011. **29**(7): p. 1064-9.
220. Chellaiah, M.A., et al., *Osteopontin deficiency produces osteoclast dysfunction due to reduced CD44 surface expression.* Molecular Biology of the Cell, 2003. **14**(1): p. 173-189.
221. Rittling, S.R., et al., *Mice lacking osteopontin show normal development and bone structure but display altered osteoclast formation in vitro.* Journal of Bone and Mineral Research, 1998. **13**(7): p. 1101-1111.
222. Suzuki, K., et al., *Colocalization of intracellular osteopontin with CD44 is associated with migration, cell fusion, and resorption in osteoclasts.* Journal of Bone and Mineral Research, 2002. **17**(8): p. 1486-1497.
223. Hirata, A., et al., *Expression profiling of cytokines and related genes in regenerating skeletal muscle after cardiotoxin injection: a role for osteopontin.* Am J Pathol, 2003. **163**(1): p. 203-15.
224. Uaesoontrachoon, K., et al., *Osteopontin and skeletal muscle myoblasts: association with muscle regeneration and regulation of myoblast function in vitro.* Int J Biochem Cell Biol, 2008. **40**(10): p. 2303-14.
225. Pfeifer, R., et al., *Cumulative effects of bone and soft tissue injury on systemic inflammation: a pilot study.* Clin Orthop Relat Res, 2013. **471**(9): p. 2815-21.
226. Forsberg, J.A., et al., *Correlation of procalcitonin and cytokine expression with dehiscence of wartime extremity wounds.* Journal of Bone and Joint Surgery-American Volume, 2008. **90A**(3): p. 580-588.
227. Hawksworth, J.S., et al., *Inflammatory Biomarkers in Combat Wound Healing.* Annals of Surgery, 2009. **250**(6): p. 1002-1007.
228. Forsberg, J.A., et al., *Do Inflammatory Markers Portend Heterotopic Ossification and Wound Failure in Combat Wounds?* Clinical Orthopaedics and Related Research, 2014. **472**(9): p. 2845-2854.
229. Dosier, C.R., et al., *Effect of cell origin and timing of delivery for stem cell-based bone tissue engineering using biologically functionalized hydrogels.* Tissue Eng Part A, 2015. **21**(1-2): p. 156-65.
230. Hettiaratchi, M.H., et al., *Heparin microparticle effects on presentation and bioactivity of bone morphogenetic protein-2.* Biomaterials, 2014. **35**(25): p. 7228-38.
231. Lopez-Valladares, M.J., et al., *Donor age and gestational age influence on growth factor levels in human amniotic membrane.* Acta Ophthalmol, 2010. **88**(6): p. e211-6.
232. Russo, A., P. Bonci, and P. Bonci, *The effects of different preservation processes on the total protein and growth factor content in a new biological product developed from human amniotic membrane.* Cell Tissue Bank, 2012. **13**(2): p. 353-61.

233. Gerber, A. and S. Gogolewski, *Reconstruction of large segmental defects in the sheep tibia using polylactide membranes. A clinical and radiographic report.* Injury-International Journal of the Care of the Injured, 2002. **33**: p. 43-57.
234. Gugala, Z. and S. Gogolewski, *Healing of critical-size segmental bone defects in the sheep tibiae using bioresorbable polylactide membranes.* Injury-International Journal of the Care of the Injured, 2002. **33**: p. 71-76.
235. Li, M.-T.A., *Treatment Strategy for Composite Tissue Limb Trauma*, in *Biomedical Engineering.* 2015, Georgia Institute of Technology. p. 182.
236. Glowacki, J., *Angiogenesis in fracture repair.* Clin Orthop Relat Res, 1998(355 Suppl): p. S82-9.
237. Portmann-Lanz, C.B., et al., *Manufacture of a cell-free amnion matrix scaffold that supports amnion cell outgrowth in vitro.* Placenta, 2007. **28**(1): p. 6-13.
238. Oyen, M.L., R.F. Cook, and S.E. Calvin, *Mechanical failure of human fetal membrane tissues.* J Mater Sci Mater Med, 2004. **15**(6): p. 651-8.
239. Niknejad, H., et al., *Properties of the amniotic membrane for potential use in tissue engineering.* European Cells & Materials, 2008. **15**: p. 88-99.
240. Guldberg, R.E., *Spatiotemporal delivery strategies for promoting musculoskeletal tissue regeneration.* J Bone Miner Res, 2009. **24**(9): p. 1507-11.
241. Barrere, F., et al., *Advanced biomaterials for skeletal tissue regeneration: instructive and smart functions.* Mater Sci Eng R-Rep, 2008. **59**: p. 38-71.